Time domain calculation of noise generated by a propeller in a flow

Michael Carley

Department of Mechanical Engineering,
Trinity College,
Dublin 2,
Ireland.

October, 1996.

A thesis submitted to the University of Dublin in partial fulfilment of the requirements for the degree of Ph. D.

Abstract

In this thesis, the problem of calculating the noise from an acoustically subsonic aircraft propeller is approached using a "moving medium" method. An established theory of noise generation by rigid bodies in motion is combined with the moving medium Green's function to develop a linear acoustic formulation for the sound radiated by a body in arbitrary motion in a uniform steady flow of arbitrary orientation.

Results from a numerical code based on this formulation are then presented and compared to experimental results from a test campaign conducted as part of the EU-sponsored SNAAP (Study of Noise and Aerodynamics of Advanced Propellers) project. Near field acoustic results from two propellers, a conventional "low speed" propeller and an advanced "high speed" design, are presented for a range of operating speeds in the high subsonic to supersonic range. Further results are presented for the far-field noise of the low speed propeller operating at a low flight Mach number. In each case the blade loading distribution used in the calculations is interpolated from experimental data.

It is found that the numerical code predicts the experimental data quite well but is more accurate in predicting the noise from the high speed propeller than the low speed design, even for supersonic blade tip speeds (up to Mach numbers of 1.08). This and other features of the numerical predictions are discussed and explained.

It is concluded that the moving medium time domain method presented is useful and can be coded for efficient prediction of propeller noise.

> Being to treat of the Doctrine of *Sounds*, I hold it convenient to premise something in the general concerning this Theory; which may serve at once to engage your attention, and excuse my pains, when I shall have recommended them, as bestow'd on a subject not altogether useless and unfruitful.

(Bishop Narcissus Marsh, one time Provost of Trinity College, Dublin. He introduced the words 'acoustics', 'phonics' and 'microphone' into the English language.)

Declaration

I declare that I am the sole author of this thesis and that all the work presented in it, unless otherwise referenced, is my own. I also declare that this work has not been submitted, in whole or in part, to any other university or college for any degree or other qualification.

I authorise the library of the University of Dublin to lend this thesis.

Michael Carley

April 19, 2002

Thanks

Thanks to

- Melea Peek.
- My family, for everything.
- Professor John Fitzpatrick, my supervisor, for his advice and encouragement at various crucial stages of this project.
- Stately, plump Garry Lyons for sharing his knowledge of, and insight into, engineering and other arts.
- Craig Meskell, for sustained Guinness-fuelled arguments about life, the universe and the nature of turbulence.
- the Sound and Vibrations and Fluids groups in the Mechanical Engineering Department and especially Gareth Bennett, Sarah Dawson, Brian MacMahon and Jan Scholten.
- Everyone in the Mechanical Engineering Department for putting up with me for the last six years.
- All at CIRA, Capuà, for their help and support during my time there and in particular Danilo Tarica and Enrico de Bernardis of the aeroacoustics group and Neill Davies of the getting safely through Neapolitan traffic group.
- The SNAAP team who have given me a remarkable introduction to the European aerospace industry.
- Dr. John Chapman of Keele University for a large amount of assistance and information which has informed much of the work in this thesis.
- Dr. Feri Farassat of Langley Research Centre, NASA, who has been most helpful and generous with his time and knowledge.
- the nice Crossair air hostesses who let me photograph the propeller on a Saab 2000 despite the fact that they must have thought I was some kind of aerosexual.
- Anyone else who's got it coming. You know who you are.

Contents

List of Figures

List of Tables

Nomenclature and abbreviations

Latin symbols

a	source radius
c	speed of sound
D	propeller diameter
$\mathbf{D}$	$\gamma\mathbf{R} - \gamma^2\mathbf{M}_\infty$
$\mathbf{f}$	force per unit area on body surface
g	retarded time function
$G(\cdot)$	Green's function
$H(\cdot)$	Heaviside function
	$H(x) = \begin{cases} 1, & x > 0 \\ 0, & x < 0 \end{cases}$
J	advance ratio
	$= \dfrac{M_\infty c}{(N/60)D}$
j	$\sqrt{-1}$
$\mathbf{l}$	surface loading
m	rotational Mach number
M_r	source-observer Mach number
M_r'	effective source-observer Mach number, $-\partial R'/\partial\tau/c$
$\mathbf{M}_s$	source Mach number
M_t	blade tip Mach number
	$= M_\infty(1 + (\pi/J)^2)^{1/2}$
$\mathbf{M}_\infty$	inflow Mach number
N	rotor speed, revolutions per minute
$\hat{\mathbf{n}}$	surface unit normal
p	pressure

p'	acoustic pressure fluctuation
p'_L	loading noise
p'_T	thickness noise
$\hat{\mathbf{r}}$	unit radiation vector
r	observer radius in cylindrical coordinates
$\mathbf{R}$	convective radiation vector, $\partial R'/\partial x_i$
R'	effective source-observer distance
S	control surface
t	time
T_{ij}	Lighthill stress tensor $= \rho v_i v_j + (p - c^2\rho)\delta_{ij}$
u_i	flow velocity
v_n	surface normal velocity
V	control volume
w_i	surface velocity
$\mathbf{x}$	observer position
$\mathbf{y}$	source position
z	observer axial displacement in cylindrical coordinates

Greek symbols

α	propeller angle of attack
β	blade pitch
γ	convection factor, $1/(1 - \lvert\mathbf{M}_\infty\rvert^2)^{1/2}$
$\delta(\cdot)$	Dirac delta function $= \dfrac{d}{dx}H(x)$
δ_{ij}	Kronecker delta $= \begin{cases} 0, & i \neq j \\ 1, & i = j \end{cases}$
ρ	fluid density
ρ_0	mean fluid density
τ	retarded time
ψ	source azimuthal angle
θ	observer azimuthal angle
θ^*	source azimuthal angle $= \Omega\tau$
Ω	rotation frequency, radian/s

Operators

D/Dt	$\partial/\partial t + \mathbf{u}.\nabla$, time differentiation in convected coordinates

Superscripts

$\bar{D}$	on a differentiation operator, generalised differentiation
p'	fluctuation of value about mean

Subscripts

p_0	mean value

Other symbols

$[\cdot]$	evaluation of quantity in brackets at retarded time(s)

Abbreviations

ARA	Aeronautical Research Association
DNW	German-Dutch Wind-tunnel
HSP	High Speed Propeller
LSP	Low Speed Propeller
SPL	Sound Pressure Level

Chapter 1

Divers remarks on acoustics

> *So the people shouted when the priests blew with the trumpets: and it came to pass, when the people heard the sound of the trumpet, and the people shouted with a great shout, that the wall fell down flat, so that the people went up into the city, every man straight before him, and they took the city.*
>
> Joshua, VI, 20.

Acoustics has deep roots.

To the Ancients, sound and light must have seemed the strangest of things. Both acting at a distance, with no obvious means of transmission, they were still real (insofar as anything is real to a philosopher). Of the two, sound was perhaps the stranger, with its links to the psychological effects of music as well as its visible physical effects (although the story of Jericho can be safely considered apocryphal). The fact that a suitably tuned string could sound in response to the plucking of a similar one must have been as mysterious then as quantum theory is today. It was in the attempt to find some explanation for sound and its effects, among other things, that the Greek natural philosophers began to develop science as we know it. One element of their study was 'harmonics' which, with astronomy, statics, optics and mathematics formed science as then constituted. Modern physical science, excluding perhaps chemistry, can be traced back to those disciplines, Kuhn [1]. Harmonics found an engineering application in the ancient world in the construction of siege engines. Hunt [2] describes how siege engines were (literally) tuned. To ensure that a projectile thrown from such a device would fly to its intended destination, the engine's cords had to be correctly tensioned. The tensioning was checked by the Ancients' equivalent of a piano-tuner who would check the note generated by each cord when plucked.

Although it was not acoustics in the modern sense, the science of harmonics was intimately related to it. It was a 'science of proportion' relating geometry, psychology and music. As scientific thought developed and the scientific and the philosophical became increasingly separated, harmonics began to disappear into other studies. As Kuhn notes [1], harmonics proper began to decline

from the fifteenth century onwards but continued to appear as an introductory chapter in treatises on composition, temperament and instrument making. It is interesting, however, to note that there was never a complete break with physical science, "Kepler, Mersenne, and Descartes all wrote on harmonics; Galileo, Huyghens, and Newton displayed interest in it; Euler's *Tentatem novae theoriae musicae* is in a longstanding tradition." By 1739, the date of Euler's publication, another study had taken the place of harmonics, "the study, both theoretical and experimental, of vibrating strings, oscillating air columns and acoustics in general."

The influence of harmonics is still felt outside the areas of music and musical theory, although more as an approach than as a body of knowledge. Within the mathematical and physical sciences, it provided a language for the study of periodic phenomena. Mathematicians, scientists and engineers still talk about 'harmonic analysis' and the 'harmonics' in a signal and it was a search for harmony that drove much of the development of astronomy from which came Newton's laws and the beginning of the science and mathematics which engineers apply today. Kepler, for instance, sought a musical and geometric harmony in the solar system [3], and called one of his works *Harmonice Mundi*, 'The Harmony of the World'. From Kepler's laws came Newton's, the fundamental theory used in any mechanical engineering practice. Within that search for harmony, harmonics was more a philosophical pursuit than a mathematical or scientific one, but as acoustics it took its modern form sooner than its relative, fluid dynamics. This may be because analytical methods work well (the same wave equation is used today, with various source terms, as was developed two hundred years ago) and that good experiments are possible with comparatively simple equipment. For example, Rayleigh [4] describes how to estimate the frequency of a source using the ear aided perhaps by some reference pitch. It is hard to think of any other field where *quantitative* measurements are possible using the direct evidence of the senses.

The word 'acoustics' was first introduced into English by Bishop Narcissus Marsh [5], sometime Provost of this college, in 1683, along with the alternative term 'phonics' whence 'microphone', a word which he also devised. Like most researchers of the time, he also saw musical theory and instrument construction as part of the field, referring to the "skill to make all sorts of *Musical Instruments*".

He recognised that the two important elements of acoustic theory are those of *generation* and *propagation*, how sound is created and how it travels—

> As to the *Object* of hearing, which is Sound, improvement has been and may be made, both as to the *Begetting*, and as to the *Conveying* or *Propagating* (which is a kind of *Conserving*) of Sounds.

Without some idea of how sound propagates from a source, a detailed knowledge of the source is useless. Similarly, an understanding of the character of the source is essential before theories of propagation are any help. Just less than three hundred years later Lighthill [6] noted that "It is hardly possible

to discuss the way in which sound is propagated without some consideration of how it has been generated, and this is equally true when the medium is in motion."

This thesis is concerned with the "Begetting" and the "Conveying" of sound "when the medium is in motion".

1.1 Aeroacoustics

The 'aero' element of aeroacoustics can also be traced back to the Greeks. Statics was originally "conceived as the theory of machines" but "as hydrostatics, the theory of fluids, it was extended during the seventeenth century to pneumatics, the 'sea of air'" [1]. From there it became fluid mechanics. Aeroacoustics is the unification of fluid dynamic (essentially large scale) and acoustic (small scale) phenomena. Acoustics can be considered as the small perturbation limit of fluid dynamics; phenomena are small fluctuations about a mean value. Typically, however, those perturbations can be detected at great distances from their sources. The fluid dynamic processes which generate the sound are usually confined to some more or less clearly defined region ('the source') and are often quite intense within that region. Aeroacoustics, as an attempt to define acoustic properties of a source in terms of those processes, tries to unify the two scales, the small perturbation, long range, acoustic scale and the large perturbation, confined region, fluid-dynamic scale.[1] This leads to serious difficulties in computing the noise from flows; as Crighton [7] points out, the errors which are always present in numerical solutions can generate more noise than the 'real' flow field, 'the numerical procedure may actually be "noisier" than the flow.' This is perhaps another reason why acoustics reached its present form so early in the history of science. Analytical methods not only work well, they often work better than computational ones.

It is only comparatively recently that sources of sound have been characterised from fundamental fluid dynamic principles, using Lighthill's theory [8]. It is more recently still that the sound radiated from solid bodies has been predicted using an exact method, the solution of Lighthill's equation due to Ffowcs Williams and Hawkings [9]. This solution has been reformulated in various ways for different problems and has proved reliable and accurate. As well as providing a method for the solution of acoustic problems it has given an insight into the physics of sound generation by flows in general and flows around solid bodies in particular. Lighthill's work has also had the pleasant side effect of shedding light on the physics of its musical ancestor. An important paper in the field is due to Howe [10] and provides a contribution to "the theory of aerodynamic noise, with applications to excess jet noise and

[1] One might, fancifully, compare the relationship of acoustics and fluid-dynamics to that of astronomy (the observation of relatively small phenomena) and cosmology (the study of very large scale forces). It must be admitted, however, that contemplation of the infinite is rarely part of an aerodynamicist's work and less often part of an acoustician's.

the theory of the flute". Quite what Euclid or the Right Reverend Father in God Narcissus Lord Bishop of Ferns and Leighlin would have made of it, it is impossible to say.

1.2 Aircraft noise

While the Ancients applied acoustics to the problem of flying rocks and buckets of Greek fire the Moderns are interested in the noise of flying humans. While the 'sonic boom' caused by supersonic aeroplanes is well known, the noise generated by subsonic transports is more likely to be actually heard by most people. Modern aircraft carry more passengers, more cheaply and over greater distances than their predecessors.[2] They also do it under more restrictive noise regulations. One of the main driving forces behind modern powerplant design is the reduction of noise. In other areas of transport this problem is not so great. In road transport the engine can be shielded so that the main source of noise in modern cars is the tyre-road contact, and it is mainly in military applications that underwater noise is of serious interest, a problem familiar from various films involving besieged submarine captains.

Civil aircraft on the other hand need to have a propeller or jet acting directly on the air to generate thrust. They also flock near inhabited areas which means that they are more annoying than military aircraft which, in peacetime at any rate, are kept away from cities. The needs of travellers also dictate that any airport will have large numbers of aircraft in transit at any one time. The need to reduce the noise generated by individual aircraft and by airports as a whole means that the acoustics of powerplant are more important than ever before, quite apart from the exotic 'stealth' considerations of military aircraft.

The study of noise generated by aircraft powerplant divides conveniently into jet noise and propeller noise with helicopter rotor noise a more complex relation of propeller noise. This roughly corresponds to a division between sound generated by turbulence and sound generated by a solid body moving in a flow. In the area of propeller noise, with the development of accurate acoustic theory and reliable methods of aerodynamic calculation, good acoustic predictions are now commonplace for standard operating conditions and attention is being directed to the more difficult cases.

1.3 Propeller noise

The work presented here deals with solid body generated noise in general and with propeller noise in particular. Recently, there has been increased

[2]For example, in 1948 it cost James Baldwin $600 to fly from New York to Paris, roughly six months wages for a New York labourer. Today, the price can be as low as IR£200, less than two weeks wages for a postgraduate engineering student.

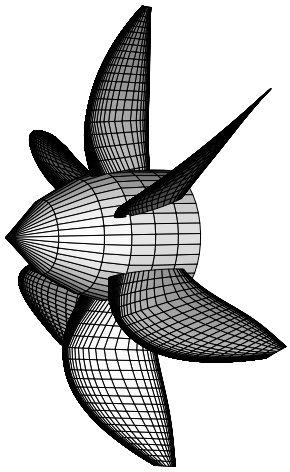

Figure 1.1: A modern high speed propeller

interest in propeller driven civil aircraft with a number of newly developed types entering service (the ATR 42, ATR 72 and Saab 2000 for example) due to the higher efficiency of propellers compared to jets. These modern propeller powered aircraft fly at higher speeds than previous designs which means that propellers are beginning to operate at transonic tip speeds. Such operating conditions will naturally cause a lot of noise and are among the main reasons for the importance of acoustics in propeller design. This has led to modern high speed designs which generally have a large number (six or more) of thin, highly swept blades, figure 1.1. Propellers of this type are being used on a number of aircraft including the recently introduced Saab 2000 and the Lockheed C-130J 'Hercules'.[3]

There are a number of factors which complicate the prediction of noise from a propeller. These are mainly related to what hapens when the propeller is attached to an aeroplane. The flow around the aircraft will obviously have some effect, causing a change in the aerodynamics and the acoustics. An important effect occurs when the propeller operates at incidence—when the

[3]A Lockheed Martin advertisement for the new C-130J (*Aviation Week and Space Technology*, April 8th, 1996), is headed "A prop that's 18% more efficient. And 100% funnier-looking." It continues "If you're thinking of snickering at the odd-looking propellers on the new C-130J Hercules, you're going to have second thoughts after reading this. Simply by twisting the blades and increasing their number to six, we've managed to give the aircraft 18% greater thrust at the same power setting.

It means at maximum gross weight, the "J" can now climb to 20,000 feet in just 14 minutes, compared to the 22 to 28 minutes of its predecessors. And with the prop's improved aerodynamic efficiency, the aircraft also uses less fuel and runs quieter."

inflow to the propeller is not parallel to the propeller axis. Figure 1.2 shows a propeller operating at some angle of attack to the inflow. Generally, 'angle of attack' is the term used to describe propeller incidence in the vertical plane and 'sideslip' the term used to describe incidence in the horizontal. Although sideslip and incidence are exactly equivalent for an isolated propeller there is a difference between them for a propeller on an aeroplane.

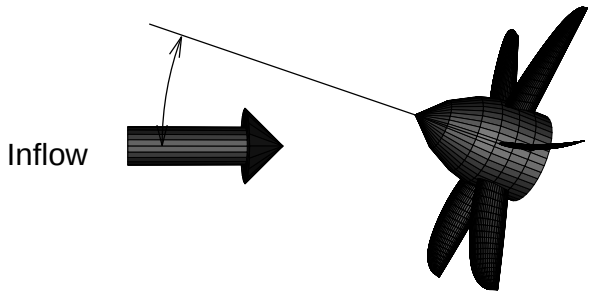

Figure 1.2: A propeller at angle of attack

When the flow is not axially symmetric, there are two effects to consider,

1. the propeller experiences varying flow conditions as it rotates so that the sound *source* distribution on the disc is not symmetric. As a blade section moves around the propeller disc, its angle of attack with respect to the inflow changes, so that the loading on the blade varies.

2. the convection conditions around the disc vary so that the sound generated by steady sources is not uniformly radiated and the *propagation* conditions are not symmetric, as demonstrated by Mani [11].

Bishop Marsh would have understood. The problem of predicting the noise generated divides neatly into one of "begetting" and one of "conveying" and the answer depends on the relative importance attached to each.

1.4 Plan of the thesis

This thesis presents a time-domain formulation for the sound radiated by a solid body moving in a steady uniform flow. The aim is to provide a formulation for the calculation of sound from a body whose motion is specified independently of that of the fluid so that effects such as crossflow on a propeller can be modelled in the time domain. More importantly, this formulation also provides a way of examining the physics of the problem and the processes which drive the observed effects of asymmetric inflow.

The next chapter presents a brief discussion of the development of propeller noise prediction methods, as well as some of the important issues in the field. It is followed by the derivation and examination of a simple, point-source, model of a propeller at angle of attack which allows the physics of the system to be investigated without the complication of using a complete model. In chapter 4 a more complete model is derived, which uses the whole surface of a propeller blade and a complete surface loading distribution in the prediction of the noise generated, these predictions being compared with experimental results in chapter 5.

Chapter 2

The prediction of propeller noise

> *Fernand Léger tells of visiting an airplane exhibition with fellow artists Duchamp and Brancusi. Duchamp, according to the story, turned to Brancusi and said, "Painting has come to an end. Who can do anything better than this propeller?" "I myself," relates Léger, "felt a preference for the motors. ... But I still remember the bearing of those great propellers. Good God, what a miracle!"*
>
> *The Existential Pleasures of Engineering*, Samuel C. Florman

The study of noise generation in general, and by solid bodies in particular, has a long history. In the past, as now, much of the work in the area has had military applications. Joshua's acoustic loading was sufficient for demolition purposes and the tuning techniques mentioned by Hunt [2] will be recalled from the previous chapter. Later on Leonardo da Vinci claimed that his proposed giant crossbow would be completely silent in operation; it is not recorded what provision he made to reduce the noise from his flying machines. Before the Industrial Revolution, most of the noise (rather than sound) of everyday life would have been generated by small scale industrial processes—forging and milling for example. Apart from arrows in flight or the odd cannonball, aerodynamically generated noise was comparatively rare. As dark Satanic Mills spread over the industrialising world, steam whistles and large furnaces blighted people's lives. This wee gem appeared in the *Mechanics' Magazine, Register, Journal, and Gazette* of the 12th of August, 1843.

> Improved blowing fan
>
> Sir,—I beg to submit to the notice of your readers a plan for preventing the disagreeable noise attending the working of fans, now very much in use among engineers and iron-foundries. These fans, your readers will recollect, are open at the sides to admit new air; now, instead of this, I propose that they should be constructed in the manner shown in the accompanying sketches, ... I think

> that in this way, the noise, which is such a nuisance to the populous neighbourhoods around iron manufactories would be completely prevented. I am, Sir, &c.
>
> Milwall X. X.

The neighbours had obviously begun to complain by 1843.

Around the start of the nineteenth century, mechanically powered vehicles became feasible and towards the end of that century, mechanically powered road and air transport began to appear. Up to then, aëronauts had made little more noise than that generated in producing the hot air for their balloons. Even when the dirigible airship came into service, air travel was relatively quiet with contemporary accounts commenting on its peaceful luxury—especially when compared to a ship or train. The environmental noise nuisance was little more than that caused ten centuries earlier by windmills, the first industrial turbomachinery.

When powered flight became possible, the situation changed. Most practical forms of air transport rely on the laws of nature and a trick of geometry. A rocket can lift a load by brute force; an aerodynamic vehicle needs some subtlety. Rocket-powered civil transports are not very common, meaning that lifting surfaces (wings or rotors for example) are needed for an aircraft to leave the ground. For such an aircraft to take off under its own steam it must generate enough thrust to accelerate to a speed where it generates a lifting force greater than its own weight. As one biographer of the Wrights [12] notes, "Whatever combination of engine and propellers they chose would have to provide sufficient thrust to achieve flying speed and sustain them in the air." They could no longer use gravity and a downhill run to get them moving. Unlike airship propulsion units, aeroplane powerplant must take the responsibility of getting a vehicle into the air as well as that of moving the vehicle through it.

2.1 The study of propeller noise

As aircraft became larger and more common, the study of their noise generation began. That study initially concentrated on the noise generated by powerplant (the obvious source of most of the noise made by any aircraft and still the most annoying). There is an excellent general history of that study as it relates to propellers by Metzger and Preisser [13] which examines the development of theoretical methods and of techniques based on empirical correlations. The two important themes in the development of theoretical methods are the inclusion of greater detail in models and the availability of greater computing power. The earliest methods used a point force model of the propeller for noise prediction. Later a thickness source was added. When the Ffowcs Williams-Hawkings solution [9] was published, full-surface models of the propeller blade began to be used. This development was aided by the

appearance of greater computing power for performing the acoustic calculations and also for the calculation of more accurate aerodynamic input. As more computing power has become available, more source mechanisms have been introduced into models, both because it has been possible to include them and because their inclusion has been required for the modelling of noise generation by more advanced propeller designs. While quadrupole terms have been used to model shock and turbulence generated noise, other mechanisms which modify the thickness and loading terms have also been included. Among these are the effects of stationary supports, non-uniform inflow (for example, the flow around a fuselage or the circulation around a wing) and the effect of another blade-row as in a counter-rotating propeller arrangement.

This chapter takes a more selective view than reference [13], taking a more direct path to the phenomena of interest in this thesis.

While X. X.'s work in the field of noise reduction was, no doubt, invaluable, the development of modern propeller noise research began in this century. By 1919 (less than twenty years after the Wrights' first powered flight), a supersonic propeller had been tested. Hawkings and Lowson [14] quote from an RAE report of 1920, which notes that a painful "crackling effect" was noticed near the propeller plane, in the "region in which the resolved part of the tip velocity in the direction of the observer exceeded the velocity of sound during some portion of a revolution of the screw." The airscrew was running at a tip speed of 1180 ft/s (354 m/s). At this stage the essential features of supersonic rotor noise were obvious,

- the change in character of the noise to a "crackling effect".
- the directivity; the character of the noise changed in a region near the propeller plane where the blade tip approached at supersonic velocity.

There is an important distinction between motion which is *acoustically* supersonic and that which is *aerodynamically* supersonic. If a body is moving supersonically relative to a fluid, the motion is aerodynamically supersonic. If a body moves towards an observer at greater than sonic velocity then the motion is acoustically supersonic. It is quite possible for motion to be aerodynamically supersonic without being acoustically supersonic. For the case of a high tip speed rotor, for example, a blade tip may move supersonically relative to the fluid but, for an observer near the propeller axis, the motion may be acoustically subsonic. The important feature is the presence and position of the observer. In the case of the RAE tests mentioned above, the change in character of the sound was noted near the propeller plane where some region of a blade was acoustically supersonic.

2.2 Noise prediction techniques

By the 1930s, Gutin [15] had derived a formulation for the prediction of propeller noise from aerodynamic parameters which gave a qualitatively correct

form for the directivity of the sound field. The first successful prediction theory, it worked adequately for low tip speed rotors. It is a frequency domain theory which predicts the strength of each discrete tone of the propeller noise field separately. Conceptually the rotating force and velocity distributions on a blade are replaced by a static distribution of fluctuating forces and velocities. In effect a moving steady force is replaced by a Fourier series in azimuthal angle on the rotor disc (see §2.4.1 below). Gutin considered only the noise generated by blade loading, which is usually the dominant noise mechanism for conventional propellers. They are, after all, designed to generate thrust. At transonic speeds, non-linear effects such as shock become important, [16], and for more accurate prediction at any speed the blade surface velocity distribution must be included.

2.2.1 Noise prediction theory

Aerodynamic noise prediction is usually based on the theory of Lighthill [8]. The well-known eighth-power law which predicts the noise power from a turbulent jet was an early success of the theory. As Powell [17] remarks, "Lighthill really did *predict* the eighth power law!", i.e. he did not know the answer in advance. Lighthill's theory starts from the exact form of the laws of mass and momentum conservation rather than from the linearised forms used in the usual development. This yields an inhomogeneous wave equation,

$$\frac{\partial^2 \rho}{\partial t^2} - c^2 \nabla^2 \rho = \frac{\partial^2 T_{ij}}{\partial x_i \partial x_j} \tag{2.1}$$

$$T_{ij} = \rho v_i v_j + (p - c^2 \rho)\delta_{ij}$$

where the source term arises from the difference between the linearised and exact forms of the equations of fluid motion. Note that the dependent variable is the fluid density, ρ. When written in this form, the equation is valid both inside and outside a source region. The term $\partial^2 T_{ij}/\partial x_i x_j$ can be estimated using scaling laws to yield the eighth power law mentioned above. $\partial^2 T_{ij}/\partial x_i x_j$ has a quadrupole directivity and is a less efficient source than the surface terms to be discussed later.

The power of Lighthill's equation lies in the fact that it is a restatement of the laws of fluid motion in a wave equation form. This has been recognised by a number of researchers who have used versions of the theory for aerodynamic calculations, for example Long [18] and Farassat [19]. In these aerodynamic calculations, compressibility is modelled using a time delay between a disturbance at one point and its effect somewhere else.

While Lighthill's theory was able to provide an insight into the source mechanisms of turbulent flows, it was the 1969 solution of equation 2.1 by Ffowcs Williams and Hawkings [9] that performed the same service for propeller noise, although earlier work was by no means superseded. The work of Lowson, for example, on the sound radiated from a moving point force [20],

is still useful as a model problem which contains the essential features of the physics of sound radiation from a moving system without the complications introduced by considering a complex geometry. Such a point-source model, also used by Gutin [15] is a valid approximation when the source region is compact, i.e. when it is small on a wavelength scale. As computing power has become cheaper and as propellers have operated at higher speeds, such point-source methods are less used for prediction purposes but they have become more important as a way of examining the physics of a problem and demonstrating certain features which would otherwise be obscured by computational issues. Simple models of this kind are also useful for parametric studies and for initial design work.

The solution of Ffowcs Williams and Hawkings [9] (see also Dowling and Ffowcs Williams [21]) is a formal mathematical manipulation which develops a solution for Lighthill's wave equation in terms of a velocity and pressure distribution over a control surface. It is usually most convenient to take this control surface to be the surface of a solid body. There also remains Lighthill's quadrupole source term in some volume around the body. The solution for the sound radiated from a moving rigid body with an impervious surface is

$$\begin{aligned} 4\pi c^2 \rho'(\mathbf{x},t) = & \frac{\partial^2}{\partial x_i x_j} \int_V \left[\frac{T_{ij}}{r|1-M_r|} \right] d^3\mathbf{y} && \text{(Quadrupole)} \\ & - \frac{\partial}{\partial x_j} \int_S \left[n_i \frac{\rho v_i v_j + p_{ij}}{r|1-M_r|} \right] dS && \text{(Loading)} \\ & + \frac{\partial}{\partial t} \int_S \left[\frac{\rho \mathbf{v}.\mathbf{n}}{r|1-M_r|} \right] dS && \text{(Thickness)} \end{aligned} \tag{2.2}$$

The "loading" and "thickness" terms are so called because of their relationship to the force distribution and geometry of the solid body respectively. The thickness noise source strength is a function of *how fast* a body moves the fluid out of its way (i.e. how the body's geometry or thickness affects the flow). The loading noise source strength depends on *how hard* the body has to push the fluid to move it. In this equation, $\rho v_i v_j + p_{ij}$ is the surface loading, r is the source-observer distance, M_r is the source-observer Mach number and v_n is the body surface normal velocity.

This equation has formed the basis of a number of noise prediction methods. In the time domain, the best known technique is that of Farassat [22] who reformulated the equations to convert the spatial derivative in the loading noise term into a time derivative making the numerical computation of the noise much easier. This is simply a matter of expanding the derivative $\partial/\partial x_j$ which yields, for the loading noise,

$$\begin{aligned} 4\pi p'_L = & \frac{1}{c} \int_S \left[\frac{1}{1-M_r} \frac{\partial}{\partial \tau} \left(\frac{l_r}{r(1-M_r)} \right) \right] dS && \text{(Far field)} \\ & + \int_S \left[\frac{l_r}{r^2(1-M_r)} \right] dS && \text{(Near field)} \end{aligned} \tag{2.3}$$

Here the loading term $n_i(\rho v_i v_j + p_{ij})\partial r/\partial x_j$ has been renamed l_r which is the component of surface loading in the direction of the observer. For this equation to be valid, it must be assumed that there is no appreciable quadrupole noise (which means, roughly, that turbulence and shocks are not very important). Then only the surface source terms contribute to the radiated sound and the relation $p' = \rho' c^2$ holds since the problem is now one of linear acoustics. Farassat's technique has been widely used and has also formed the basis of two integral formulations for linearised aerodynamics (one subsonic body formulation due to Long [18], and one for transonic and supersonic bodies due to Farassat [19]). As noted above, this is due to the fact that Lighthill's original theory is essentially a restatement of the laws of fluid dynamics or, if you prefer, that acoustics is really linearised aerodynamics.

In the frequency domain, the method of Hanson has achieved a certain fame [23]. Often an approximate far-field form of his theory is used which has proven quite accurate for most applications. Frequency and time domain methods of noise prediction are examined in §2.4.1.

2.3 Technological advances

By the 1940s, the "sound barrier" was seen as the immediate goal of aircraft development. This led to the development of jet powerplant reliable enough for use in commercial transports. The availability of jet and then turbofan propulsion caused a move away from propeller driven aeroplanes. In recent years, the trend has been to return to propellers due to

- the higher efficiency of turboprop powerplant.
- the development of a market for smaller aircraft for regional traffic and for "narrow" routes—services which do not carry enough passengers to make the use of large, turbofan-powered, aircraft profitable.

The aircraft being used operate at higher cruise speeds than their predecessors which means that their propellers are operating transonically. As new materials and manufacturing methods have become available, advanced designs have become practical, leading to the wide-chord, highly swept blades now being seen. This has also led to new challenges in noise prediction as the problems of complex, non-linear, source mechanisms and high source-observer velocities have arisen.

Figure 2.1 shows one trend in the development of modern aircraft powerplant. Over the past forty years the specific fuel consumption of turboprop and jet/turbofan engines has continued to fall. In the case of turbofans it can be seen that the shift to higher bypass ratios has greatly improved their efficiency. And since McCormick [24] notes in a discussion of trends in powerplant development, "a turboprop is simply an extension of the turbofan to a higher bypass ratio", one would expect turboprop plant to be more widely used. The

problem is that at high subsonic Mach numbers the efficiency of propellers drops markedly due to compressibility effects. The modern challenge is to develop propellers that can operate at higher speeds to take advantage of the higher efficiency of turboprop engines, as seen in the example of the Pratt and Whitney 120 in figure 2.1.

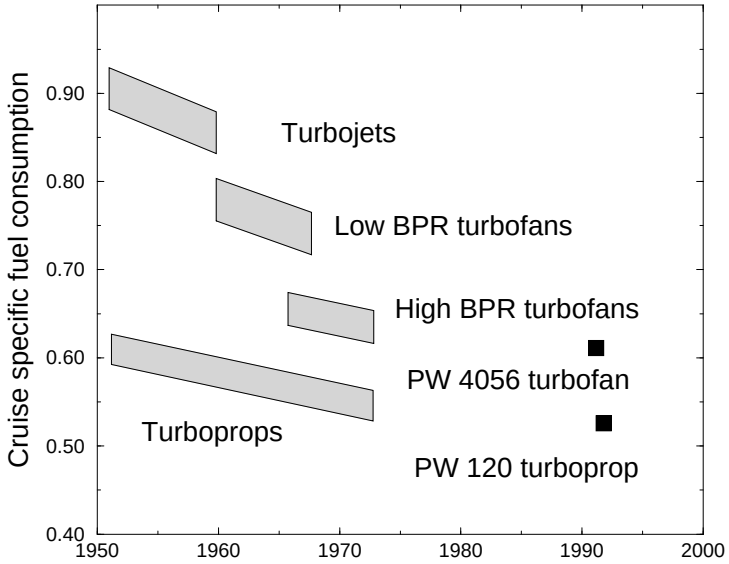

Figure 2.1: Trends in propulsion development (BPR—bypass ratio) including two modern Pratt and Whitney engines. Data from McCormick [24]

Some preliminary results for an advanced eight-bladed turboprop design tested at NASA's Lewis research centre are shown in figure 2.2. The efficiency of the propeller falls off quite rapidly around a Mach number of 0.73 but the design goal shown (80% efficiency at 0.8 Mach number) is certainly achievable.

As a further example of the possible gains to be made from propeller design, figure 2.3 shows the effect of blade sweep on the efficiency of a counter-rotating propeller tested by Rolls-Royce [25]. The swept blade has much higher efficiency than the conventional design over the higher Mach number range and has a peak around a Mach number of 0.8, offering the possibility of efficient high-speed propeller driven aircraft.

2.3.1 Modern research

Over the past decade or so, there have been a number of research programmes examining advanced propeller designs. Notably the NASA Propfan Test Assessment (PTA) aeroplane has been used for flight testing of open and ducted

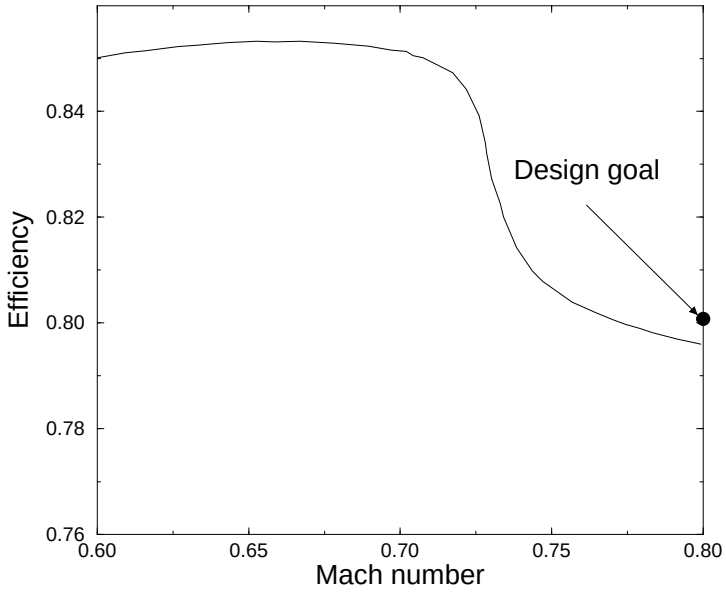

Figure 2.2: Test data for an advanced turboprop design tested at NASA Lewis. Data from McCormick [24]

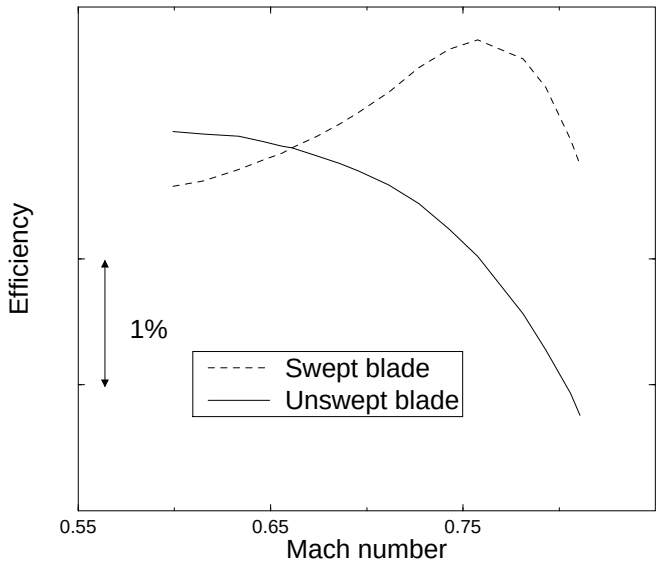

Figure 2.3: Effect of blade sweep on counter-rotating propeller efficiency. Data from Kirker [25]

single- and counter-rotation propellers. Woodward and Loeffler [26], give an account of tests conducted using this aircraft. Fokker [27], Dowty Rotol [28, 29, 30] and Rolls-Royce [25], have all published data from propeller noise tests conducted in European wind-tunnels, and in the United States Hamilton Standard [31], and General Electric [32], have done likewise. In the case of Rolls-Royce and the two American companies, work has been done on counter-rotating propellers as well as on single-rotation types. Results from these tests were published between 1987 and 1994, indicating great interest (i.e. interest great enough for aerospace companies to spend money) in propeller development generally, and in propeller acoustics in particular.

The NASA Lewis tests on a Hamilton Standard SR-7L single rotation propeller [26], used the PTA to carry a propeller and various acoustic and aerodynamic instrumentation and a Learjet flying in formation for far field noise measurements. Noise data were also taken on the ground to test atmospheric propagation models. More extensive ground noise tests are described by Garber and Willshire [33]. They found a large variation in noise levels for tests conducted under nominally identical conditions. They ascribed this to the effects of propagation through the atmosphere. There was "no clear correlation [of atmospheric turbulence] with the observed short-term sound level variability." They also emphasise the interdependence of variables in the system, noting that, for example, reducing the propeller rotation speed may reduce the peak noise level, but the associated change in directivity may well cause the noise at a given point to become greater than it was at the higher rotation speed.

Dittmar and Stang [31] describe wind-tunnel tests on a 2/9 scale Hamilton Standard SR-7A. They found that the maximum blade-passage-frequency tone's sound pressure level increased and then levelled off or decreased with increasing helical tip Mach number, for a given advance ratio. They conclude that this "points to the use of faster rotating propellers as a possible method to limit cabin noise while maintaining high flight speed and efficiency."

Trebble details tests carried out on a full size [28], and on a one fifth scale [29], Dowty Rotol R212 propeller. He notes that the data are consistent with "the simplifying suggestion ... that the effective noise source is at the propeller tip", which has been demonstrated with some rigour by Crighton and others [34, 35, 36], using Hanson's far field model [23] and asymptotic techniques. It was found that for a subsonic propeller, the tip region is exponentially dominant over the inboard part of the blade in determining harmonic strength. For supersonic propellers, the point on the blade which approaches the observer at sonic velocity is algebraically dominant, followed in importance by the tip.

2.4 Issues in propeller noise prediction

Some of the general issues concerning the prediction of noise generated by propellers are considered. The important points are

- time domain or frequency domain?
- moving observer or moving medium?
- formulations and algorithms.
- incidence effects.

2.4.1 Time and frequency domain methods

The main division in propeller noise prediction theories is that between frequency domain and time domain methods. They are precisely equivalent but, in general, frequency domain methods are more elegant and easier, especially for mathematical analysis. A frequency domain method is one which predicts the strength of each harmonic of the noise from a propeller directly while a time domain method yields a time record, typically for one revolution of the propeller. A frequency domain method replaces the rotating source distribution on a propeller blade with a stationary distribution over the propeller disc. This has the advantage of eliminating the rotational component of the source motion from the calculations, as demonstrated in appendix A. The moving source distribution as a function of time is replaced by its Fourier series as a function of azimuth. Figure 2.4 shows how a rotating point source, a delta function of azimuthal angle and time, can be represented by the first few terms of its Fourier series. The source distribution used for the acoustic calculation is then a set of modes distributed over the propeller disc with each of these modes being one of the components of the Fourier series of the azimuthal source distribution, as shown in figure 2.4.

Frequency domain methods have fewer of the difficulties associated with the singularities which are often encountered in the calculation of sound from a high speed body. They are also more useful in the aeronautical industry when it is necessary to meet the standards of, for example, the Federal Aviation Regulations. Since these regulations are based on an estimated human response to sound which varies with frequency (based on an A-weight filter, for example), it is usually most convenient to calculate directly the strength of those harmonics which are perceived as most annoying (those in the 1–5kHz range, [37]). Further, the effect of the atmosphere on propagation of the generated sound can depend on the frequency of that sound [38] so that in estimating the expected community annoyance, it is easier to work in the frequency domain.

Time domain techniques, however, do have some advantages over frequency domain methods. The first is that propellers are not the only moving bodies

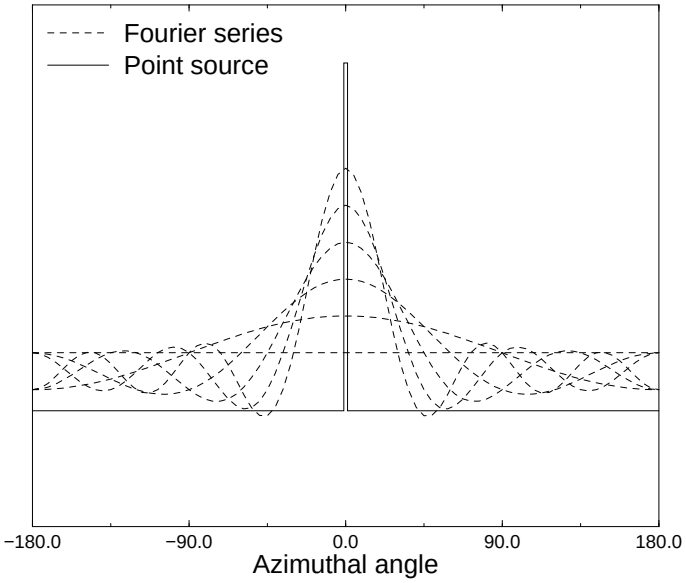

Figure 2.4: The representation of a point source by the first few terms of its Fourier series

which make noise. In calculating the sound from a body which is not moving periodically there is no convenient frequency domain method for calculating the sound radiated. Secondly, it is often easier to think about physical processes happening over time rather than in the somewhat abstract frequency domain. The time domain method gives an insight into the physics which might be less easily found in a frequency domain formulation. Finally, for research (rather than design) purposes, a time domain method offers the possibility of looking at phenomena such as turbulence which can be difficult to include in a frequency domain model.

For prediction purposes, the decision of which method will be used is usually made on grounds of convenience. Time domain methods usually work by calculating the sound from one blade and then summing suitably shifted records, one for each blade, to find the net signal from the rotor. For a many-bladed rotor such as a turbine fan, a very large number of points must be calculated in the initial time series to ensure sufficient resolution in the final result. If a frequency domain method is used, only the strength of harmonics which will actually appear in the final result need be calculated.

On the other hand, for very high speed rotors, time-domain methods are often favoured. As the tip speed of the rotor increases, the noise generated becomes more and more impulsive, consisting of a train of very short impulses. These impulses have a Fourier series which decays very slowly with harmonic

number so that an accurate noise prediction requires a very large number of harmonics to be calculated.

In summary, there is no particular preferred method for low speed, low blade-number rotors. For rotors with many blades, frequency domain methods are more efficient while for very high speed rotors, time domain techniques are faster.

2.4.2 'Moving medium' and 'moving observer' formulations

The problem of the noise generated by a propeller in the cabin of an aircraft or on its fuselage can be examined either as a 'moving observer' or a 'moving medium' problem. In the first case, an observer is assumed to translate forward at the same speed as the propeller, for example a passenger in an aircraft in flight. In a 'moving medium' case, the propeller and observer do not translate and there is a flow over both—the case of a wind-tunnel test. Wells and Han [39] have found that a time-domain 'moving-medium' approach greatly reduces the time required to compute the noise from a propeller in an axial flow and a 'moving medium' method has been used by Mani [11] and Hanson [40] in the frequency domain to examine the effect of asymmetric inflow (angle of attack), as mentioned above. In this thesis, a 'moving medium' technique is used which allows the convective influence on propeller noise to be 'decoupled' from the rotational and unsteady loading effects.

The prediction of noise from an aerodynamic source is a question of estimating the noise generated by a solid body, a flow or both of these. In aerodynamics, the problem of a body moving in a still fluid is equivalent to that of flow over a body. When we consider the acoustic problem, the presence of an observer complicates the issue. In most previous time-domain work (e.g. Farassat [22, 41]), a reference frame is chosen so that the fluid is stationary. There are cases where such a formulation is the only one which can be used, for example that of an accelerating aircraft. As a rule however, the case of constant velocity motion is of most interest and in that case a moving medium formulation is useful. Wells and Han [39] develop such a formulation which is equivalent to Farassat's formulation 3 [41]. They use this method to ease the calculation of the noise from translating propellers, claiming a sixfold reduction in computational effort. They do not, however, apply their method to the problem of a propeller at incidence, as their technique was developed for the case of an axial inflow. Spiegel [42] applies a moving medium method to the problem of helicopter noise (the extreme case of incidence) but he also does not allow for an arbitrary inflow angle which would make the calculation of sound from a propeller at angle of attack quite tricky.

2.4.3 Formulations and algorithms

There is an important distinction to be drawn between *formulations* and *algorithms*. While most interest has been in the development of formulations of the acoustic equations, the details of numerical implementation are not often made explicit. As the Ffowcs Williams-Hawkings equation, in its different forms, is exact, it should be possible to find exact solutions for the radiated sound, as long as the fluid dynamic data are exact. But as Brentner [43] notes, "the veracity of the input data *and the numerical approach* both play major roles in determining the accuracy of the acoustic prediction" [emphasis added]. In other words, the answer depends on how exactly the question is asked. Brentner goes on to detail a number of different integral formulations for the sound radiated from a surface and also looks at the different numerical methods which can be used to perform the required integrations. The sensitivity of different formulations to the numerical methods used to implement them is an issue which is becoming important in computational acoustics as the novelty of being able to make good predictions wears off. As Brentner [43] points out, "the discipline of computational acoustics is becoming more discerning—an assessment of the solution accuracy is also needed along with the acoustic prediction."

2.4.4 A propeller at incidence

The problem of a propeller operating at some angle of attack is closely linked to the increased restrictions on the noise an aircraft may make near an airport. Typically, an aeroplane near an airport is taking off or landing, i.e. it is operating at an angle of attack. Unfortunately, it is under these conditions that noise prediction becomes more difficult as the propeller sound field develops a marked asymmetry.

The standard explanation for this effect is that as the effective angle of incidence for a blade changes (due to varying flow conditions around the propeller disc), the force distribution over the blade fluctuates and this unsteady source distribution affects the noise radiated. In other words, it is an *aerodynamic* effect. Recently, Mani [11] has pointed out an additional mechanism which relies on the *acoustic* effect of a moving medium. He calculates the effect of asymmetric convection on the steady pressure distribution, to first order in crossflow Mach number, and demonstrates that this is equivalent to an unsteady acoustic source. There is also an earlier, less general, method due to Stuff [44], who calculated the sound field due to a point force in arbitrary motion in a uniform flow—essentially the moving medium equivalent of Lowson's work [20]. To estimate the effect of incidence on the sound from a propeller, he follows Gutin's approximation of the propeller as a point force at 80% of the blade radius [15]. Taking a Fourier series of the acoustic signature yields an estimate of the harmonic strength in the near and far fields. Both of these techniques indicate the general physics of propeller noise but suffer

from the point force approximation which leads to an underestimation of the higher harmonics of the signal.

Mani's analysis uses a frequency domain formulation, a very sensible approach which minimises the complexity of the problem. This is because the propeller can then be modelled as a translating disc rather than as a set of sources moving along a helical path. In this thesis, a time-domain formulation is presented and used to explain the source of the asymmetry of the sound field in terms of the physics of a moving source rather than in terms of spinning modes. This approach has been used by Hanson and Parzych [45] and by Hanson [40] to develop exact frequency domain formulations which include the convective effect of an angle of attack.

2.5 Currently available methods

Having seen some of the decisions to be made in deciding how to predict propeller noise, representative examples of the currently available methods of noise prediction can be examined. In the time domain, there are three basic methods of noise prediction using a full description of the blade surface and the aerodynamics, which can be arranged according to the choices made for the frame of reference (moving medium or moving observer) and for the range of source velocities to be considered (subsonic only or supersonic). Representative samples of these techniques are

- Farassat 1A [22], a moving observer, subsonic source method.
- Farassat 3 [41], a moving observer, supersonic source technique.
- Wells & Han [39], a moving medium, supersonic source formulation.

These methods and the choices made in developing them are summarised in table 2.1. As incidence effects are of interest in propeller noise, it is worth noting that the formulae of Farassat are the most flexible in this respect as they allow for the general case of an accelerating aircraft, for example a turning helicopter. The method of Wells and Han, like the technique developed in this thesis is less general (allowing only for axial inflow or steady aircraft motion).

2.5.1 Farassat 1A

The method of Farassat [22] for subsonic propellers in a stationary medium is one of the most widely used time domain techniques. It uses an integration over the actual surface of the blade to predict the noise generated by the various aerodynamic sources and, as it contains a Doppler factor, it will not work when a point on the blade approaches the observer at the sonic velocity. The main advantages of this technique are that it can be quite easily coded and that it is efficient, requiring evalulation of the acoustic integrals on the actual surface of the blade unlike Farassat's method 3 described in §2.5.2. It

gains some efficiency by the expansion of the spatial derivative in the Ffowcs Williams-Hawkings equation to a time derivative (see equation 2.3). If the formulation used the spatial derivative, the integral would need to be evaluated for a number of observer positions to allow numerical calculation of the divergence of the integral. Using the time derivative removes this necessity and allows all of the quantities in the equation to be evaluated using data from one retarded time calculation and one observer position.

2.5.2 Farassat 3

This technique developed by Farassat [41], is a powerful and elegant method which removes the difficulties associated with singularities caused by supersonic motion of a source. The formulation is developed starting from the usual solution of the wave equation, a convolution of a Green's function and a source distribution. Using certain properties of generalised functions, this solution is developed to give a formula which contains no Doppler factor but where integration is carried out over the retarded surface of the propeller blade, the surface made up of the position of each point on the blade at the retarded time corresponding to a given observer time point. The method works well for supersonic rotors but is computationally intensive. Because blade surface elements become very distorted at high speeds integrating over them requires exhaustive calculation. In practice both Farassat 1A and Farassat 3 are used in the same code, with Farassat 3 reserved for those blade surface elements that actually need it (i.e. those which approach the observer at supersonic speeds) and Farassat 1A for the inboard, subsonic part of a blade where source-observer speeds are low enough to cause no difficulties.

2.5.3 Wells and Han

Wells and Han [39] have recently published a moving medium equivalent of Farassat 3. Like that method it uses an integration over the acoustic planform of a blade to predict the noise generated. By using a moving medium Green's function, they absorb the translational component of the propeller and observer velocity into the equations rather than having to include them in the computation. Their formula for thickness noise is

$$4\pi c^2 \rho' = \frac{\partial}{\partial t} \int_S \frac{\rho_0 v_n}{R^*} \left(1 - M_\infty \frac{\partial R}{\partial x_1}\right) dS - \int_S \frac{\rho_0 v_n}{R^{*2}} \frac{\partial R}{\partial x_1} dS \qquad (2.4)$$

where S is a retarded surface. This formulation is more efficient than Farassat 3A (it requires one sixth of the processor time) although more restrictive as it only allows for the case of uniform translation of the propeller and observer.

2.5.4 A moving-medium, subsonic method

The technique to be developed in this thesis (chapter 4) will fit into table 2.1. It will be a moving-medium, subsonic propeller technique taking into account the aerodynamic and acoustic effects of incidence. This will allow the time domain calculation of noise from a propeller in a flow and will also show explicitly the effect of incidence on the Doppler amplification of the radiated noise.

2.6 Summary

The time-domain noise prediction formulae described in §2.5 can be fitted into a matrix according to their main characteristics. This matrix characterises the *formulation* used in each case independently of the numerical methods used to implement them (see the reference to Brentner [43] in §2.4.3).

	Moving observer	Moving fluid
Subsonic body only	Farassat 1A, §2.5.1	
Supersonic bodies	Farassat 3, §2.5.2	Wells & Han, §2.5.3

Table 2.1: Matrix of current time-domain noise prediction techniques

The object of the work developed in this thesis is to fill in the gap in the table (see table 4.1, page 41).

Chapter 3

The sound from a point source moving in a flow

If I ventured in the slipstream, ...

Astral Weeks, Van Morrison

In this chapter, a Green's function for a stationary source in a uniform flow is used to derive an equation for the sound radiated from a moving point source. This 'point source' approach has a long pedigree (see Gutin [15], Lowson [20] and Stuff [44] for example) as it is simpler than a solution for a finite solid body, being amenable to analytic investigation, and allows the essential features of the physics to be examined, unclouded by computational difficulties. Here, such a model indicates explicitly the effect of the interaction of source and fluid motion on the radiated sound. Certain features of the problem of a source rotating in an asymmetric flow can then be examined before introducing the complications of chapter 4, where equations for the sound radiated by solid bodies are derived.

3.1 Sound from a source moving in a uniform flow

The first stage in developing a theory of sound radiated by a solid body in a flow is to introduce a Green's function for the system.

The starting point for this derivation is the Green's function given by Lakhtakia et. al. [46] for sound radiation in a steady uniform flow, with a source at $\mathbf{y}$, an observer at $\mathbf{x}$ and a flow of Mach number M_∞ in the x_3

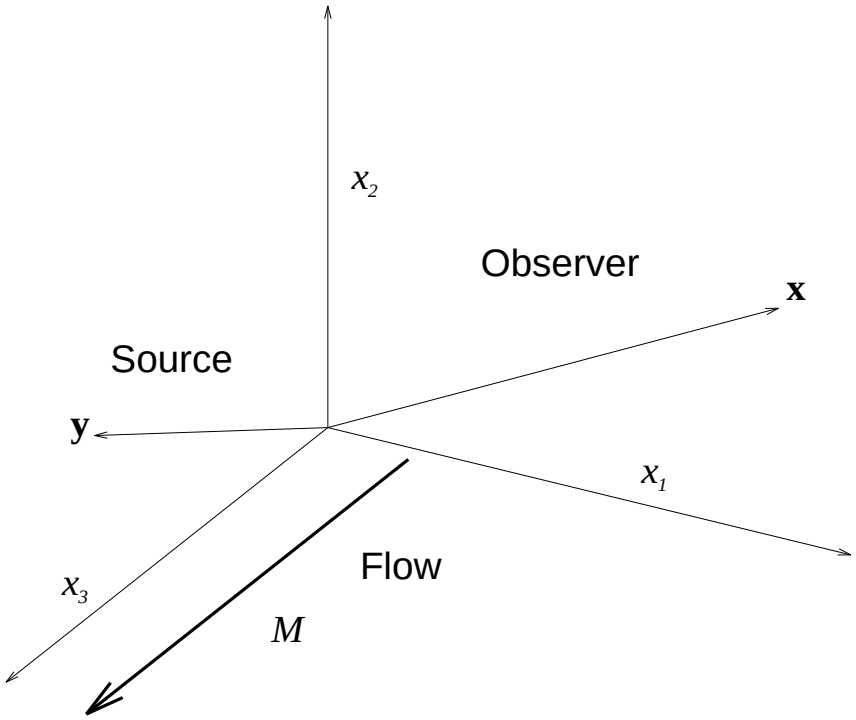

Figure 3.1: Arrangement of source, observer and flow for equation 3.1

direction, figure 3.1,

$$G(\mathbf{x},t;\mathbf{y},\tau) = \gamma\frac{\delta(\tau - t + \gamma R'/c - \gamma^2 M_\infty(x_3 - y_3)/c)}{4\pi R'}, \tag{3.1}$$
$$R' = [(x_1-y_1)^2 + (x_2-y_2)^2 + \gamma^2(x_3-y_3)^2]^{1/2},$$
$$\gamma^2 = \frac{1}{1-M_\infty^2}$$

This has the same form as the usual $1/R$ Green's function except that there are now two different distances to take into account. One, R', is the distance used for calculating attenuation and the other, $\gamma R' - \gamma^2 M_\infty(x_3 - y_3)/c)$ is used in working out the retarded time. It is common in the literature to refer to R' as the amplitude radius and $\sigma = \gamma R' - \gamma^2 M_\infty(x_3 - y_3)$ as the phase radius. Sound is attenuated more travelling through the flow than it would be in a still medium. Perhaps unexpectedly, the attenuation is symmetric, sound travelling upstream is attenuated by the same amount as sound travelling downstream. The only difference in propagation is that the delay depends on the direction in which the sound travels, as noted by Lighthill [6] who also points out that this has been confirmed by careful experiment.

Equation 3.1 can easily be adapted to the case of a flow of arbitrary direc-

tion, $\mathbf{M}_\infty$,

$$G(\mathbf{x},t;\mathbf{y},\tau) = \gamma\frac{\delta(\tau - t + \gamma R'/c - \gamma^2\mathbf{M}_\infty.(\mathbf{x}-\mathbf{y})/c)}{4\pi R'}, \tag{3.2}$$
$$R' = (|(\mathbf{x}-\mathbf{y})|^2 + \gamma^2|\mathbf{M}_\infty.(\mathbf{x}-\mathbf{y})|^2)^{1/2},$$
$$\gamma^2 = \frac{1}{1-|\mathbf{M}_\infty|^2},$$

so that the phase radius is now $\sigma = \gamma R' - \gamma^2\mathbf{M}_\infty.(\mathbf{x}-\mathbf{y})$.

3.1.1 Source motion

Source motion effects are included in the usual fashion for this problem, e.g., Dowling and Ffowcs Williams [21]. The sound from a source distribution over the volume V is given by integrating the source distribution multiplied by the appropriate Green's function over time and space,

$$p'(\mathbf{x},t) = \int_{-\infty}^{\infty}\int_V G(\mathbf{x},t;\mathbf{y},\tau)s(\mathbf{y},\tau)\,dV\,d\tau, \tag{3.3}$$

For a point source, at a position $\mathbf{y}(\tau)$,

$$p'(\mathbf{x},t) = \int_{-\infty}^{\infty}\int_V \gamma\frac{\delta(g)}{4\pi R'}\,dV\,d\tau, \tag{3.4}$$
$$g = \tau - t + \gamma R'/c - \gamma^2\mathbf{M}_\infty.(\mathbf{x}-\mathbf{y})/c, \tag{3.5}$$

The integration over τ can be performed immediately using the methods of generalised function theory, e.g. Farassat [47],

$$\int_{-\infty}^{\infty} f(x)\delta(g(x))\,dx = \left[\frac{f(x)}{|dg/dx|}\right]_{x=x^*}$$

where the notation $[\cdot]_{x=x^*}$ denotes evaluation of the term in brackets at the roots of $g(x)$, $x = x^*$. If $g(x)$ has more than one root the term is evaluated at each of these roots and the solution is the sum of the terms evaluated at each of the roots.

Then, for the sound from a point source moving in a flow $\mathbf{M}_\infty$,

$$p'(\mathbf{x},t;\mathbf{y},\tau;\mathbf{M}_\infty) = \gamma\frac{\delta(g)}{4\pi R'|1+\gamma\partial R'/\partial\tau/c + \gamma^2\mathbf{M}_\infty.\dot{\mathbf{y}}/c|} \tag{3.6}$$

if the observer is stationary ($\dot{\mathbf{x}} = 0$).

The notation of this equation can then be modified to bring it into line

with the more familiar form for a moving source

$$p'(\mathbf{x},t;\mathbf{y},\tau;\mathbf{M}_\infty) = \gamma \frac{\delta(g)}{4\pi R'|1-\gamma M'_r + \gamma^2 \mathbf{M}_\infty.\mathbf{M}_s|}, \tag{3.7}$$

$$M'_r = -\frac{\partial R'}{\partial \tau}/c,$$

Source-observer Mach number

$$\mathbf{M}_s = \frac{\partial \mathbf{y}}{\partial \tau}/c.$$

Source Mach number

The equation for the radiated sound has acquired an extra term related to the convection velocity as well as the usual term derived from the motion of the source towards the observer. It is important to note that for a source whose motion is confined to a plane, with the flow $\mathbf{M}_\infty$ perpendicular to that plane, the term $\mathbf{M}_\infty.\mathbf{M}_s$ is identically zero and there is no convection effect on the Doppler factor. It is also worth noting that equation 3.7 could be derived from the standard stationary-medium expression with the observer and source given some velocity. The source velocity would be given by $c(\mathbf{M}_s - \mathbf{M}_\infty)$ and the observer velocity would be $-c\mathbf{M}_\infty$. Inserting these expressions into the Doppler factor and into the retarded time calculation would yield equation 3.7.

3.2 The sound from a rotating source in crossflow

Equation 3.7 can be used as a simple model to look at the effect of angle of attack on the noise radiated by a propeller. For comparison, a simple frequency domain model will also be introduced.

3.2.1 Time domain calculations

The first diagrams show the value of equation 3.7 in the time domain for a source in a flow. The parameters of interest are tip rotational Mach number $m = \Omega a/c$ and crossflow Mach number M_x and observer radius r, and azimuth θ. The observer is in the plane of rotation. It should be noted that for a purely axial flow, the term $\mathbf{M}_\infty.\mathbf{M}_s$ vanishes and convection affects only the retarded time and source-observer distance, just as for a stationary source.

Figure 3.4a shows the value of p' for one revolution of a source with rotational Mach number $m = 0.74$, crossflow Mach number 0.1 and axial flow Mach number 0.3. Notation is shown in figures 3.2 and 3.3. Also shown in figure 3.4a is the delay between sound emission and reception, $t - \tau$, over one revolution. The magnitude of p' is strongly affected by the changing orientation of the observer. As well as the usual Doppler effect on the amplitude there is an interaction between the source motion and the flow. This causes

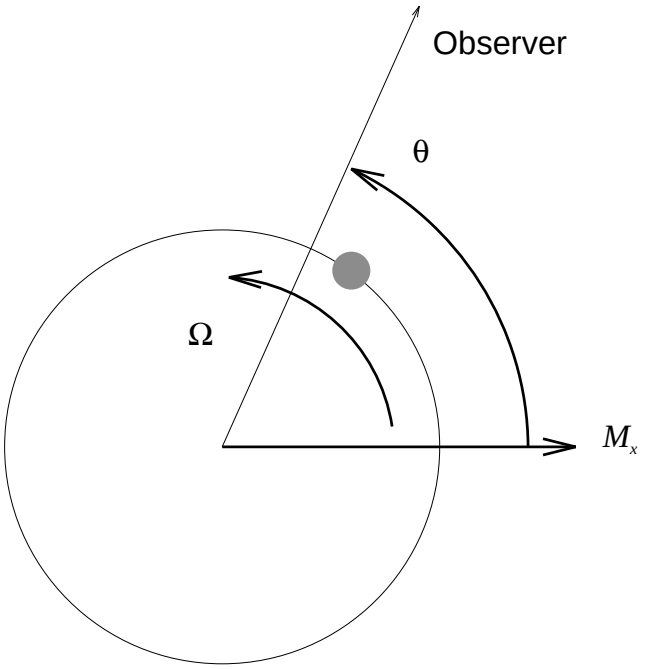

Figure 3.2: An acoustician's propeller

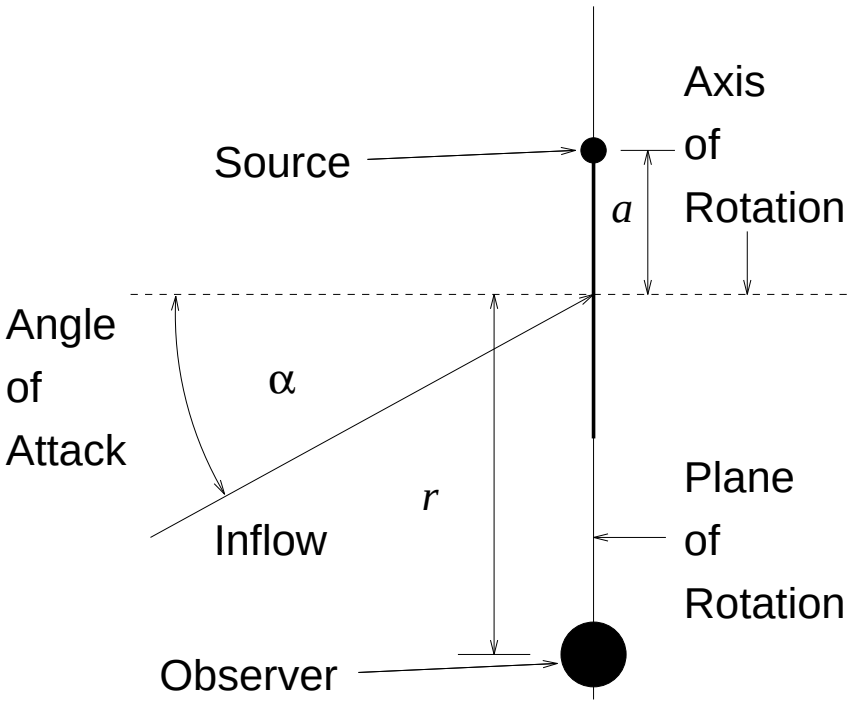

Figure 3.3: Definition of angle of attack

the large difference between the signal at 0° and that at 180°. As would be expected the peak in magnitude occurs at the maximum rate of change of retarded time or equivalently at the maximum source-observer approach velocity in the fluid-fixed reference frame. Physically, the sound arriving at an observer is 'compressed' or 'expanded' by the variations in retarded time. For a source in a stationary fluid, this variation depends only on the source velocity but when there is a flow, the interaction of source motion and convection changes the retarded time relationships and the rate of energy transmission. For the upstream positions, the large peak occurs because of the high rate of change of retarded time as the source approaches the observer at its maximum velocity.

To help visualise the effect of crossflow on the sound amplitude $\gamma^2\mathbf{M}_\infty.\mathbf{M}_s$, which is proportional to the component of source velocity in the upstream direction, can be plotted against source-observer Mach number $\gamma M_r'$, figure 3.4b. This is roughly analogous to a phase-plane diagram for a dynamical system. Some obvious rules help in interpreting these diagrams,

- the peak in the acoustic signal corresponds to the point where $\gamma^2\mathbf{M}_\infty.\mathbf{M}_s - \gamma M_r'$ has its greatest negative value—on the extreme right hand side of the trajectory.
- the highest possible peak in the acoustic signal will occur for a trajectory which goes into the bottom right hand corner of the plot.
- because the motion is periodic, twice per revolution both $\gamma^2\mathbf{M}_\infty.\mathbf{M}_s$ and $\gamma M_r'$ equal zero.
- due to the source periodicity a trajectory will be symmetric about a line through the origin of the plot.
- if the trajectory passes through the origin of the plot there is no Doppler amplification at that point—the convective and source-motion amplification effects cancel each other out. This can only happen for an observer position on the cross-flow axis. For it to happen, $\partial R'/\partial\tau$ and $\mathbf{M}_\infty.\mathbf{M}_s$ must be zero simultaneously. This happens when the source velocity is normal to the crossflow and at the same time the source is at its closest to, or furthest from, the observer.
- for a system with no crossflow the "phase-plane" diagram would be a horizontal line as $\mathbf{M}_\infty.\mathbf{M}_s$ is always zero, as noted above.

As can be seen from figure 3.4b (the near-field case) and figure 3.5b, the far-field diagram, only two trajectories in each plot have a crossover point and that crossover is at the origin in each case. All the other trajectories are closed loops with no crossovers. In the far-field case, figure 3.5b, the 0° trajectory is almost circular. This is because the source-observer vector changes very little and $M_r' = \mathbf{M}_s.\hat{\mathbf{r}}$ where $\hat{\mathbf{r}}$, the source-observer vector, is practically constant.

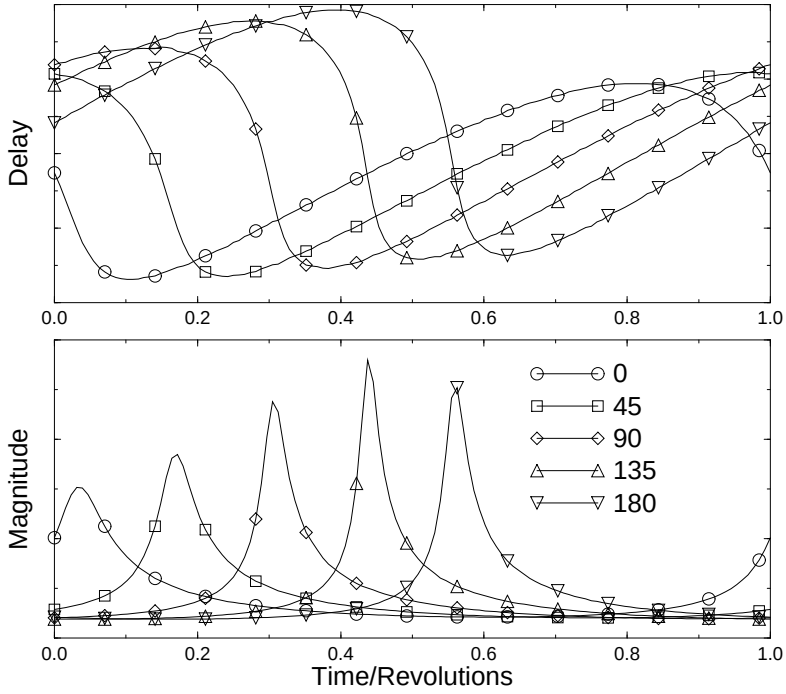

(a): Magnitude and delay for one revolution

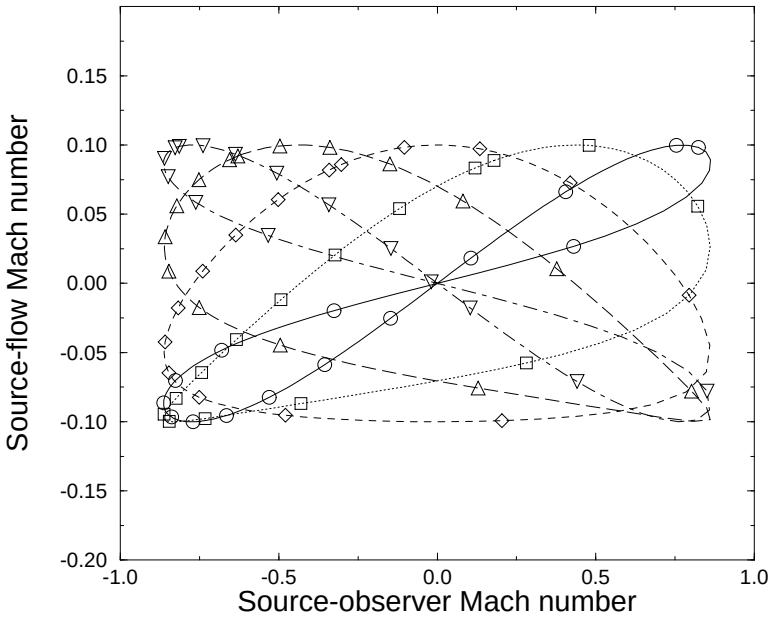

(b): "Phase plane" plot, notation as in (a)

Figure 3.4: Acoustic signal and Mach number plots for $m = 0.74$, $M_x = 0.1$, $r = 2$

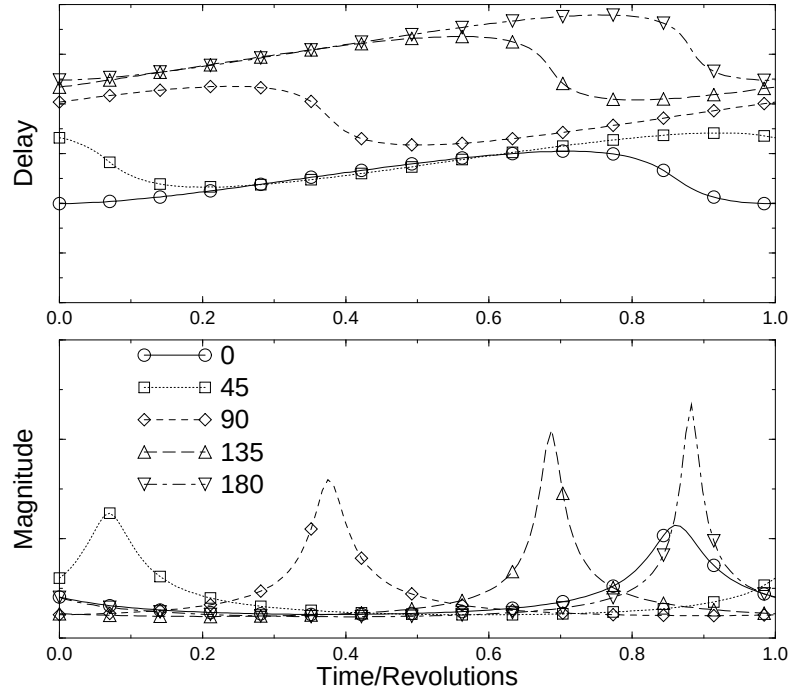

(a): Magnitude and delay for one revolution

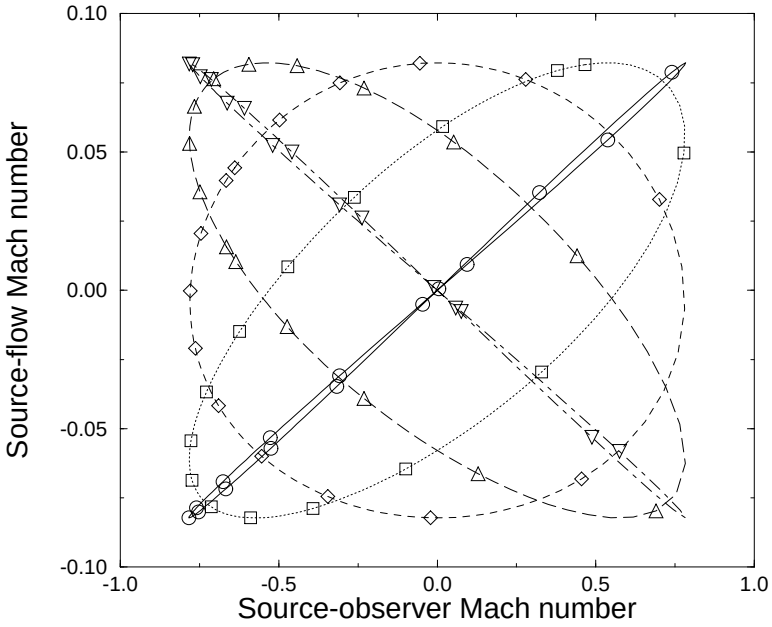

(b): "Phase plane" plot, notation as in (a)

Figure 3.5: Acoustic signal and Mach number plots for $m = 0.74$, $M_x = 0.1$, $r = 20$

This is typical of the far-field noise; it is controlled by changes in source-observer velocity rather than by changes in their separation. In the near-field case, changes in distance are important, which shows up in the trajectory in figure 3.4b which is definitely not circular.

3.2.2 Frequency domain

An equivalent equation for the sound from a rotating source can be derived in the frequency domain; see appendix A. The frequency domain method has the advantage of being simpler for this model problem. Results are presented here to demonstrate the equivalence of the two approaches. From appendix A, the strength, h_m, of the mth harmonic is

$$h_m = \frac{1}{\pi}\int_0^{2\pi} \gamma \frac{\exp(-j\Omega(\gamma R'/c - \gamma^2 \mathbf{M}_\infty.(\mathbf{x}-\mathbf{y})/c))}{4\pi R'} \exp(-jm\psi)\, d\psi. \quad (3.8)$$

For comparison with the time domain results, a time record p' will be used,

$$p'(t) = \sum_{m=1}^{m=N} \Re(h_m \exp(jm\Omega t)), \quad (3.9)$$

with N the number of harmonics to be considered. Figure 3.6 shows comparisons of the time domain acoustic signal and the frequency domain equivalent calculated with forty harmonics. There is a very good match at all observer positions although the frequency domain technique does not quite capture the sharpness of the peaks.

Using the frequency domain formulation of equation 3.8 the effect of crossflow on the harmonic strengths can be calculated directly. This can be done computationally using the exact formulation given or analytically using a far or near field approximation. The problem of the effect of convection on the sound from a propeller at incidence has been examined by Mani [11] who found, using a frequency domain method and a far field approximation, that the effect of asymmetric convection on the radiated noise can be greater than the effect of unsteady loading.

Figure 3.8 shows the effect of a crossflow on the first, second and fifth harmonics of the sound from a point source. The observer is twenty source radii from the axis of rotation, in the far field. The obvious point is that higher harmonics are more strongly affected than lower ones. In each case, the maximum effect is in the upstream direction. Figure 3.7 shows similar data for an observer two source radii from the rotation axis. Here, because of the additional effect of a changing source-observer distance, the maximum effect is nearer 135°.

It may seem strange that the maximum in the sound field is in the upstream direction but this is consistent with the time domain data. Looking again at equation 3.7, it is the term $\mathbf{M}_\infty.\mathbf{M}_s$ which controls the strength of the peak in the time record. This has its largest negative value when the source is moving

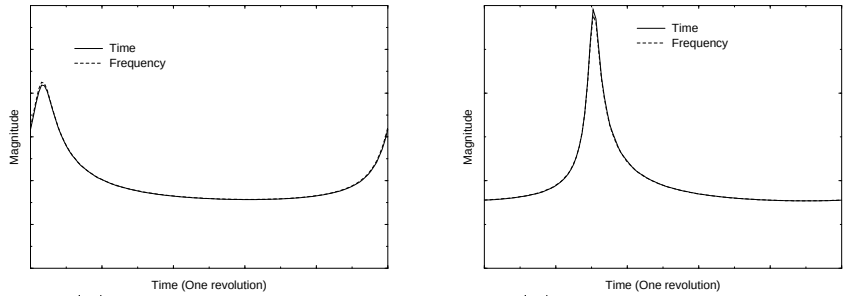

(a): observer at 0°

(b): observer at 90°

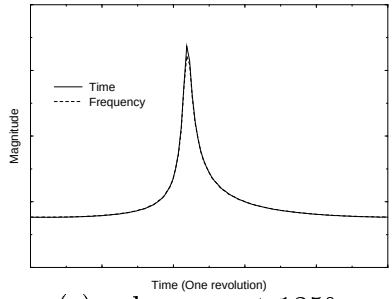

(c): observer at 135°

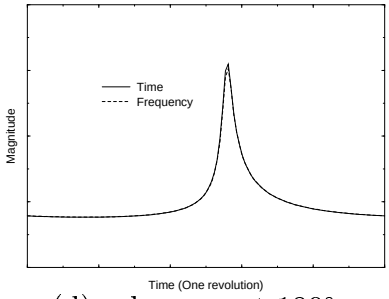

(d): observer at 180°

Figure 3.6: Time domain acoustic signal and frequency domain equivalents $m = 0.74$, $M_x = 0.1$, $r = 2$.

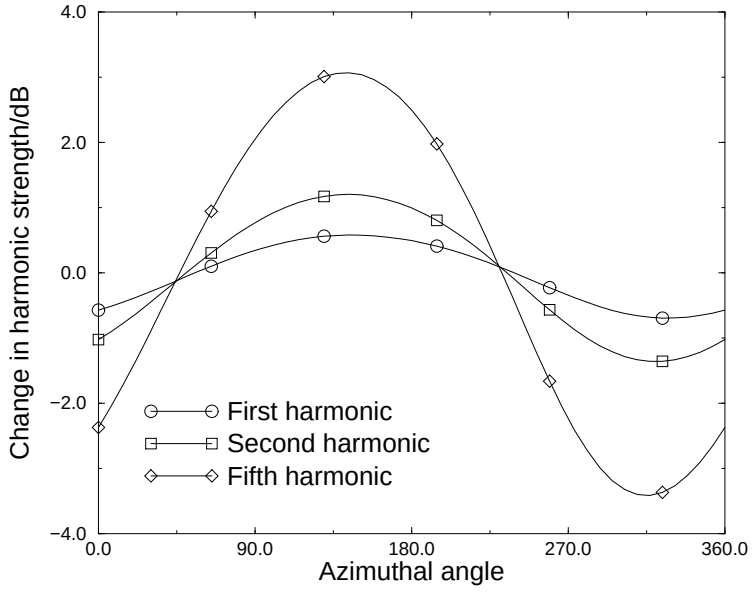

Figure 3.7: Effect of crossflow on harmonics in near field.

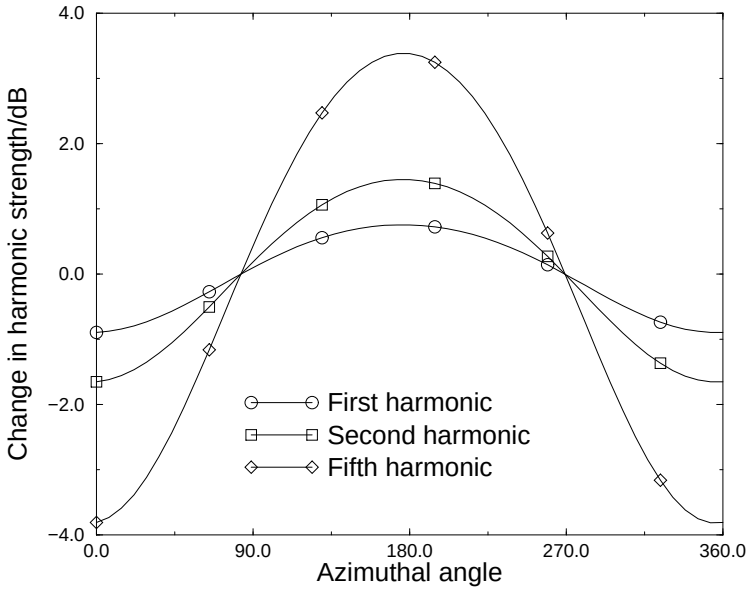

Figure 3.8: Effect of crossflow on harmonics in far field.

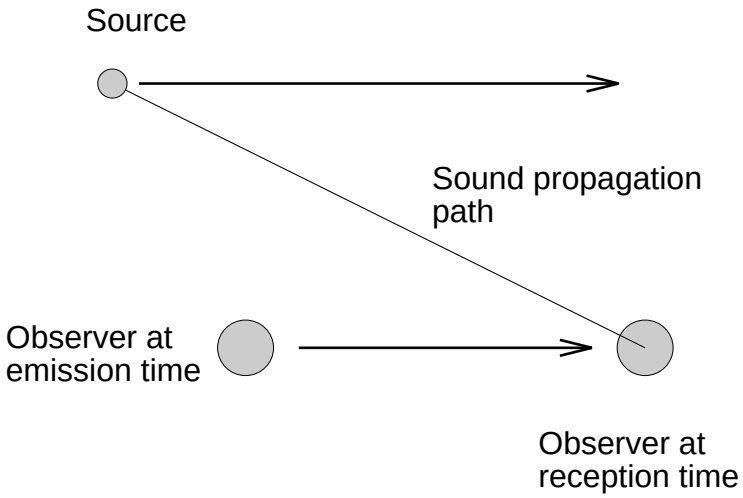

Figure 3.9: Effect of motion on acoustics.

upstream. Alternatively, looking at the problem in terms of a source and observer both moving with some mean velocity, the source-observer velocity is higher in the upstream direction than in the downstream.

Consider the situation of figure 3.9 with a source at position $\mathbf{y} - \mathbf{u}t$ and an observer at $\mathbf{x} - \mathbf{u}t$ in a stationary medium, with $\mathbf{u} = c\mathbf{M}_\infty$. Then the sound heard by the observer is given by the stationary medium Green's function,

$$\frac{\delta(\tau - t + R/c)}{4\pi R},$$

and in this case R will be

$$R = |\mathbf{r} - \mathbf{u}(t - \tau)|,$$

with

$$\mathbf{r} = \mathbf{x} - \mathbf{y}.$$

It is then simple to solve $\tau - t + R/c = 0$ for $t - \tau$,

$$t - \tau = -\gamma^2 \mathbf{M}_\infty.\mathbf{r}/c \pm \gamma(\mathbf{r}.\mathbf{r} + \gamma^2(\mathbf{M}_\infty.\mathbf{r})^2)^{1/2}/c,$$

with '$\pm$' replaced by '$+$' for causality ($t > \tau$) in the subsonic case. This is, naturally, identical to the retarded time expression given for the moving medium case. It can be seen that the effect of the translation is to allow the observer to forward during the period of passage of a wavefront from the source. If it moves forward of the source then the component of the source velocity in its direction is increased and the effect of the motion (or equivalently the fluid motion) is a Doppler amplification. If the observer is behind the source when a wavefront arrives then the Doppler amplification becomes an attenuation—the component of velocity towards the observer is reduced.

3.3 In conclusion

An existing Green's function for the sound radiated from a source in a uniform flow has been used to solve the problem of a source executing arbitrary motion in a steady uniform flow of arbitrary direction. This solution has then been examined with particular reference to the case of a rotating source in a crossflow—a simple model of the acoustics of a propeller. A consideration of this system has indicated the origin of the asymmetric noise field around a propeller operating at incidence. The interaction of source and fluid motion (the source and propagation effects mentioned on page 3) drives the observed variation in acoustic power distribution.

Chapter 4

Sound radiated from a rigid body in a steady uniform flow

But that propeller I left in Bilbao—
I ought to tell you about it now.

That Propeller I Left in Bilbao, Paul Durcan

The development of the acoustic theory for a real moving body now becomes the problem of incorporating the moving medium Green's function into a model for the radiation of sound from a finite body in a flow. The most convenient method is to use a set of manipulations similar to those of Farassat [22], where the source terms for the wave equation are written using generalised functions and convolved with the Green's function in the usual fashion. If certain properties of generalised functions are used this allows the development of a powerful formulation which does not contain a Doppler factor so that singularities are avoided and calculations of the noise from transonic and supersonic bodies are possible, as in the work of Farassat [41] and, in the supersonic propeller equivalent of the work presented here, Wells and Han [39]. Here, formulae which do have a Doppler factor are developed. This is because formulae of the type mentioned above usually require more computation than the conventional form and so are best used only when required. Furthermore, formulae of the usual type are more easily interpreted and are more helpful in examining the physics of the system.

4.1 Noise from a solid body

In this section, established methods are applied to the surface source terms of a solid body, giving a finite body equivalent of the point source equation of chapter 3. This leads to a useful reformulation of the equations of sound generation by a solid body which allows convective effects to be examined independently of the body's motion.

4.1.1 Use of generalised functions

In the following development, generalised functions are used to handle the source terms in the wave equation, a technique which has been used by Farassat in a number of papers, [22, 41] and which is explained in reference [47].

In essence, generalised functions provide a method of "restricting" quantities in some way. This is especially true in multidimensional space. In chapter 3 a (one-dimensional) delta function of time was used to state the relationship between retarded time and reception time. A similar technique can be used in three dimensions, in dealing with geometrical relationships. If a surface in space is specified by a function $f(\mathbf{x}, t)$,

$$f(\mathbf{y}, t) \begin{cases} < 0, & \text{inside the surface} \\ = 0, & \text{on the surface} \\ > 0, & \text{outside the surface} \end{cases},$$

and the convention of Farassat that

$$|\nabla f| = 1$$

is adopted so that

$$\nabla f = \mathbf{n} \qquad \text{the unit surface normal}$$

it becomes quite simple to restrict quantities to some specified region by multiplying by the *Heaviside* or *Dirac delta* functions. The Heaviside function,

$$H(x) = \begin{cases} 1, & x > 0 \\ 0, & x < 0 \end{cases},$$

restricts a quantity $Q(\mathbf{x}, t)$ to the region outside a surface using the expression $H(f)Q$. The delta function can be used in a similar manner to restrict a quantity to a surface, $\delta(f)Q$. In the development of the moving medium acoustic analogy, equation 4.6, Heaviside functions are used to require that the equations of momentum and continuity be considered outside the surface of interest. When these equations are differentiated, the delta functions generated will be interpreted as a statement that the source terms affected are to be restricted to the surface defined by f.

4.2 A moving medium acoustic analogy

The arrangement is shown in figure 4.1. The surface is given by $f(\mathbf{x}, t) = 0$. The surface normal $\mathbf{n} = \partial f / \partial x_i$ is also required.

The wave equation for a solid body moving in a uniform steady flow is now derived. The geometry for the system is shown in figure 4.1, using the surface

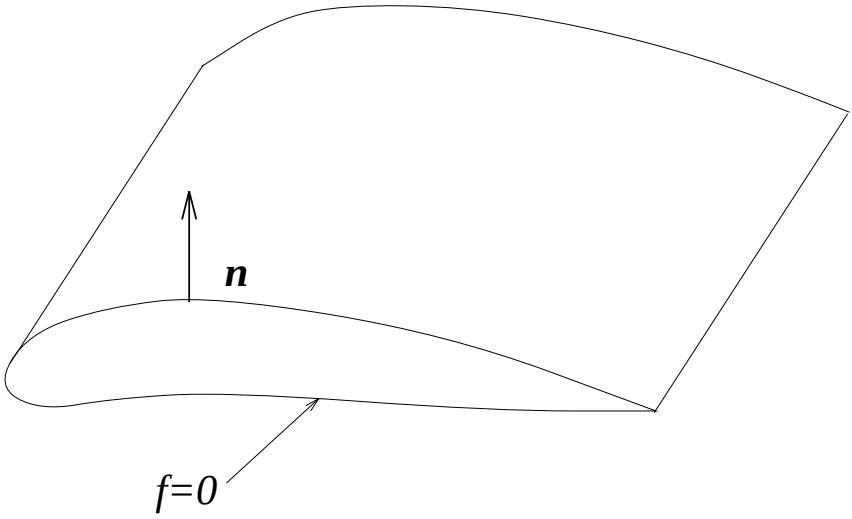

Figure 4.1: The surface definition for rigid body noise

definition $f(\mathbf{x}, t) = 0$ discussed above. A slightly more complex derivation for the case of flow along one coordinate axis can be found in Wells and Han [39]. The approach here is more general, considering the case of an inflow of arbitrary direction. The starting point is the equations of momentum and continuity (see e.g. Panton [48]) modified by multiplication with a Heaviside function of $f(\mathbf{x}, t)$ which defines the surface of the body of interest. Multiplying by $H(f)$ is simply a means of stating that the equations are valid only in the space outside the surface f. It is further required that $|\nabla f| = 1$, in accordance with the convention of Farassat [47]. The equations are, replacing $\partial/\partial t$ with $D/Dt = \partial/\partial t + u_i \partial/\partial x_i$,

$$H(f)\left(\frac{D\rho'}{Dt} + \frac{\partial}{\partial x_i}(\rho v_i)\right) = 0, \tag{4.1}$$

$$H(f)\left(\frac{D}{Dt}(\rho v_i) + \frac{\partial}{\partial x_j}(p_{ij} + \rho v_i v_j)\right) = 0. \tag{4.2}$$

These can be rewritten, since $H(f)dg/dx = \bar{d}/dx(H(f)g(x)) - g(x)\delta(f)$, where the bar on a differentiation operator signifies generalised differentiation,

$$\frac{\bar{D}}{Dt}(H(f)\rho') + \frac{\bar{\partial}}{\partial x_i}(H(f)\rho v_i) = \delta(f)\frac{\partial f}{\partial x_i}[\rho_0(w_i - u_i) + \rho(v_i + u_i - w_i)], \tag{4.3}$$

$$\frac{\bar{D}}{Dt}(H(f)\rho v_i) + \frac{\bar{\partial}}{\partial x_j}(H(f)(p_{ij} + \rho v_i v_j)) = \delta(f)\frac{\partial f}{\partial x_j}(\rho v_i(u_j - w_j + v_j) + p_{ij}), \tag{4.4}$$

with w_i the velocity of the body surface. It can be seen that the delta function restricting the source quantities to the surface f as discussed in the previous section arises naturally from the use of the Heaviside function in equations 4.1

and 4.2. Then, differentiating equation 4.3 with respect to time and subtracting from it the divergence of 4.4,

$$\begin{aligned}\left(\frac{D^2}{Dt^2} - c^2\frac{\partial^2}{\partial x_i^2}\right)\rho' = &\frac{\bar{D}}{Dt}\left([\rho_0(w_i - u_i) + \rho(v_i + u_i - w_i)]\delta(f)\frac{\partial f}{\partial x_i}\right) \\ &- \frac{\bar{\partial}}{\partial x_i}\left([\rho v_i(u_j - w_j + v_j) + p_{ij}]\delta(f)\frac{\partial f}{\partial x_j}\right) \\ &+ \frac{\partial^2}{\partial x_i \partial x_j}(p_{ij} + \rho v_i v_j) - c^2\frac{\partial^2 \rho}{\partial x_i^2},\end{aligned} \tag{4.5}$$

with quantities now restricted to the support of $H(f)$ (i.e. only to be considered outside the surface f). Then, since for an impermeable surface $w_i \partial f/\partial x_i = (u_i + v_i)\partial f/\partial x_i$, equation 4.5 can be rewritten,

$$\begin{aligned}\left(\frac{D^2}{Dt^2} - c^2\frac{\partial^2}{\partial x_i^2}\right)\rho' = &\frac{\bar{D}}{Dt}[\rho_0 v_n \delta(f)] && \text{(Thickness)} \\ &- \frac{\bar{\partial}}{\partial x_i}[l_i \delta(f)] && \text{(Loading)} \\ &+ \frac{\partial^2 T_{ij}}{\partial x_i \partial x_j}, && \text{(Quadrupole)}\end{aligned} \tag{4.6}$$

where v_n is the surface normal velocity $v_i \partial f/\partial x_i$ and l_i is the force exerted by the surface on the fluid.

4.3 Thickness noise

The solution of the convected wave equation for thickness noise is found by convolving the source terms in equation 4.6 with the Green's function introduced in equation 3.2,

$$4\pi p'_T = \gamma\left(\frac{\bar{\partial}}{\partial t} + u_i\frac{\bar{\partial}}{\partial x_i}\right)\int_\tau\int_{\mathbf{y}} \frac{\rho_0 v_n \delta(f)}{R'}\delta(g)\, d\mathbf{y}\, d\tau. \tag{4.7}$$

The first integration, over τ, is quite simple and is carried out in the same way as in the point-source problem in the previous chapter,

$$4\pi p'_T = \gamma\left(\frac{\bar{\partial}}{\partial t} + u_i\frac{\bar{\partial}}{\partial x_i}\right)\int_{\mathbf{y}} \frac{\rho_0 v_n \delta(f)}{R' dg/d\tau}\, d\mathbf{y}. \tag{4.8}$$

The integration over the source region, $\mathbf{y}$, is performed using the identity (Farassat [47], equation 3.80, also appendix B)

$$\int_{\mathbf{x}} \phi(\mathbf{x})\delta(f)\, d\mathbf{x} = \int_{f=0} \phi(\mathbf{x})\, dS \tag{4.9}$$

with S the surface defined by $f = 0$. This yields

$$4\pi p'_T(\mathbf{x},t) = \gamma \left(\frac{\partial}{\partial t} + u_i \frac{\partial}{\partial x_i} \right) \int_S \left[\frac{\rho_0 v_n}{R'(1 - \mathbf{M}_s.(\gamma \mathbf{R} - \gamma^2 \mathbf{M}_\infty))} \right] dS \quad (4.10)$$

where $[\cdot]$ indicates evaluation of the function inside the brackets at retarded time τ, S is the blade surface and $\mathbf{M}_s$ is the source velocity in the fixed reference frame, $\mathbf{R} = \partial R'/\partial x_i$,

$$\begin{aligned} \mathbf{R} &= (\mathbf{r} + \gamma^2 (\mathbf{M}_\infty.\mathbf{r})\mathbf{M}_\infty)/R', \\ \mathbf{r} &= \mathbf{x} - \mathbf{y}. \end{aligned} \quad (4.11)$$

The spatial derivative can be expanded to a time derivative and the time derivatives brought under the integral sign to give a formula for thickness noise

$$\begin{aligned} 4\pi p'_T = \gamma \int_S \left[\frac{1}{1 - \mathbf{M}_s.\mathbf{D}} \frac{d}{d\tau} \left(\frac{\rho_0 v_n (1 - \mathbf{M}_\infty.\mathbf{D})}{R'(1 - \mathbf{M}_s.\mathbf{D})} \right) \right] dS \\ -\gamma c \int_S \left[\frac{\rho_0 v_n \mathbf{M}_\infty}{R'(1 - \mathbf{M}_s.\mathbf{D})} \cdot \left(\frac{\mathbf{R}}{R'} - \frac{\gamma}{c} \frac{\dot{\mathbf{R}}}{1 - \mathbf{M}_s.\mathbf{D}} \right) \right] dS, \end{aligned} \quad (4.12)$$

where the 'radiation vector', $\mathbf{D}$, is equal to $\gamma \mathbf{R} - \gamma^2 \mathbf{M}_\infty$.

4.4 Loading noise

The solution of the loading noise equation is

$$4\pi p'_L = -\gamma \frac{\bar{\partial}}{\partial x_i} \int_\tau \int_{\mathbf{y}} \left[\frac{\delta(g)}{R'} l_i \delta(f) \right] d\mathbf{y}\, d\tau. \quad (4.13)$$

where l_i is the ith component of the force per unit area on the fluid. This can be manipulated in the same way as the thickness noise equation above to give

$$4\pi p'_L = -\gamma \frac{\partial}{\partial x_i} \int_S \left[\frac{l_i}{R'(1 - \mathbf{M}_s.(\gamma \mathbf{R} - \gamma^2 \mathbf{M}_\infty))} \right] dS. \quad (4.14)$$

Then, expanding the spatial derivative, this becomes

$$\begin{aligned} 4\pi p'_L = \frac{\gamma}{c} \int_S \left[\frac{1}{1 - \mathbf{M}_s.\mathbf{D}} \frac{d}{d\tau} \left(\frac{\mathbf{l}.\mathbf{D}}{R'(1 - \mathbf{M}_s.\mathbf{D})} \right) \right] dS \\ +\gamma \int_S \left[\frac{\mathbf{l}}{R'(1 - \mathbf{M}_s.\mathbf{D})} . \left(\frac{\mathbf{R}}{R'} - \frac{\gamma}{c} \frac{\dot{\mathbf{R}}}{1 - \mathbf{M}_s.\mathbf{D}} \right) \right] dS. \end{aligned} \quad (4.15)$$

This formulation can be considered to complete table 2.1, the matrix of time-domain methods,

	Moving observer	Moving fluid
Subsonic body only	Farassat 1A [22]	Equations **4.12**, **4.15**
Supersonic bodies	Farassat 3 [41]	Wells & Han [39]

Table 4.1: Updated matrix of time-domain noise prediction techniques

4.5 Computational considerations

It is worth briefly noting the advantage of developing the equations 4.15 and 4.12 for an arbitrary inflow vector $\mathbf{M}_\infty$. If only axial inflow cases were considered it would still be possible to calculate the noise from a propeller at incidence by notionally tilting the propeller to introduce an angle of attack. In principle, this is no more difficult than the simple axial inflow case, but in practice it requires transformations of the type given by Hanson and Parzych [45]. While these transformations can easily be coded for computation, they are quite time consuming and can add substantially to the calculation of retarded time, the largest part of the noise calculation.

A neater way of doing these calculations is to fix the propeller in a vertical plane and 'tilt' the inflow and the observer position to set up an angle of attack. Then no transformations are needed in calculating the blade position and there is a saving in computational time. The chance of an error being introduced in the trigonometric formulae used for the transformations is also reduced.

Finally, it should also be borne in mind that equations 4.12 and 4.15 are practically identical in form. The differences are in the source terms and in the factors leading each integral. This means that there is very little extra computational work involved in calculating the predicted sound once the retarded time calculations have been carried out especially as many of the quantities involved (R' and $\mathbf{M}_s$, for example) are calculated during the retarded time calculation anyway. Recognising this, equations 4.12 and 4.15 could be combined in a form which would be more efficient for noise prediction,

$$4\pi p' = \frac{\gamma}{c}\int_S \left[\frac{1}{1-\mathbf{M}_s.\mathbf{D}}\frac{d}{d\tau}\left(\frac{\rho_0 c v_n + (\mathbf{l}-\rho_0 c v_n \mathbf{M}_\infty).\mathbf{D}}{R'(1-\mathbf{M}_s.\mathbf{D})}\right)\right] dS$$
$$+\gamma\int_S \left[\frac{\mathbf{l}-\rho_0 c v_n \mathbf{M}_\infty}{1-\mathbf{M}_s.\mathbf{D}}.\left(\frac{\mathbf{R}}{R'}-\frac{\gamma}{c}\frac{\dot{\mathbf{R}}}{1-\mathbf{M}_s.\mathbf{D}}\right)\right] dS. \qquad (4.16)$$

In the next chapter, numerical predictions of the noise from a propeller operating under various conditions are compared to experimental results.

Chapter 5

Experimental validation

But before you base a law on this case test it two or three times and see whether the tests produce the same effects.

Leonardo da Vinci

The final stage of noise prediction was the implementation of the formulation of chapter 4 in a numerical code and the comparison of noise predictions generated by that code to measured data. This raised the issue of determining the strength of the thickness and loading source terms. The thickness noise component presented no special difficulties as its source strength can be determined directly from known characteristics of the blade and fluid motion. The loading noise, being dependent on the blade surface pressure, was a more difficult problem.

In comparing the loading noise predicted by the theory presented in chapter 4 with the results from experiment, it was decided to use measured blade surface pressures rather than those predicted by a CFD code. There were two reasons,

- it was felt that experimentally measured surface pressures would be more reliable as they would be taken from tests conducted under known conditions rather than using nominal parameters.
- both steady and fluctuating blade surface pressures were available, allowing for the possibility of using a 'full' model for angle of attack calculations. No numerical predictions of unsteady pressure were available.

5.1 Experimental data

Between February and September, 1995, acoustic and aerodynamic tests were conducted in the transonic wind-tunnel of the Aircraft Research Association, Bedford, England and in the DNW low speed wind-tunnel at Emmeloord in the Netherlands. Two six-bladed propellers were tested. The first, low

speed, propeller (LSP) was of conventional design while the second, high speed, propeller (HSP) used an advanced, wide-chord blade. At the time of writing, low-speed, far-field data were not available for the HSP so that only LSP results are presented for those conditions.

Appendix D contains details of the test conditions (rotation speed, inflow Mach number and angle of attack) and microphone positions for the LSP and HSP at ARA and for the LSP at DNW. Details of the propellers and of their instrumentation are given in appendix E.

5.2 Methodology

The method adopted in generating the pressure distribution was to interpolate from the measured pressures onto a blade mesh which had been used for CFD calculations. This proceeded in two stages. First, the pressure distribution around each blade section containing pressure tappings was evaluated using linear interpolation between tapping positions. Then these chordwise pressure distributions were linearly interpolated onto the blade mesh. Linear interpolation was used on the grounds that any more sophisticated interpolation technique would mean making extra assumptions about the nature of the pressure distribution and would introduce the possibility of errors due to the interpolation scheme. In effect, it was assumed that the aerodynamic measurement points were closely enough spaced to make linear interpolation accurate.

5.2.1 Steady pressure distribution

The calculation of the steady pressure distribution was a problem of estimating the pressure at the nodes of the blade surface mesh, based on the known pressures at the pressure tapping positions. The first stage was to estimate a pressure distribution around each section containing a set of pressure tappings as shown in figure 5.1.

This yielded data for a number of sections, with a complete interpolated pressure distribution for each of them. The final step was to interpolate between these sections onto the sections of the CFD mesh to estimate a pressure distribution for the whole blade. This was quite straightforward except near the blade root and at the tip, past the outboard tappings. At the blade root, the condition that the gauge pressure be zero was imposed. In the case of the tip, the surface pressure was held constant from the last known pressure outwards. It is known from the work of Parry and Crighton [49] that the noise from a propeller depends very strongly on the gradient of the blade loading near the tip, so that assuming a constant pressure near the tip should underestimate the noise generated. Finally, for the DNW tests, the blade gauge pressures were scaled to give the same propeller thrust as that measured in the wind-tunnel tests. This was not found necessary for the ARA data.

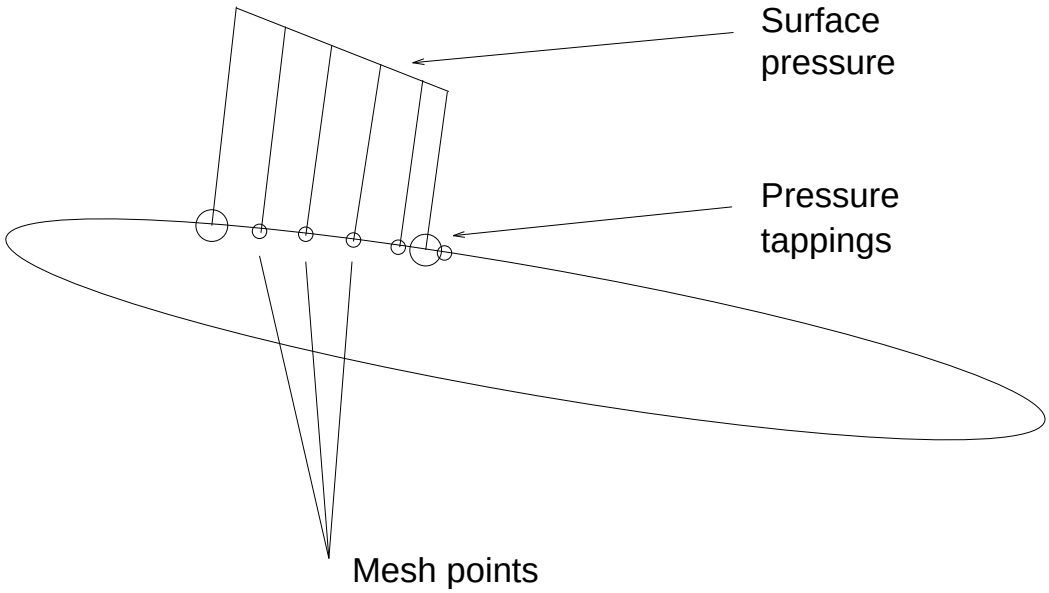

Figure 5.1: Interpolation of section pressure distribution

5.2.2 Unsteady pressure distribution

As it is practically impossible, on both technical and financial grounds, to populate a blade as densely with unsteady pressure transducers as with static pressure tappings, the unsteady pressure data were somewhat sparser. As transducers were placed especially densely at one blade section, it was decided to assume that that section was representative of the blade as a whole and, in particular, that the ratio of unsteady to steady pressure was the same at all sections so that the unsteady pressure at other sections could be determined by simple scaling. The unsteady pressure was input to the numerical code in the form of coefficients of a Fourier series (amplitude and phase). These coefficients were determined by averaging the measured waveform to calculate a "single-revolution" unsteady pressure and then extracting the Fourier coefficients from that time record. The sampled records were synchronised using the once-per-revolution pulse from the propeller.

5.2.3 Numerical implementation

The essential features of the implementation of the formulation derived in chapter 4 (the numerical calculation of the acoustic integrals and the interpolation of the surface pressure distribution) are described in appendix C.

As mentioned above the unsteady loading is specified in the frequency domain for numerical accuracy. As the time derivatives of the loading are required, it seemed better to use unsteady loading data in a form where numerical differentiation would not be required. Also, in most cases, the frequency domain information is much more compact than the corresponding

time record. For the results presented here five components of the blade unsteady loading were used, at multiples of the propeller rotation frequency, although the code is not limited to periodic variations in loading.

To find the observer time record, the observer time is stepped over the required range. At each time point, the retarded time for each node on the blade mesh is calculated using the Newton-Raphson method, [50], to solve equation 3.5 for $g = 0$. The various kinematic factors and source strengths required at each node are then calculated and stored. Storing all these data is somewhat wasteful of memory but is done to allow them to be written to a file and examined later, for example as in figure 5.34. The acoustic pressure at the observer time is then found by integrating equations 4.12 and 4.15 over the blade surface. Integration is performed assuming a linear variation of quantities between mesh nodes (see §C.1.2).

The results from the calculations are output separately for each of the four integrals of equations 4.12 and 4.15, first the single blade signal and then the superposed whole-propeller record.

5.3 High speed, near-field results

In the results plotted here, and in the low speed case, the axial coordinate is positive in the upstream direction, i.e. the flow is from right to left across the directivity plots. In each case where experimental data are plotted, only data points which could be clearly distinguished as harmonics of the propeller noise signal are plotted.

5.3.1 Low speed propeller

Near field results for the low speed propeller are presented at the end of this section. Table 5.1 lists the axial inflow cases by advance ratio and inflow Mach number. It is worth bearing in mind that at constant advance ratio, tip Mach number is linearly proportional to inflow Mach number.

J	$M_\infty = 0.6$	$M_\infty = 0.65$	$M_\infty = 0.7$
3.238	5.2	5.3	5.4
3.597	5.5	5.6	5.7
4.625	5.8	5.9	5.10

Table 5.1: Low speed propeller, near field axial inflow figures

The tests conducted for $J = 3.238$ and $J = 3.597$ were for a blade pitch of 54.9°. The $J = 4.625$ test was carried out at a pitch setting of 61.8°. Only steady pressure measurements were used in the interpolated blade loading for these tests.

The first set of tests for a blade pitch setting of 54.9°, an advance ratio of 3.238 and inflow Mach numbers 0.60, 0.65 and 0.7 (figures 5.2, 5.3 and 5.4 respectively) have plenty of data points available for comparison. In each case the directivity is in error with the peak in the predicted directivity being downstream of the experimentally measured maximum. In the lowest speed case, figure 5.2, the maximum value of the first harmonic is quite accurately predicted but this is the best match in these plots. In figures 5.3 and 5.4, where the blade tip Mach numbers are greater than 0.9, the predictions are not as accurate. The tip Mach number of 0.9 is significant as it can be taken as the beginning of the range where non-linear sources are important (see Magliozzi et. al. [16] and §5.6.2).

The next three sets of data were taken under the same conditions as those described in the previous paragraph but at an advance ratio of 3.597 (i.e. at a lower rotational speed). Here there are not as many experimental data points available (the propeller was simply not as noisy at the lower speeds) and the numerical predictions are not as good. In the 0.6 and 0.65 inflow Mach number cases, it overpredicts the maximum sound pressure level and in all three cases the directivity prediction is quite poor, having features not seen in the experimental results.

Figures 5.8 to 5.10 show results and predictions for the propeller at a blade pitch of 61.8°, an advance ratio of 4.625 and inflow Mach numbers of 0.6, 0.65 and 0.7. The same trends are evident here as in the previous results; the lowest inflow Mach number case has the best agreement with experimental results and that agreement worsens at higher blade tip speeds. There is an error in the directivity in each case (the position of the maximum is incorrect) but the absolute value of the peak SPL compares well with the experimental result in the higher Mach number cases.

The angle of attack effect is shown in figures 5.11 to 5.14 for an advance ratio of 4.047, an inflow Mach number of 0.7 and a blade pitch setting of 61.8° as before. In the case of the 0° angle of attack the predicted first harmonic is a very good match with experiment and agrees much better than in the $J = 4.625$ case shown before. This may be due to the inclusion of estimated unsteady loading or simply because the propeller makes more noise at lower advance ratios. In the 3° case the match is not as good but the general shape of the directivity curve has been captured quite well. Figure 5.14 shows a comparison of a time averaged waveform for one revolution of the propeller and a prediction of that signal for both angles of attack. As might be expected from the spectral data the 0° case matches quite well in both the amplitude and position of the peaks in the signal. In the 3° case the agreement is also quite good for the position of the peaks but the amplitudes are underpredicted.

Finally figure 5.15 summarises some of the data and shows the experimental and predicted variation in the propeller-plane first harmonic as a function of inflow Mach number.

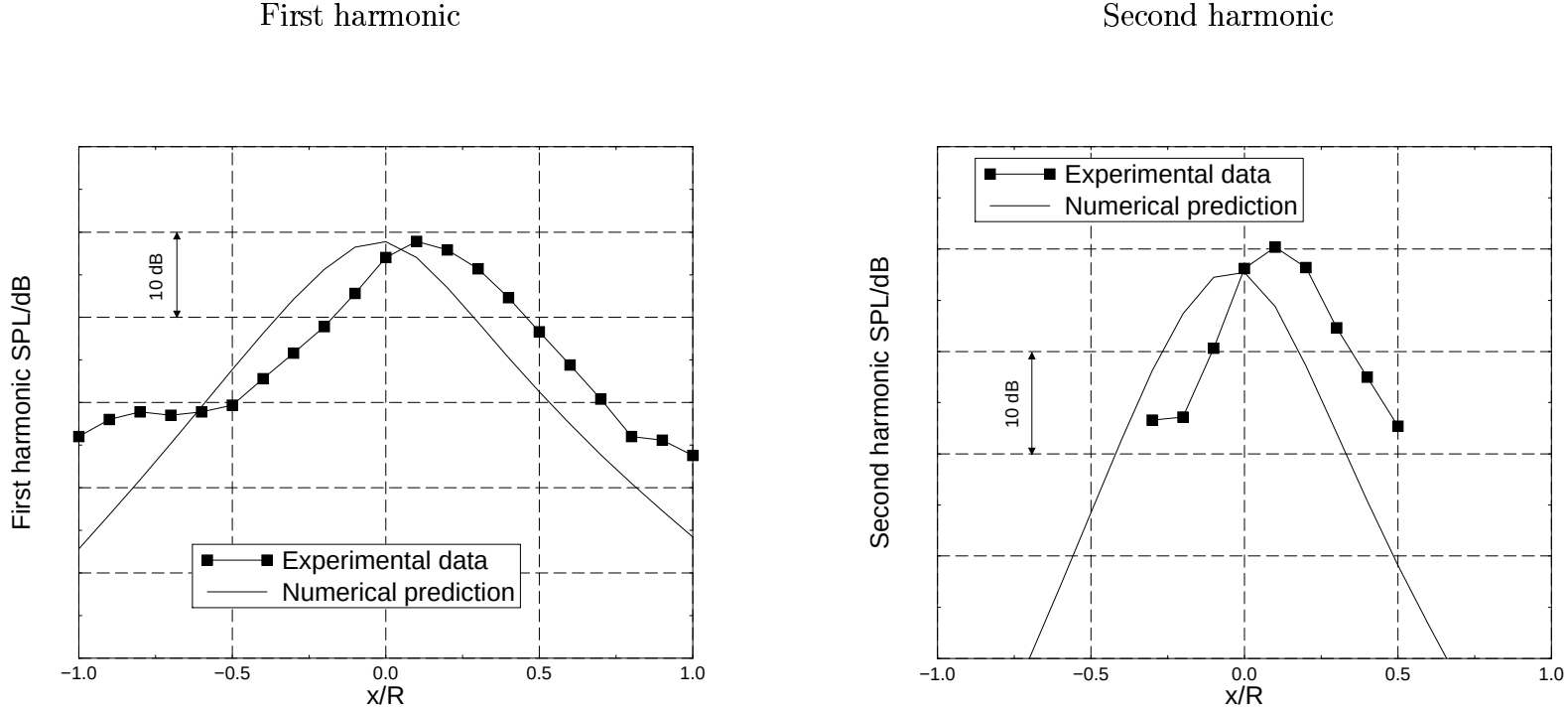

Figure 5.2: Low speed propeller, near-field axial directivity, $\beta = 54.9°$, $J = 3.238$, $M_\infty = 0.6$, $M_t = 0.84$

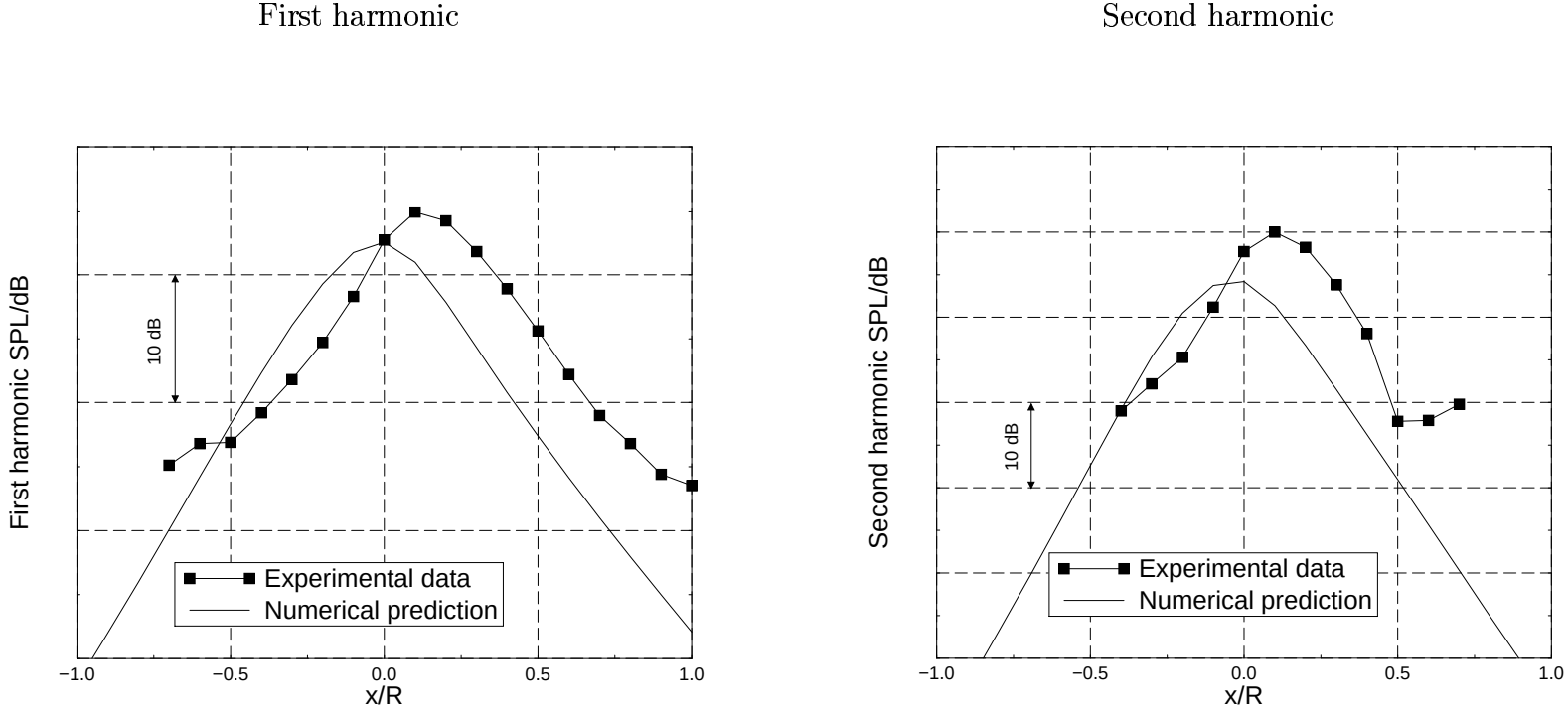

Figure 5.3: Low speed propeller, near-field axial directivity, $\beta = 54.9°$, $J = 3.238$, $M_\infty = 0.65$, $M_t = 0.91$

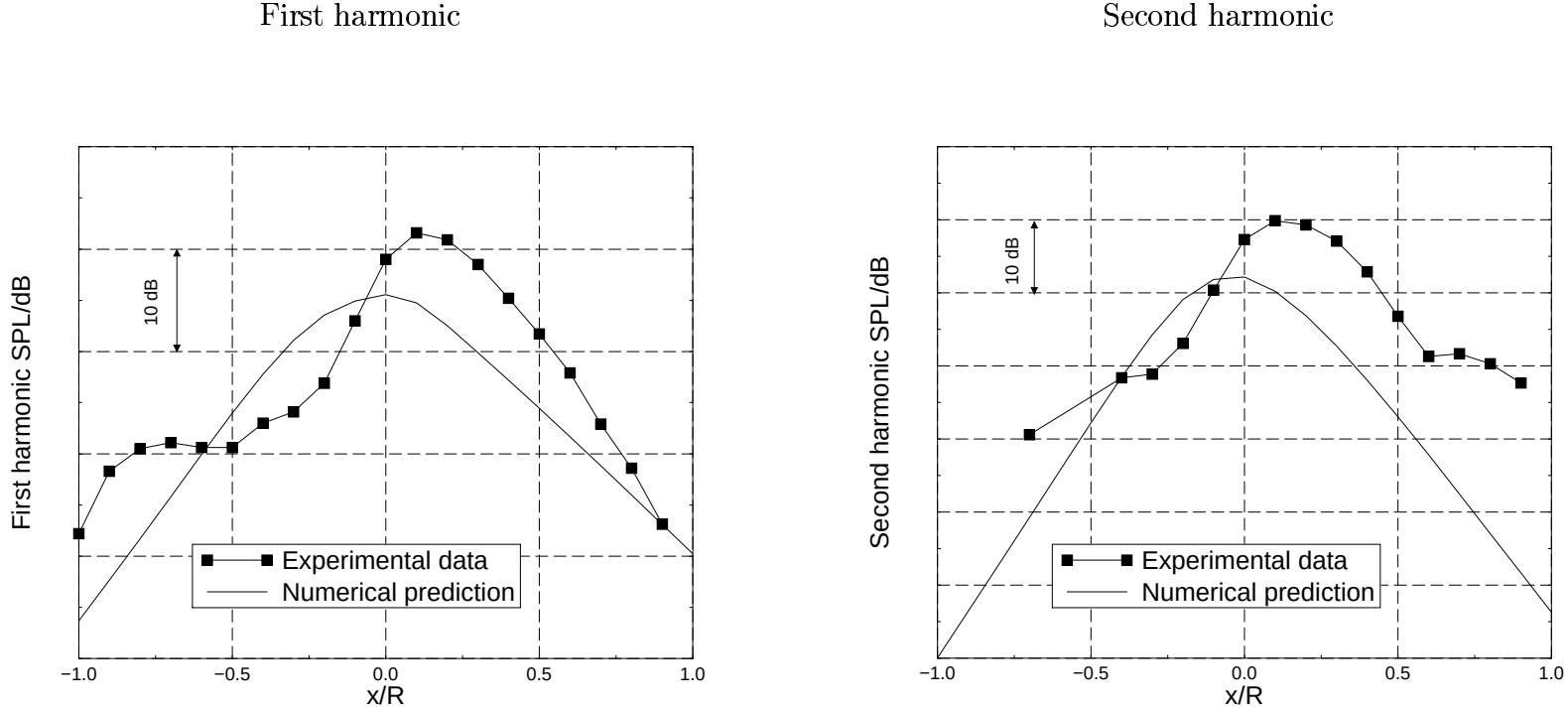

Figure 5.4: Low speed propeller, near-field axial directivity, $\beta = 54.9°$, $J = 3.238$, $M_\infty = 0.70$, $M_t = 0.98$

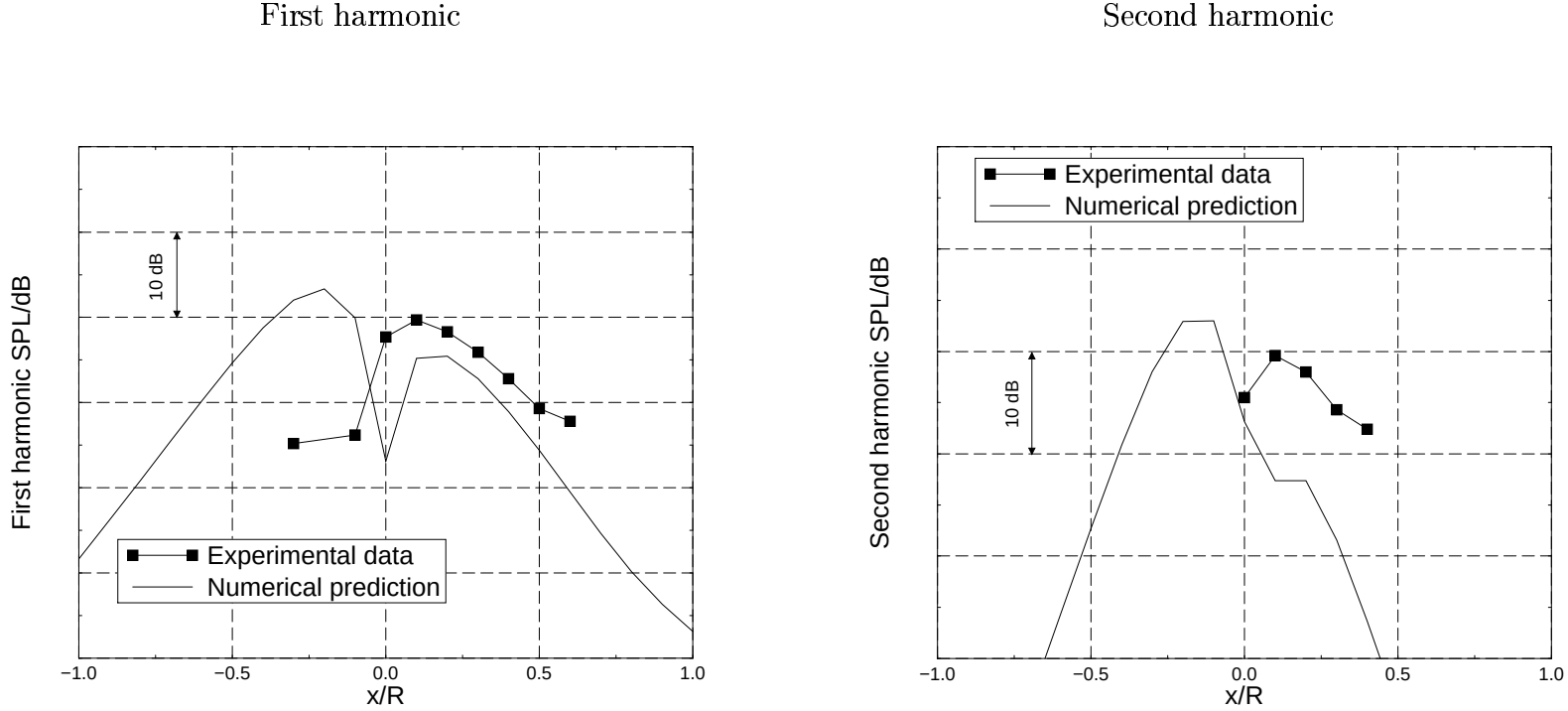

Figure 5.5: Low speed propeller, near-field axial directivity, $\beta = 54.9°$, $J = 3.597$, $M_\infty = 0.60$, $M_t = 0.8$

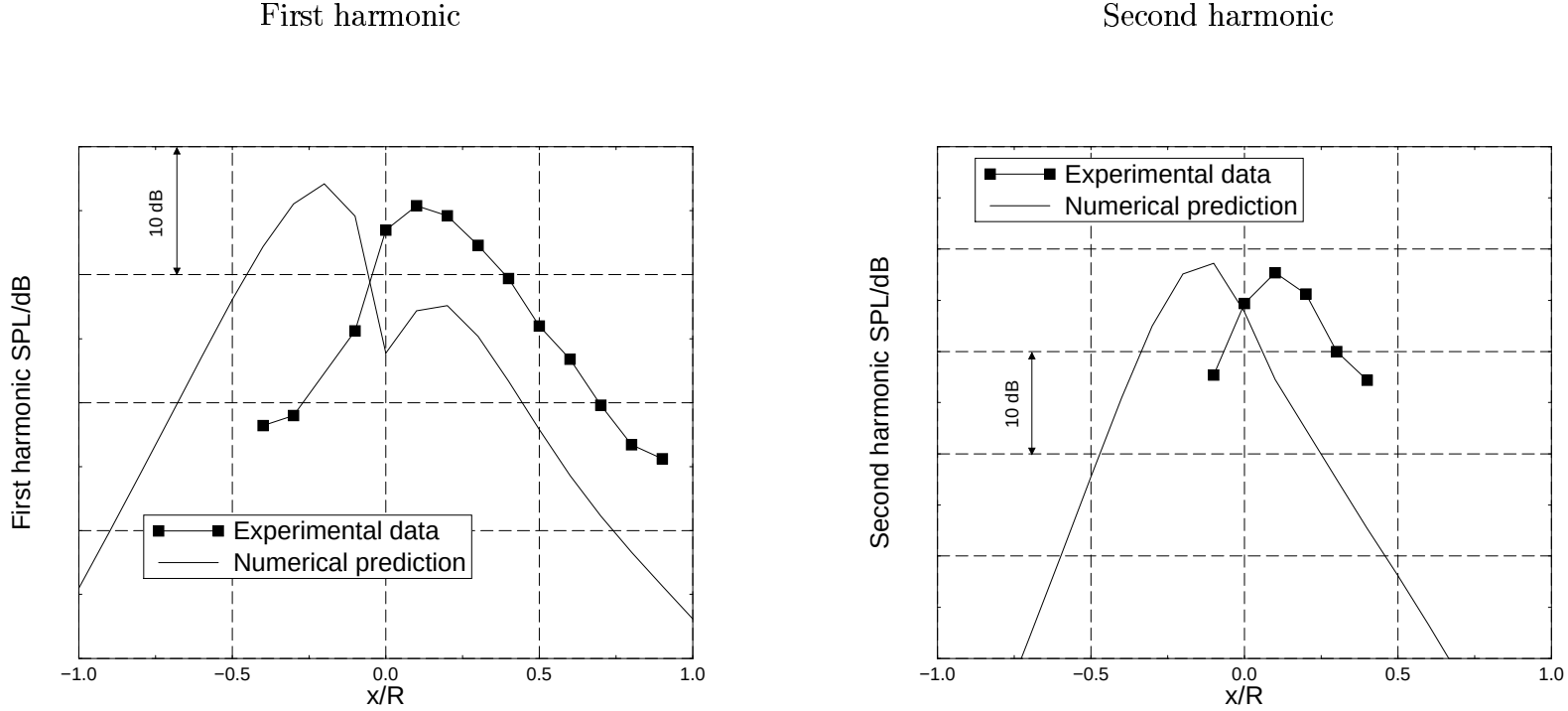

Figure 5.6: Low speed propeller, near-field axial directivity, $\beta = 54.9°$, $J = 3.597$, $M_\infty = 0.65$, $M_t = 0.86$

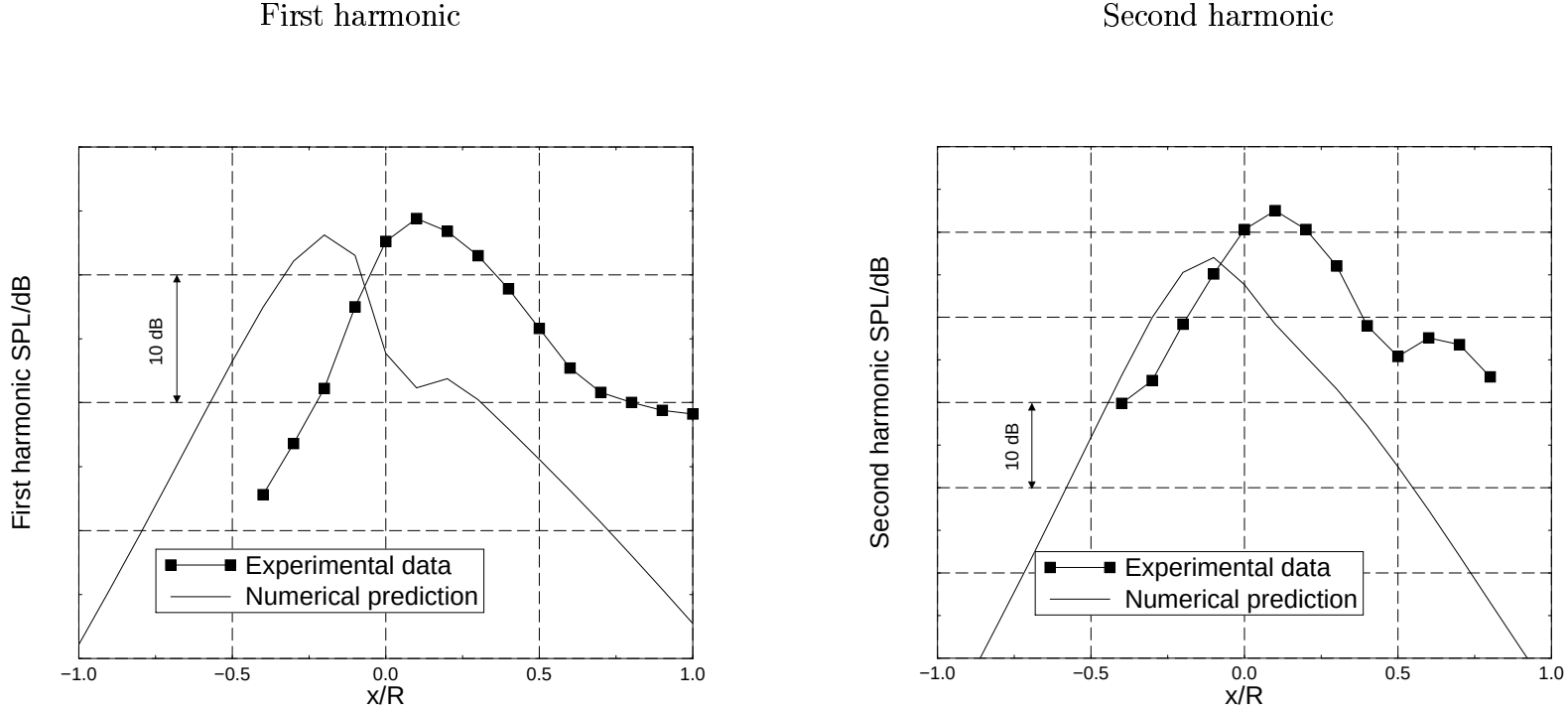

Figure 5.7: Low speed propeller, near-field axial directivity, $\beta = 54.9°$, $J = 3.597$, $M_\infty = 0.70$, $M_t = 0.93$

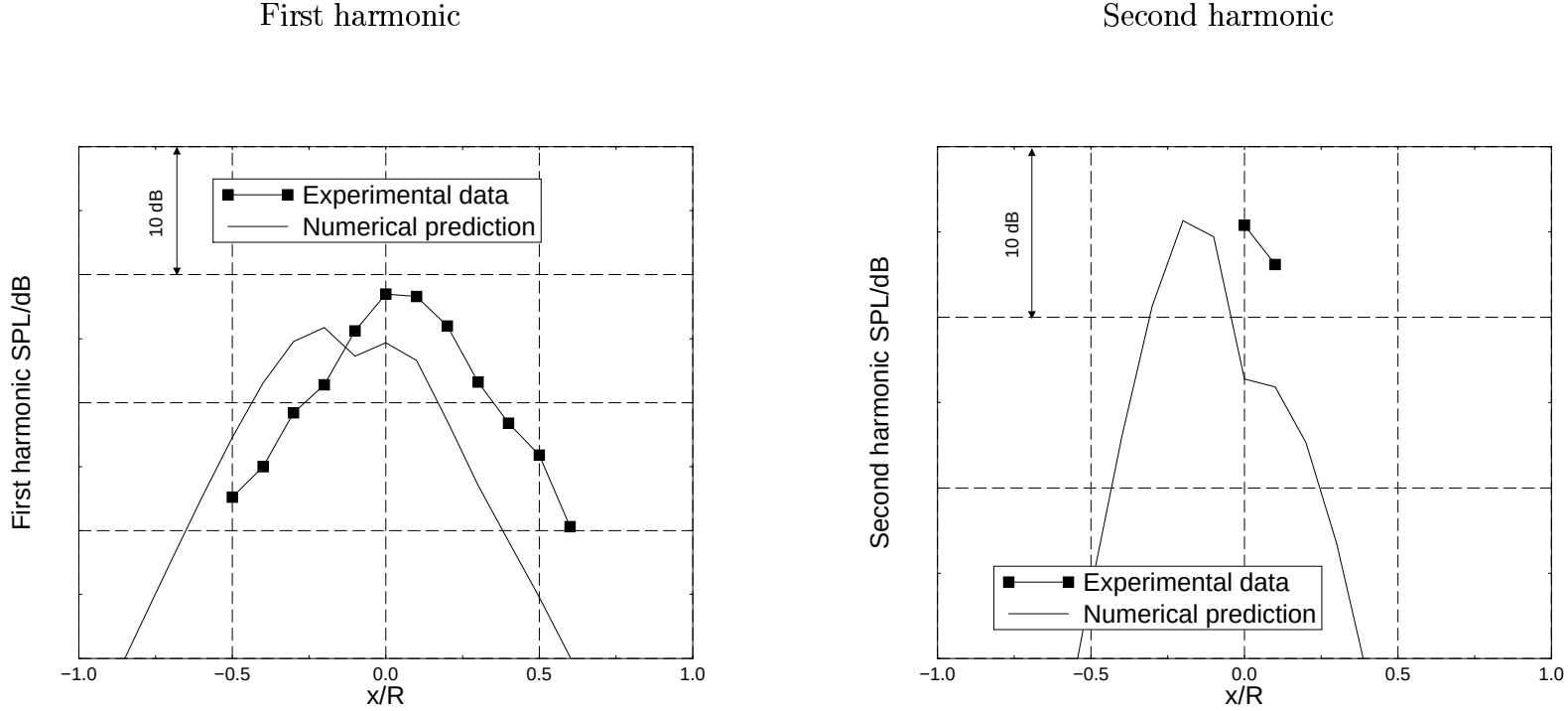

Figure 5.8: Low speed propeller, near-field axial directivity, $\beta = 61.8°$, $J = 4.625$, $M_\infty = 0.60$, $M_t = 0.73$

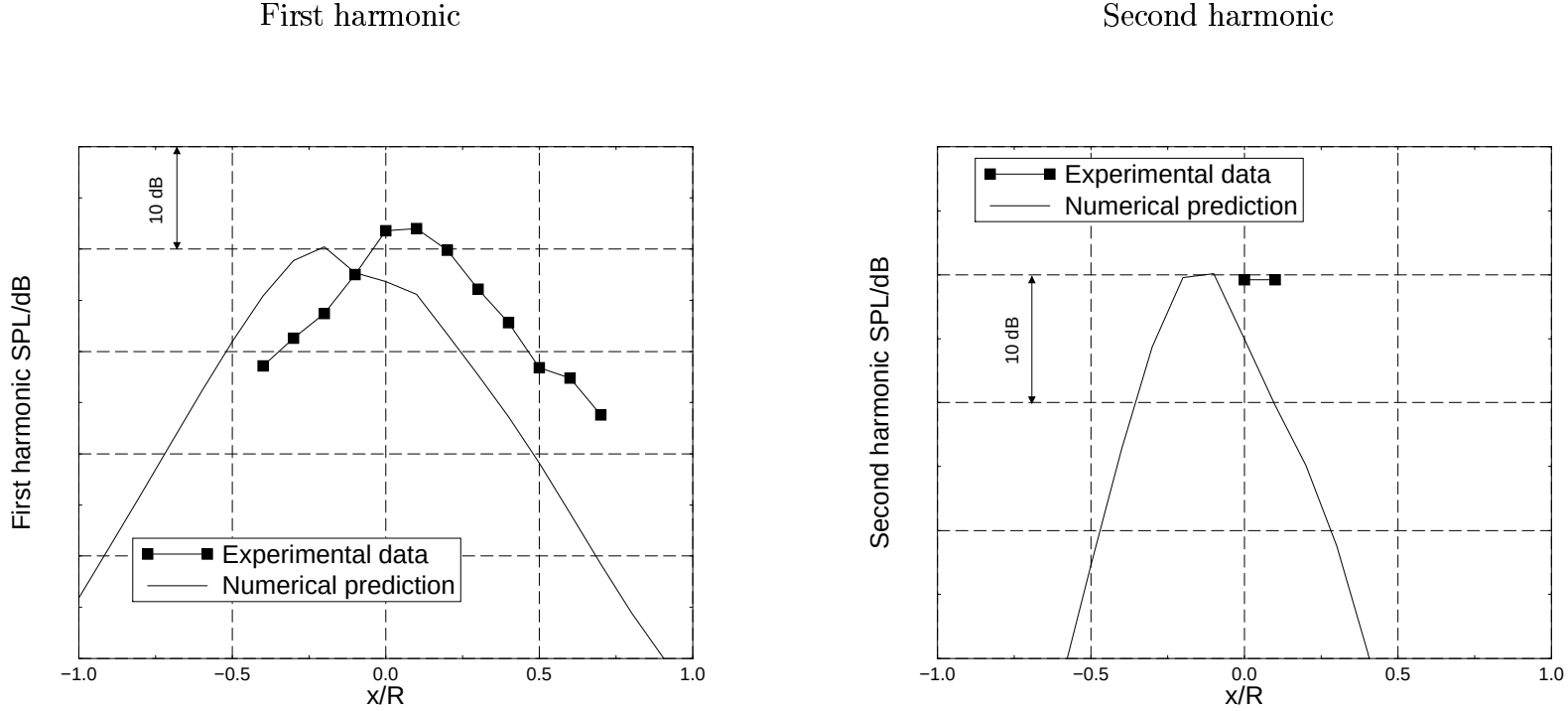

Figure 5.9: Low speed propeller, near-field axial directivity, $\beta = 61.8°$, $J = 4.625$, $M_\infty = 0.65$, $M_t = 0.79$

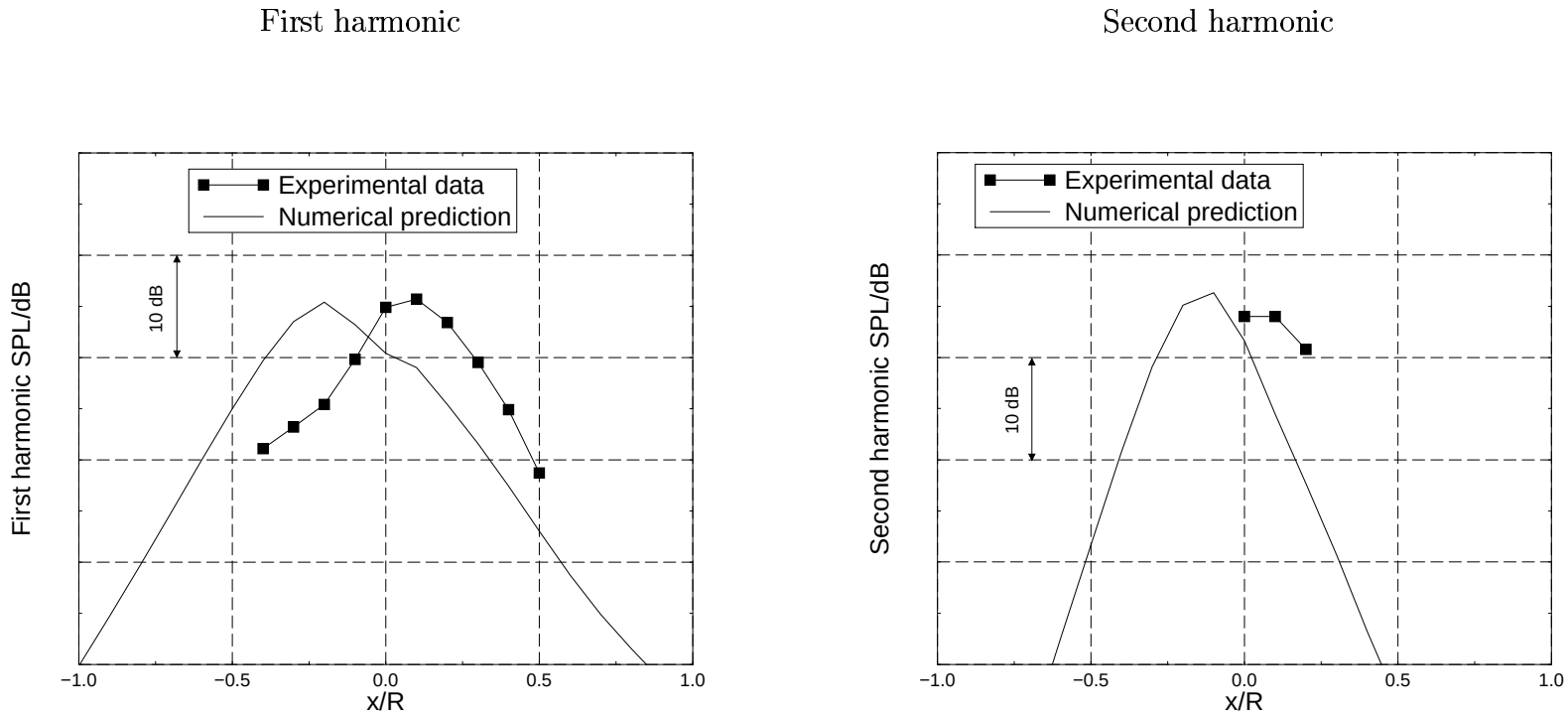

Figure 5.10: Low speed propeller, near-field axial directivity, $\beta = 61.8°$, $J = 4.625$, $M_\infty = 0.70$, $M_t = 0.85$

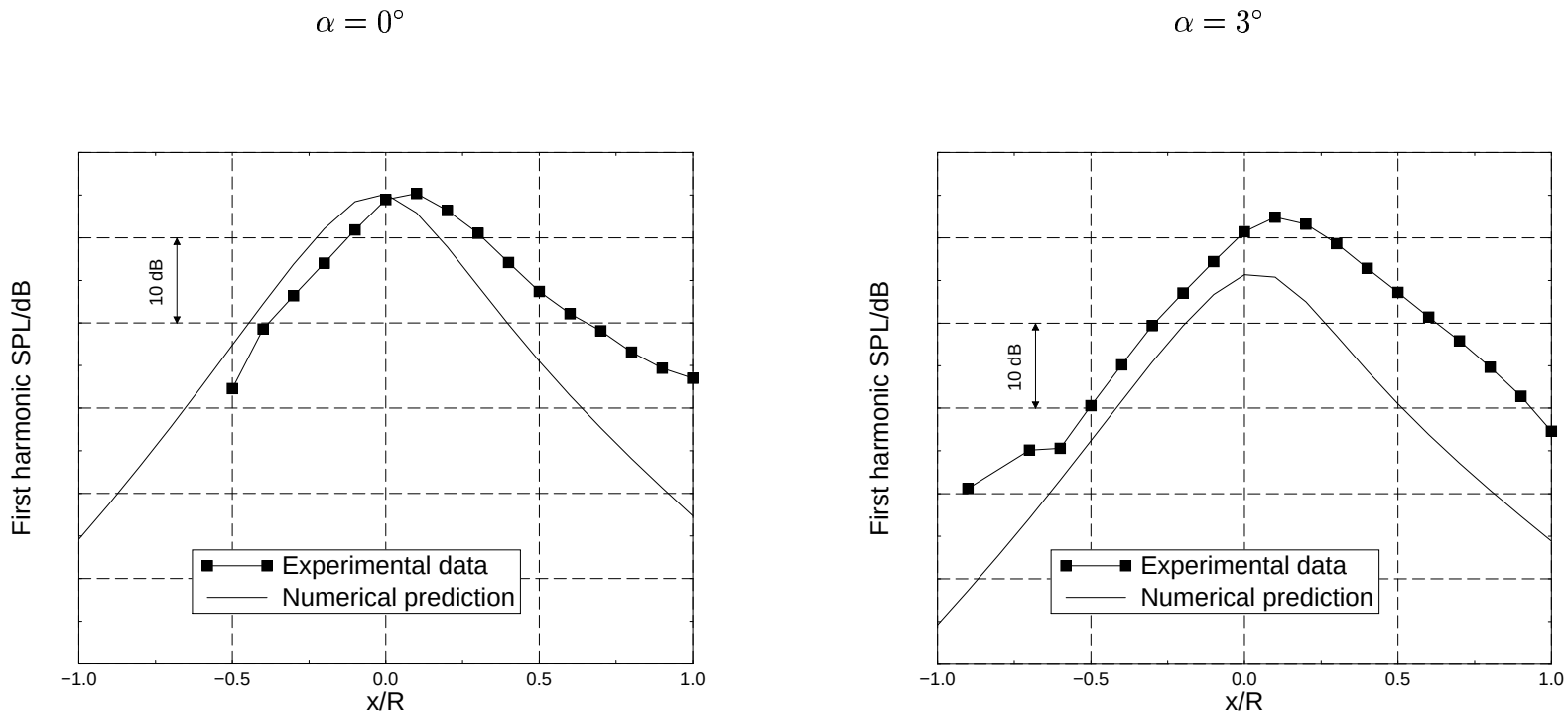

Figure 5.11: Low speed propeller, $\beta = 61.8°$, first harmonic near-field axial directivity, $M_\infty = 0.7$, $J = 4.047$, $M_t = 0.88$, angle of attack effect

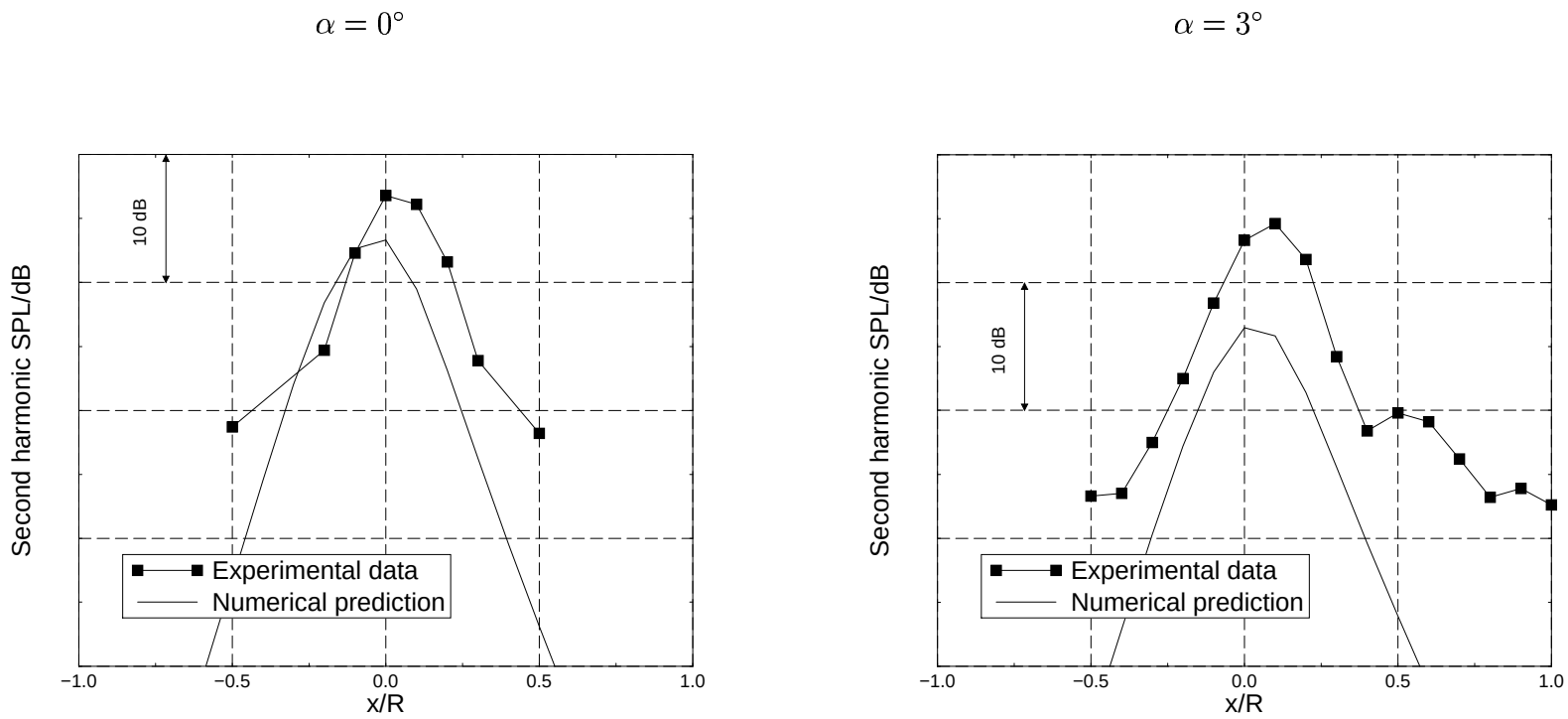

Figure 5.12: Low speed propeller, $\beta = 61.8°$, second harmonic near-field axial directivity, $M_\infty = 0.7$, $J = 4.047$, $M_t = 0.88$, angle of attack effect

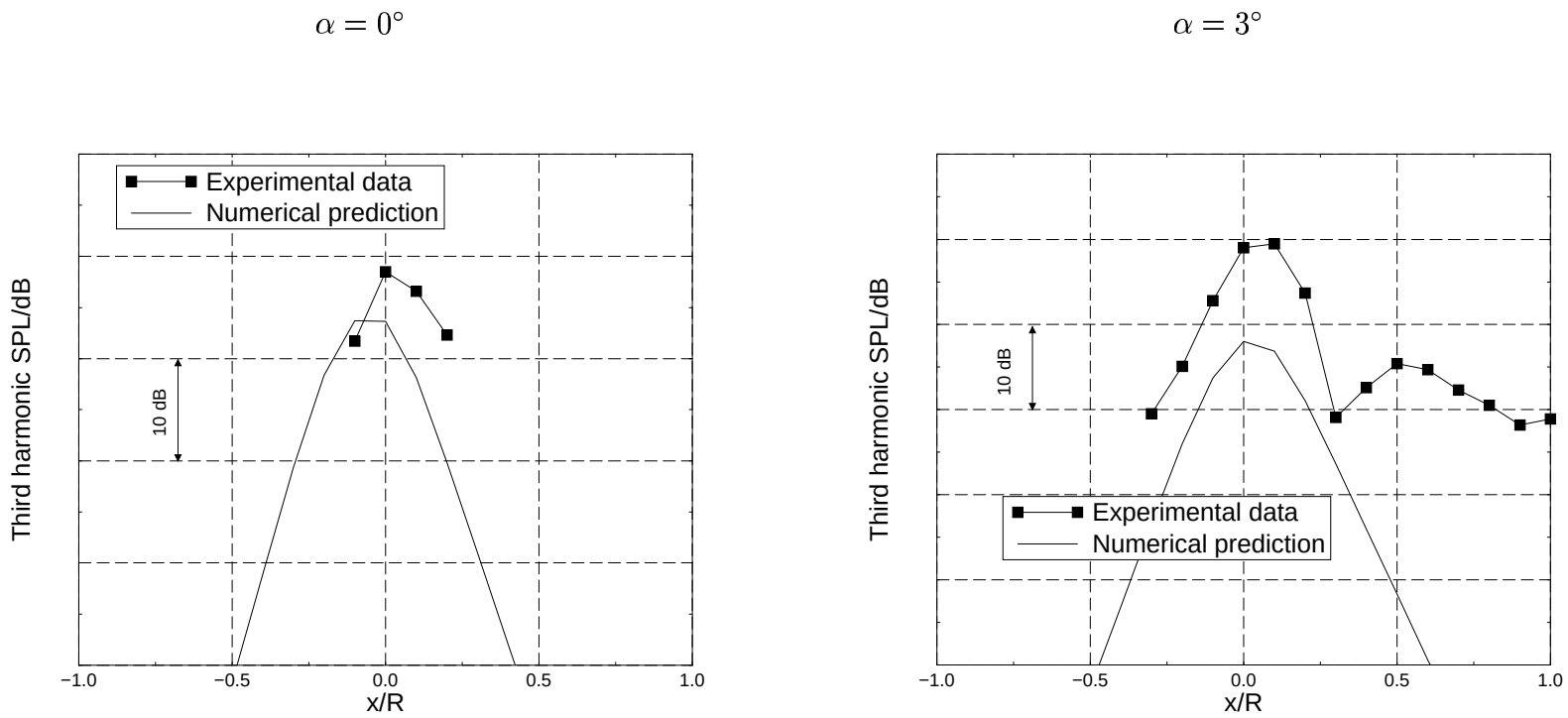

Figure 5.13: Low speed propeller, $\beta = 61.8°$, third harmonic near-field axial directivity, $M_\infty = 0.7$, $J = 4.047$, $M_t = 0.88$, angle of attack effect

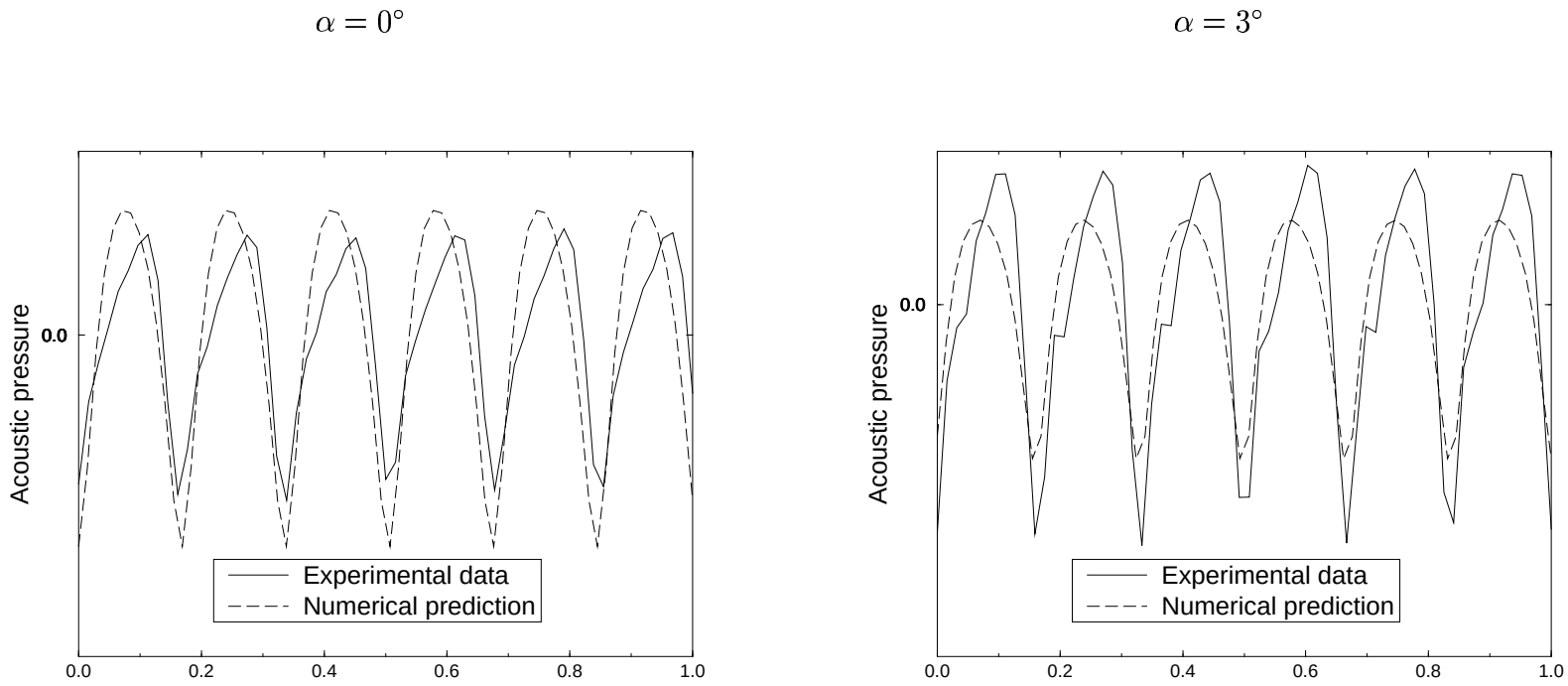

Figure 5.14: Low speed propeller, $\beta = 61.8°$, near-field time records, $M_\infty = 0.7$, $J = 4.047$, $M_t = 0.88$, in-plane, r/R=1.22, angle of attack effect

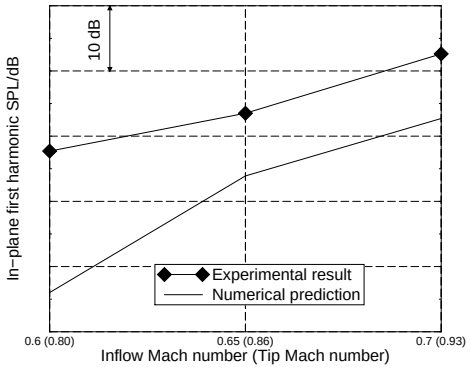

$\beta = 54.9°,\ J = 3.597$

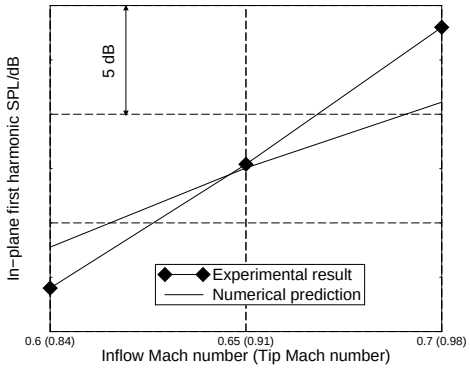

$\beta = 54.9°,\ J = 3.238$

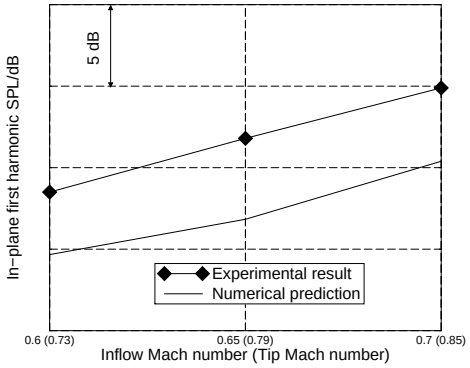

$\beta = 61.8°,\ J = 4.625$

Figure 5.15: Low speed propeller, near field acoustic trends

5.3.2 High speed propeller

For the high speed propeller, two sets of graphs are presented. The first, figures 5.16–5.18, show results over a range of high subsonic tip Mach numbers, while figures 5.19–5.21 show results for a range of supersonic tip Mach numbers. Both tests were conducted in an axial inflow. Figure 5.22 summarises the predicted and measured acoustic trends.

Figures 5.16 to 5.18 show results for a propeller speed of 4200 rpm, a blade pitch setting of 61.1° and inflow Mach numbers of 0.74, 0.76 and 0.78. The agreement of predicted and experimental results, especially for the first harmonic, is surprisingly good in the light of the low speed propeller data presented in §5.3.1. Even for the highest speed case, figure 5.18, where the blade tip Mach number is 0.99, the in-plane prediction matches the experimental result very well.

The next set of results, figures 5.19 to 5.21, were taken at a propeller speed of 5123 rpm with the blade tip Mach number greater than unity in each case. Even under these extreme conditions, the theory has held up well with one serious deviation, the spike in figure 5.21.

Finally, a set of time domain comparisons are shown for two propeller speeds (4200rpm and 5123rpm) and inflow Mach numbers ranging from 0.74 to 0.78 in figures 5.23 to 5.25.

Possible reasons for the good agreement of experiment and theory in these high speed cases are discussed in §5.3.3, as is the sharp spike in the directivity plot in figure 5.21.

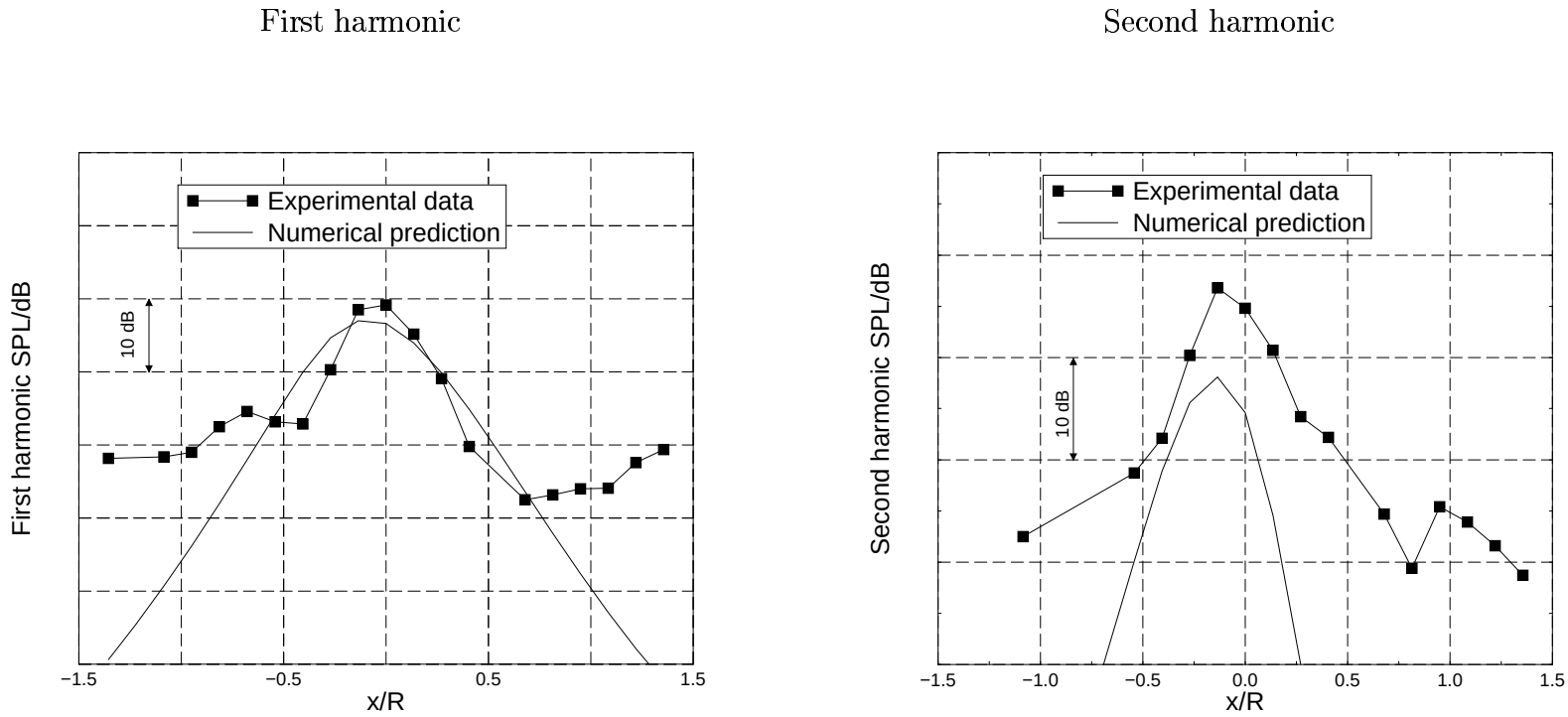

Figure 5.16: High speed propeller, near-field axial directivity, $\beta = 61.1°$, $N = 4200$rpm, $M_\infty = 0.74$, $M_t = 0.96$

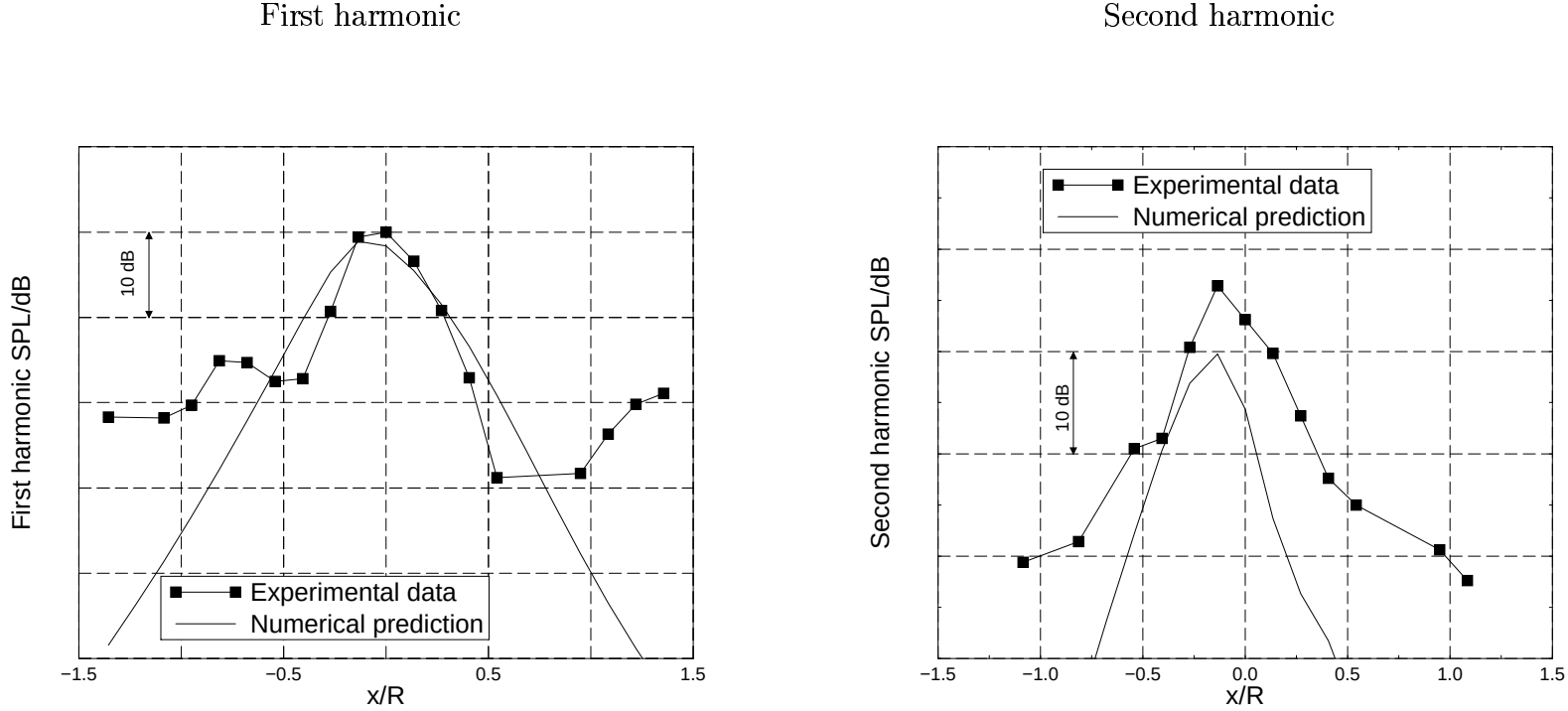

Figure 5.17: High speed propeller, near-field axial directivity, $\beta = 61.1°$, $N = 4200$rpm, $M_\infty = 0.76$, $M_t = 0.97$

First harmonic

Second harmonic

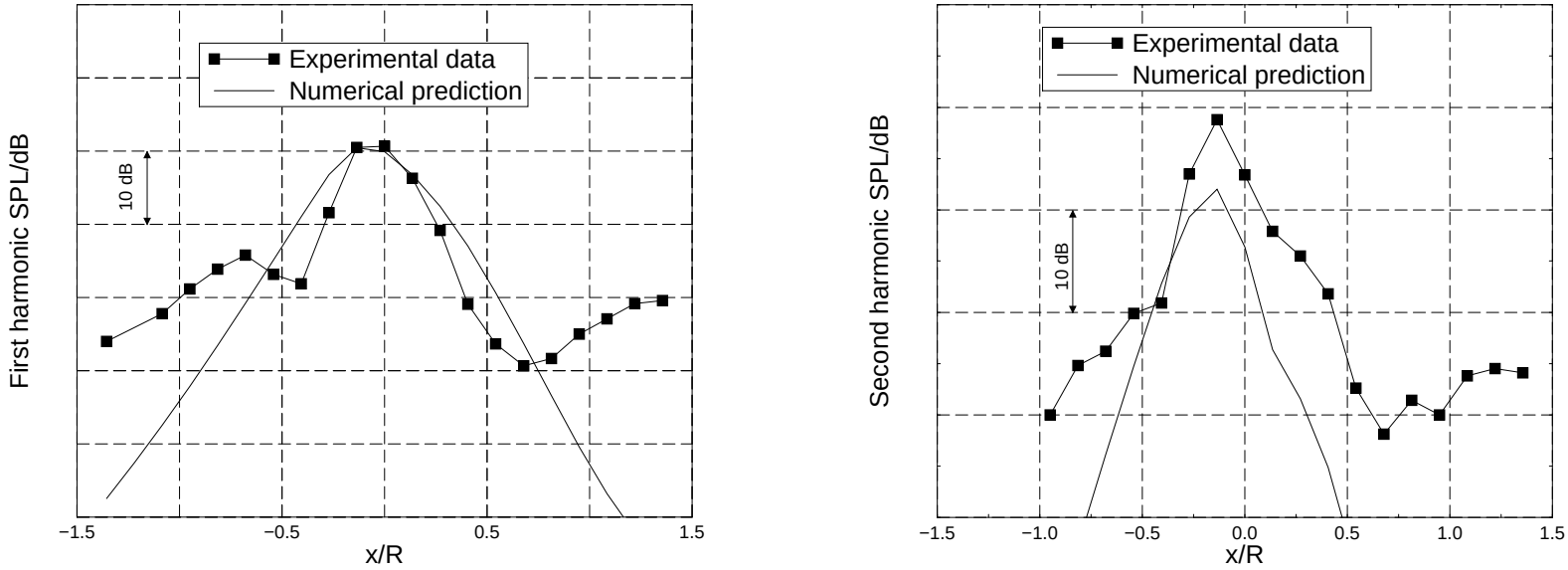

Figure 5.18: High speed propeller, near-field axial directivity, $\beta = 61.1°$, $N = 4200$rpm, $M_\infty = 0.78$, $M_t = 0.99$

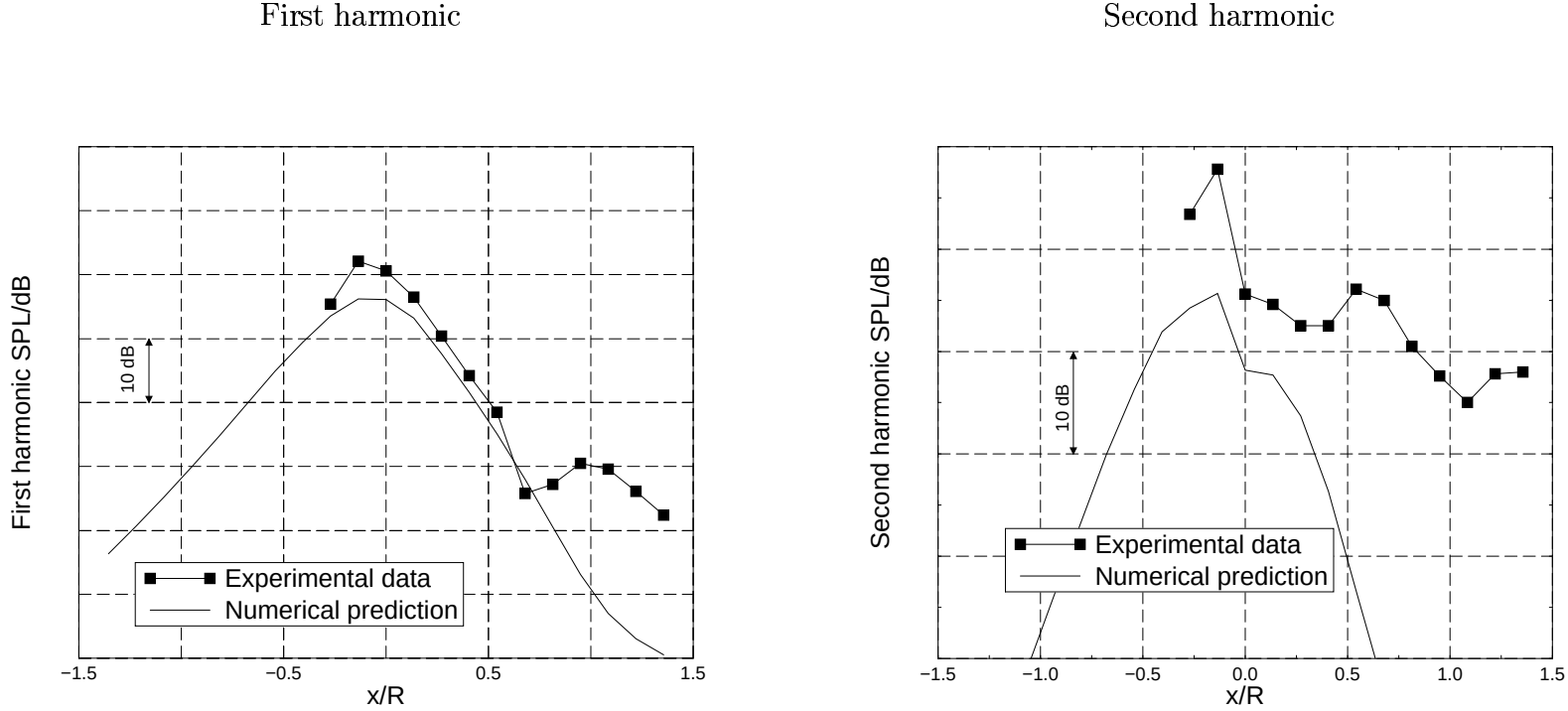

Figure 5.19: High speed propeller, near-field axial directivity, $\beta = 61.1°$, $N = 5123$rpm, $M_\infty = 0.74$, $M_t = 1.05$

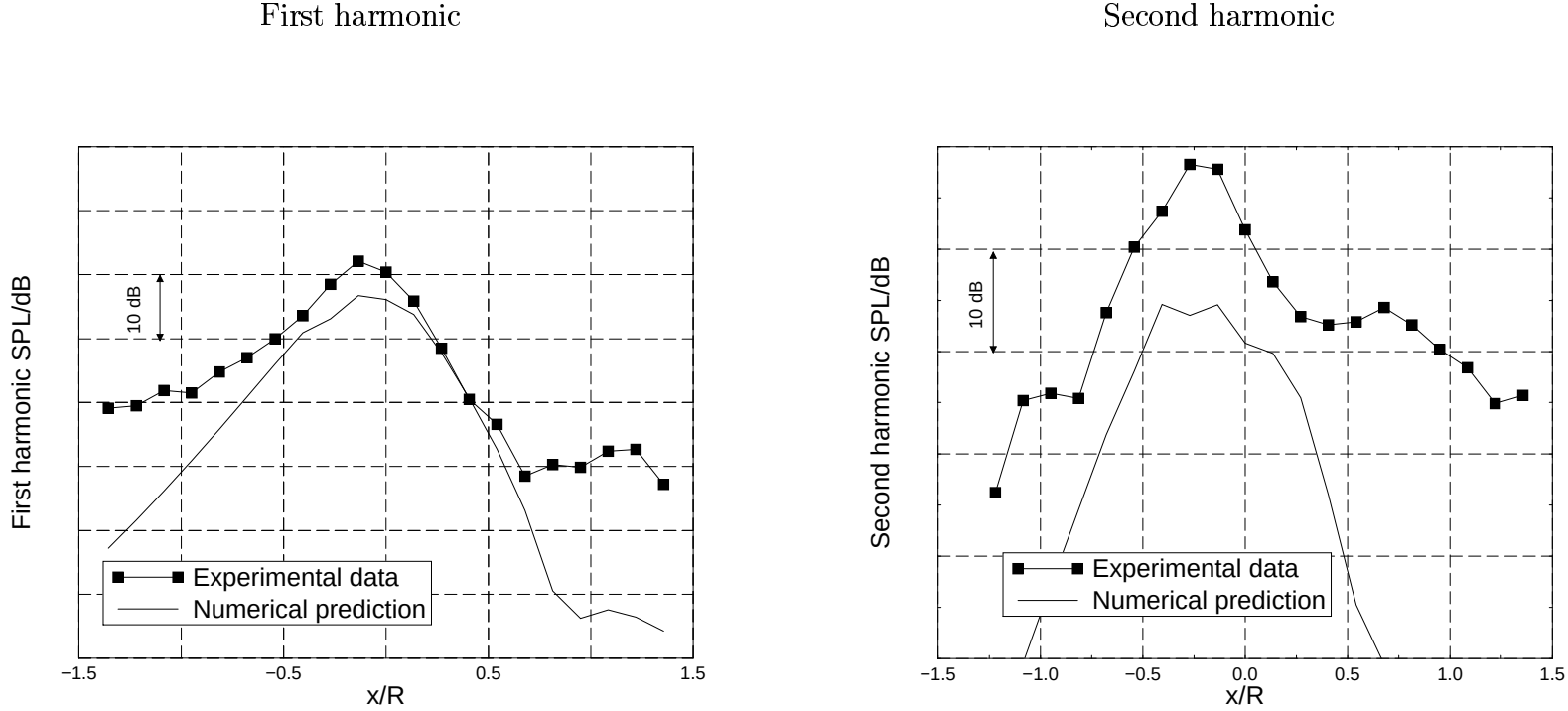

Figure 5.20: High speed propeller, near-field axial directivity, $\beta = 61.1°$, $N = 5123$rpm, $M_\infty = 0.76$, $M_t = 1.06$

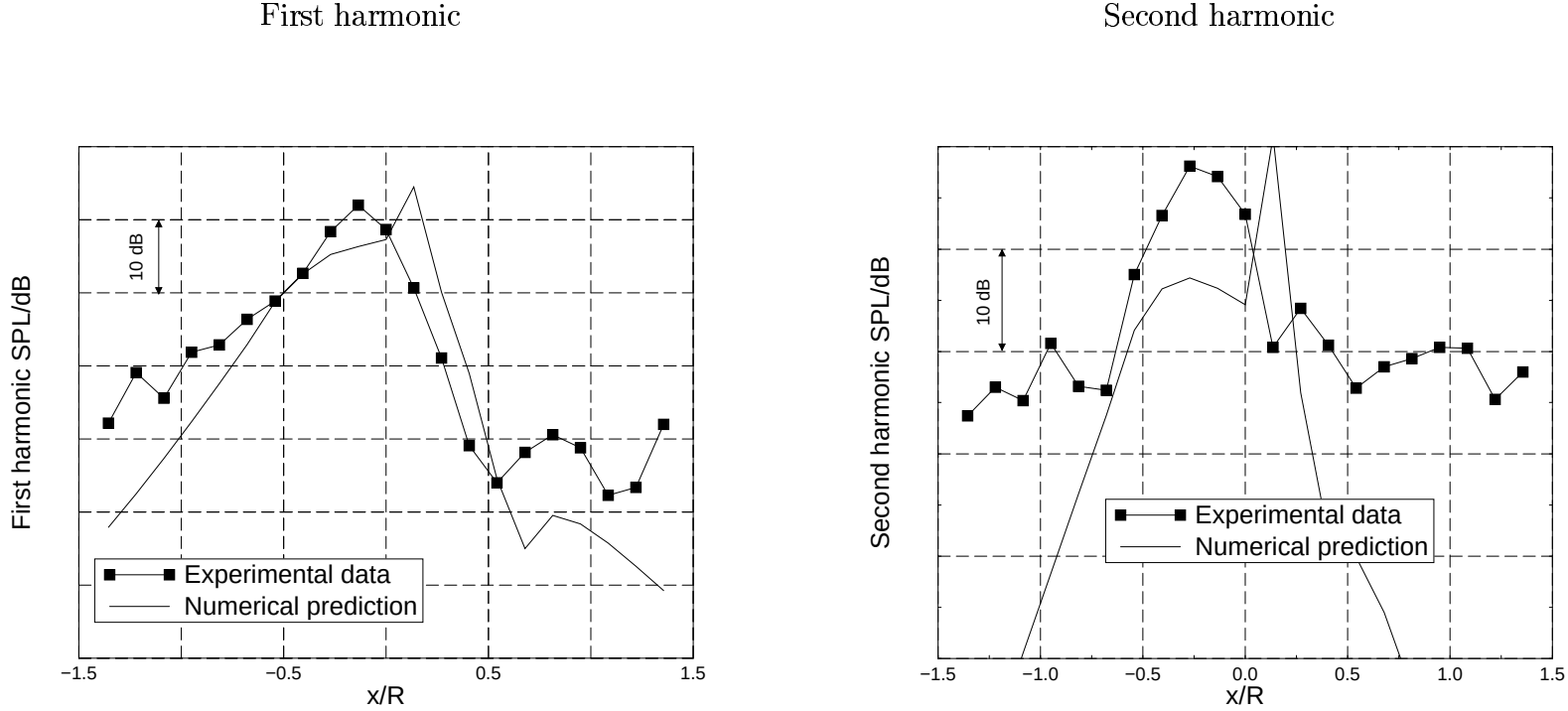

Figure 5.21: High speed propeller, near-field axial directivity, $\beta = 61.1°$, $N = 5123$rpm, $M_\infty = 0.78$, $M_t = 1.08$

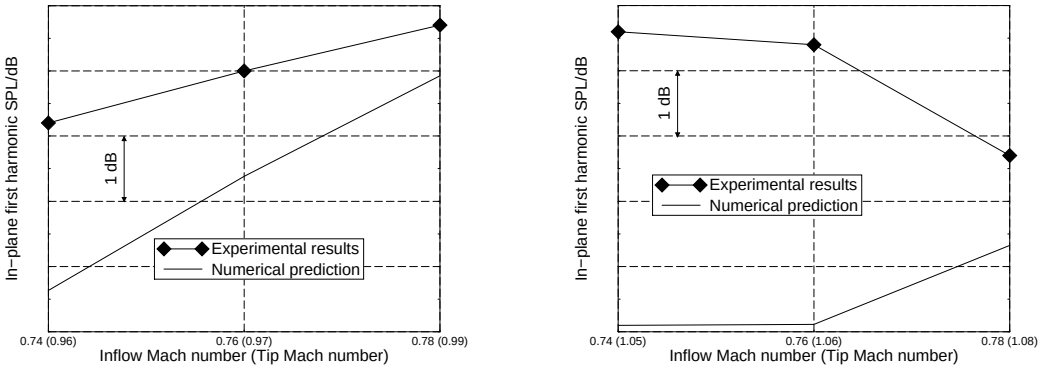

$\beta = 61.1°$, $N = 4200$rpm $\beta = 61.1°$, $N = 5123$rpm

Figure 5.22: High speed propeller, near field acoustic trends

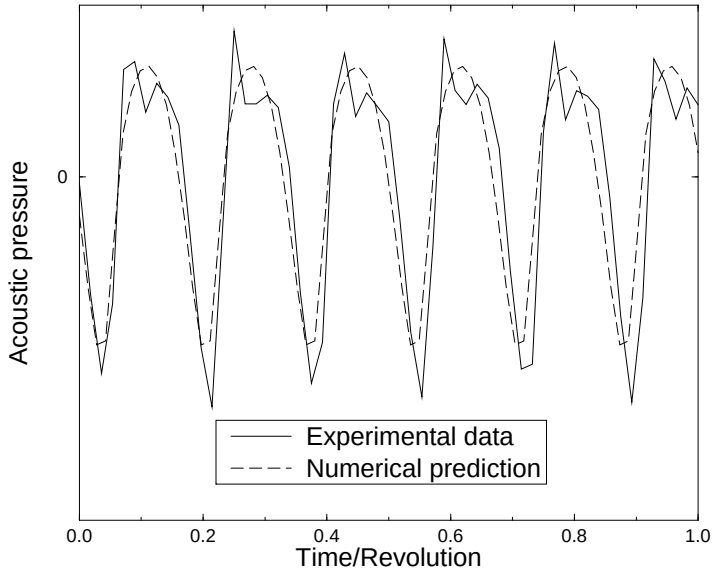

$\beta = 61.1°$, $N = 4200$rpm

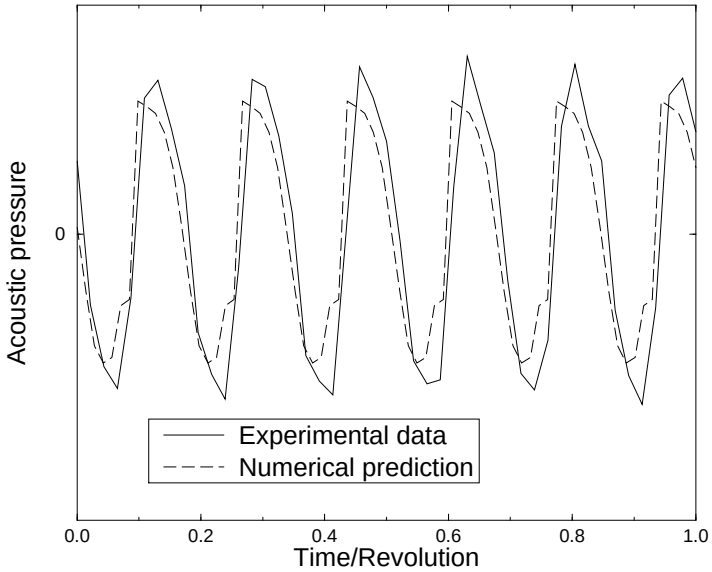

$\beta = 61.1°$, $N = 5123$rpm

Figure 5.23: Time domain comparison for HSP, $M_\infty = 0.74$, in-plane, r/R=1.22

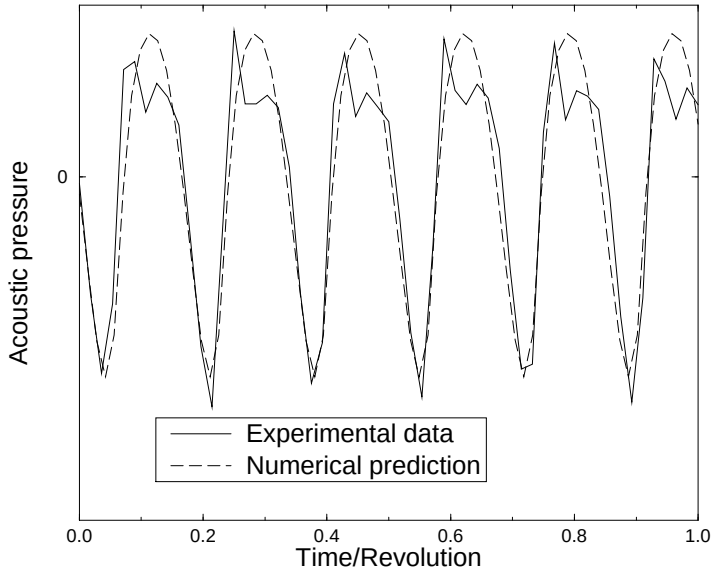

$\beta = 61.1°$, $N = 4200$rpm

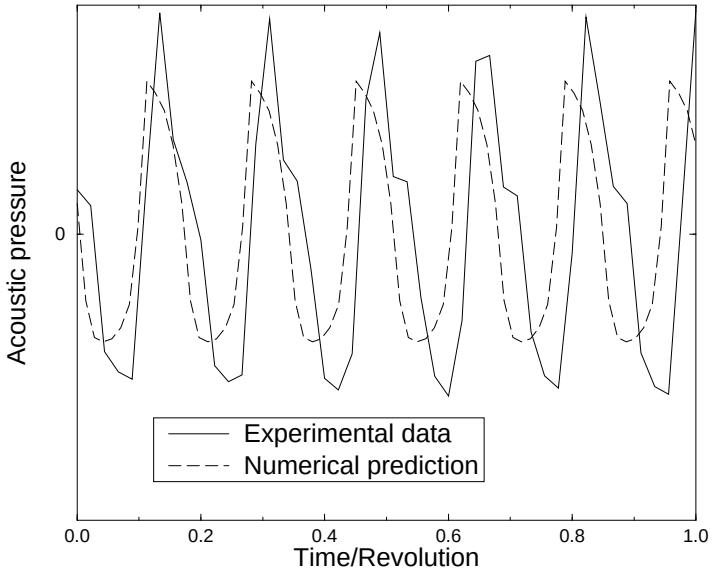

$\beta = 61.1°$, $N = 5123$rpm

Figure 5.24: Time domain comparison for HSP, $M_\infty = 0.76$, in-plane, r/R=1.22

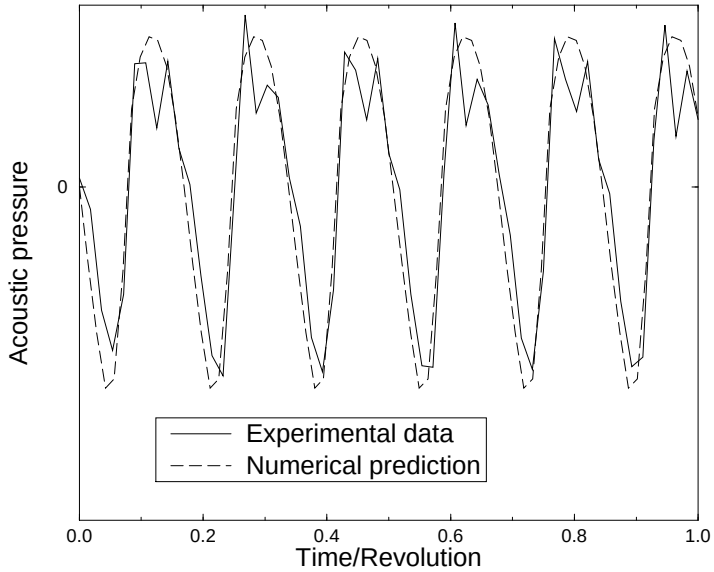

$\beta = 61.1°$, $N = 4200$rpm

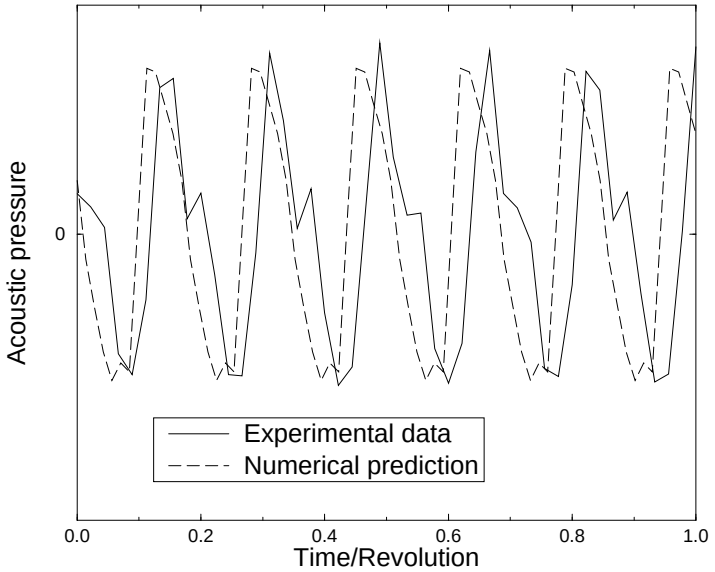

$\beta = 61.1°$, $N = 5123$rpm

Figure 5.25: Time domain comparison for HSP, $M_\infty = 0.78$, in-plane, r/R=1.22

5.3.3 Discussion

Two features of the predicted results are immmediately apparent. In general, predictions are more accurate for higher blade tip and inflow speeds and the HSP predictions are more accurate than the LSP results.

Looking first at the LSP tests, the predictions for 61.8° pitch are better than those at 54.9° and in each case the lower advance ratio (i.e. higher tip speed) results are the more accurate. This may simply be because at higher tip speeds the tunnel background noise did not contaminate the acoustic signal as much as in the lower speed cases. In those cases with better predictions there were more data points available for comparison which might lead one to believe that these data were more reliable than those from the 'quieter' tests. Another possible cause of error, especially for the in-plane measurements, is non-linearity in the source terms but discussion of this is postponed to a later section.

The other obvious feature, the fact that the HSP predictions, even for tip Mach numbers as high as 1.08, were better than those for the LSP, is perhaps not so surprising in hindsight. The HSP blades, thin and highly-swept, were expressly designed to operate at high speed without suffering from large compressibility effects so that the effect of non-linear sources on the acoustics would not be as great as for the LSP. Also, the HSP was also somewhat louder than the LSP so that the data from it should be more reliable. Even for the second harmonic in figures 5.16–5.18 and figures 5.21–5.21 there are many data points available for comparison. Finally, at transonic tip Mach numbers, the noise field is dominated by the thickness noise so that errors caused by the interpolated blade pressure distribution would be less important, see §5.6.1.

Turning to the trend data in figures 5.22 and 5.15 the effects of tip speed and pitch become clearer. In the LSP case, figure 5.15, the first predicted trend only starts to look right over the second half of the inflow Mach number range, in the second (higher speed) case the absolute levels are well predicted but with an error in the slope and the third case the prediction is consistently good over the range of speeds.

In the HSP plots, figure 5.22, the predictions are consistently good, within 5 dB of the experimental result over all the Mach numbers considered, including tip Mach numbers up to 1.08, and within 3 dB for the subsonic tip cases. In the time domain comparisons, figures 5.23 to 5.25, the comparisons are very good for both shape and amplitude with some loss of detail around the peaks but with the overall shape of the signal well-captured.

Finally, the angle of attack results presented are just acceptable. In the 3° angle of attack case, both the first and second harmonics are underpredicted. Given that the underprediction is far greater than in the 0° case, it seems to be the estimation of the unsteady pressure distribution that is causing the error. More detailed discussion of this problem can be found in §5.6.

5.4 Low speed, far-field results

Unfortunately, only data for the low-speed propeller were available at the time of writing so no HSP results are presented here.

5.4.1 Low speed propeller

Far-field noise data for the LSP are presented in figures 5.26 and 5.27. A very good agreement in both level and trends is evident in each case, in particular in the first plot in figure 5.26 and in the second plot in figure 5.27. This good match may be due to a number of things including source compactness and a lack of non-linear effects.

At the low speeds used in these tests, non-linear effects such as shocks are not important. In particular, this means that sudden changes in the blade loading distribution which might be 'lost' during interpolation are not expected and should not affect the results. Also, at low rotation speeds the propeller is a compact acoustic source. This means that a very simple model is adequate to predict the noise radiated (a Gutin [15] formulation for example). Since, in these cases, the interpolated propeller loading was scaled to give the measured thrust, a good match between prediction and experiment is only to be expected—it is possible to get a reasonably good match to the directivity knowing only the thrust and torque on the propeller at low blade tip speeds.

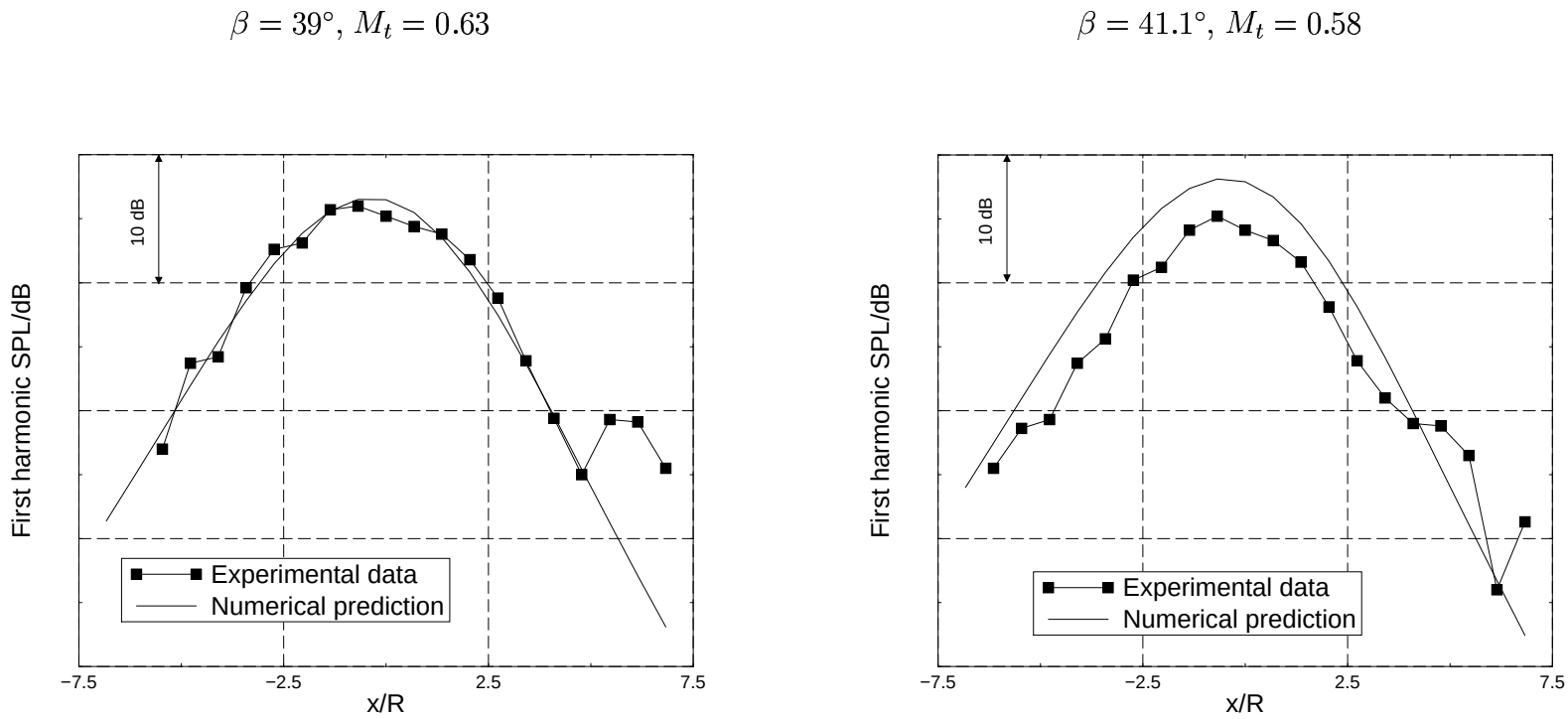

Figure 5.26: Low speed propeller, far-field axial directivity, axial inflow, first harmonic, $M_\infty = 0.2$

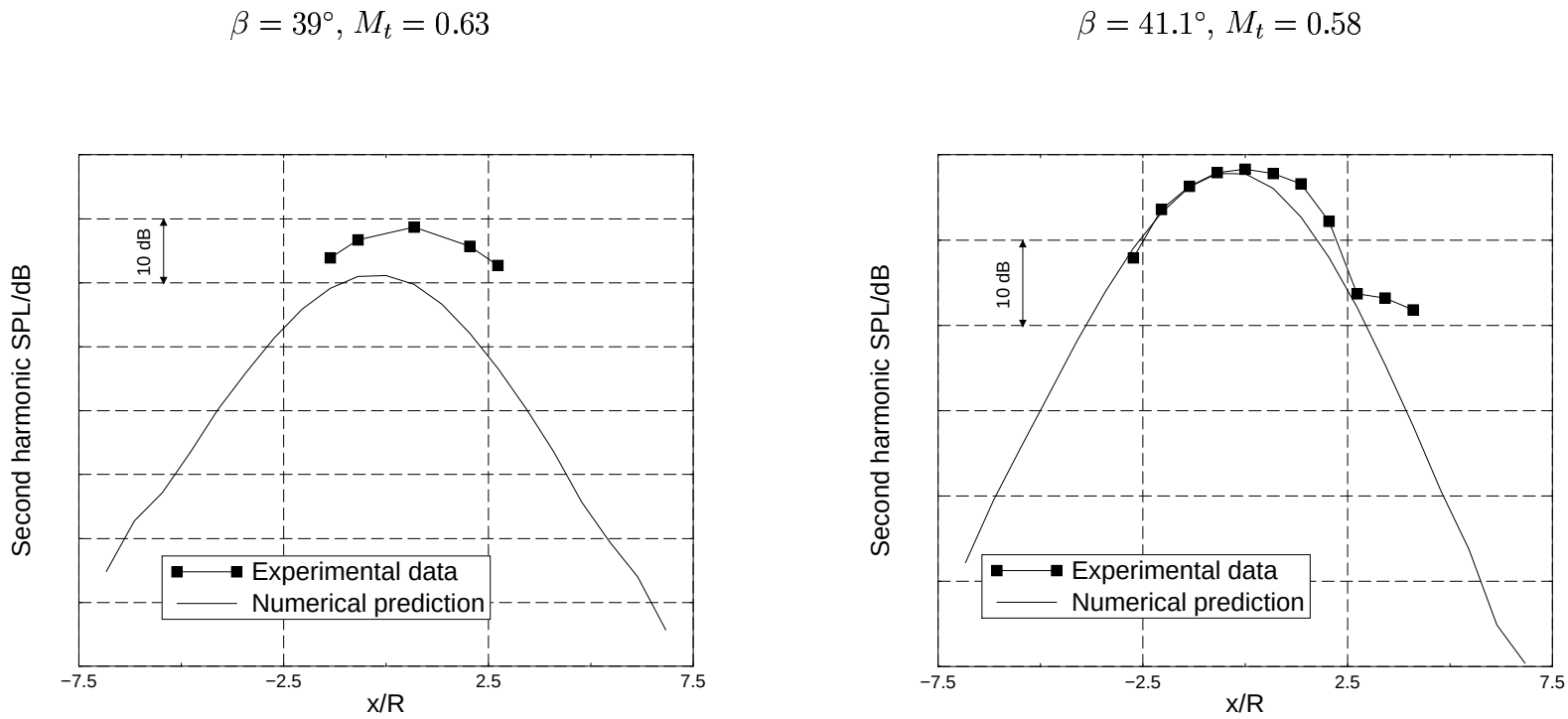

Figure 5.27: Low speed propeller, far-field axial directivity, axial inflow, second harmonic, $M_\infty = 0.2$

5.5 Prediction quality

The experimental data and numerical predictions presented in figures 5.2 to 5.27 exhibit a number of features some of which are obvious and some of which are obvious in hindsight. Overall the best results are those in figure 5.26, low speed results for the low speed propeller. This might be expected—these were the least demanding test conditions. What only becomes obvious with hindsight is that in the high Mach number tests, as mentioned above, the high speed propeller predictions are better than those for the low speed design.

This might appear surprising at first but is due to the fact that, tautologically, the high speed propeller was designed to operate at high speed. It is highly swept, quite thin and has a wide chord. It was expressly designed not to suffer from compressibility effects when operating in the supersonic and transonic regimes. The low speed propeller on the other hand, of a more conventional design, has quite a thick blade and is bound to suffer from non-linear effects under these operating conditions and the noise prediction accuracy suffers accordingly.

5.5.1 Time domain comparison

The most important comparisons are those of the predicted and measured time domain signals. Figure 5.14 shows two such records for the low speed propeller, for 0° and 3° angle of attack, while figures 5.23 to 5.25 show time record comparisons for the high speed propeller at 0° incidence over a range of transonic and supersonic tip Mach numbers.

In the 0° case for the LSP the comparison is quite good, with the negative pressure peaks (which have a large thickness noise contribution) accurately captured in position and only slightly overpredicted in magnitude. In the angle of attack case, the position of the negative peak is also quite accurate although its strength is underpredicted. It is hard to tell exactly how bad this underprediction is as the experimental data fluctuate quite badly but at worst it is no worse than the error in the 0° case. This is encouraging as the thickness noise contributes most strongly to the negative pressure peak, figure 5.28.

One might imagine that this observation is nothing special (calculation of the thickness noise source is trivially simple) but it does demonstrate that we can have confidence in the model and in the thickness noise part of the prediction. And since the comparison is based on a time record, it is possible to isolate the contribution of the two sources and get some idea of their accuracy separately. (With a frequency domain theory this would only be possible by synthesising time records and comparing them to experimental results.) Unless the model is grossly incorrect (possible but unlikely—it has worked well for more than twenty-five years) the negative peak can be ascribed to the thickness source, leaving the loading term to explain the positive peak.

The positive peak is not as well predicted as the negative. There are a number of possible reasons. The first of these is that the theory is grossly

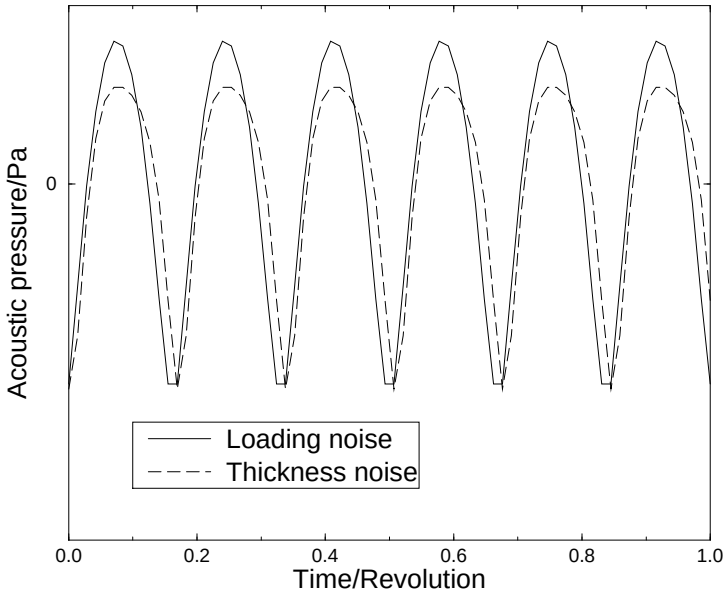

Figure 5.28: Thickness and loading noise contributions for the LSP, 0° case

incorrect and the accurate prediction of the negative peak was simply good luck. As mentioned above this is unlikely; the theory has worked quite well up to now and has been used in many different forms. A more plausible cause is some error in the blade pressure distribution which is causing the loading noise to be incorrectly predicted. This possibility is considered in more detail in §5.6.1. On the whole the time domain results presented lead one to believe that the theory is accurate and that the errors in the predictions are due to limitations in the input data accuracy rather than to inaccuracy in the theory *per se*.

For the HSP the results are far better than one might expect at these tip Mach numbers (but see §5.6.5). In each case the shape and amplitude of the waveform are well predicted. In figure 5.24 the 5123rpm prediction is too low in amplitude and for the same case in figure 5.25 the phase is incorrect but these errors are quite minor compared to the other results in this set of figures. The only major concern is the failure of the numerical method to capture the jagged detail around the positive (loading) peaks of the signal. This could be due to errors in the interpolated pressure distribution (see §5.6.1) or to inadequate spatial resolution in the blade mesh causing the higher harmonics to be underpredicted.

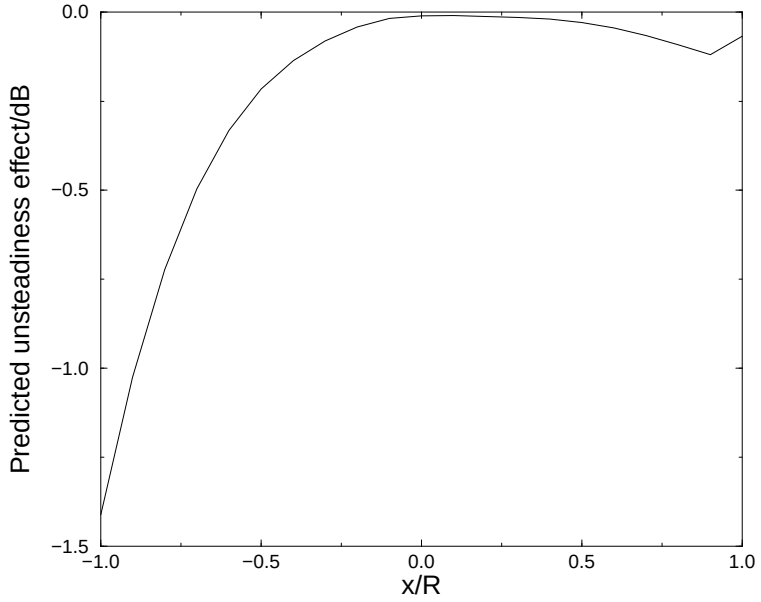

Figure 5.29: Effect of including unsteady loading estimate, $\alpha = 0°$

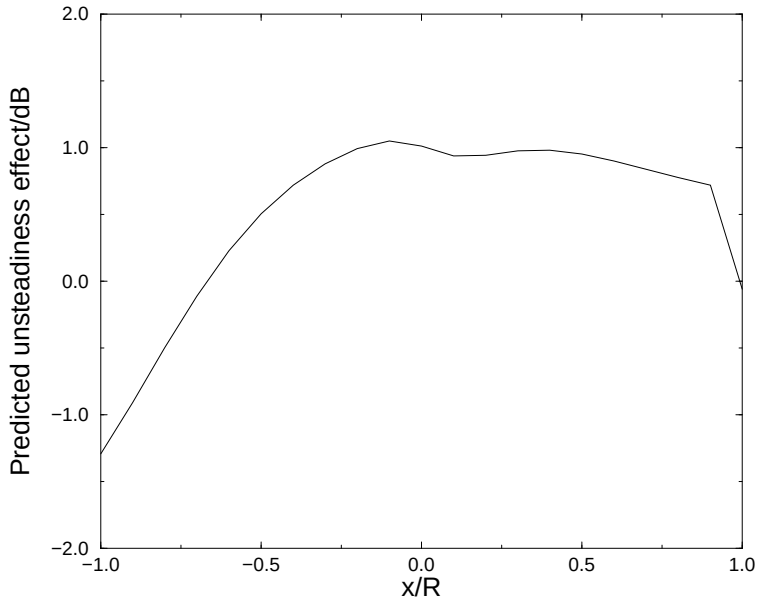

Figure 5.30: Effect of including unsteady loading estimate, $\alpha = 3°$

5.5.2 Unsteady loading effects

An estimate of the unsteady loading effect on the acoustic signal's first harmonic is shown in figures 5.29 and 5.30 which are based on the angle of attack data given in figures 5.11 to 5.14. Each plot shows the difference between the SPL predicted with and without an estimate of the blade unsteady loading calculated as

$$\mathrm{SPL}_{\text{unsteady loading}} - \mathrm{SPL}_{\text{no unsteady loading}}$$

It can be seen that in the zero incidence case the effect of the unsteady loading is minimal except at quite a large distance downstream of the propeller (about one blade radius). This is as it should be—the unsteady loading is not very large at zero nominal incidence.

In the 3° angle of attack case, the effect of including an estimate of the unsteady loading is greater, increasing the first harmonic SPL by around 1dB over much of the upstream part of the directivity, although it causes a drop in the SPL of 1.4dB in the downstream direction.

5.6 Prediction errors

Errors in numerical predictions can be divided up into 'real' errors (errors of theory or the numerical implementation of the theory) and 'domain' errors (the use of the theory outside its strict domain of validity). The main 'real' error to be considered is that introduced in estimating the blade surface pressure distribution. The effects of some other sources of error, related to the range of validity of the theory are shown in figure 5.31. These include

- non-linear sources discussed in §5.6.2.
- wind-tunnel reflection, see §5.6.3.
- supersonic sources considered in §5.6.4.

5.6.1 Errors of implementation

The most important error is that introduced in the interpolation of the blade surface pressure distribution. There are two important inaccuracies. The first is that interpolation is inherently a smoothing technique which can smear out certain features of the pressure distribution, especially those which lie between pressure tappings. A sudden change in pressure on the real blade, for example, will become a smooth ramp between two tappings when interpolation is carried out.

The second error is due to the fact that some *extrapolation* of values is unavoidable, especially in the blade tip region. There is an upper limit on

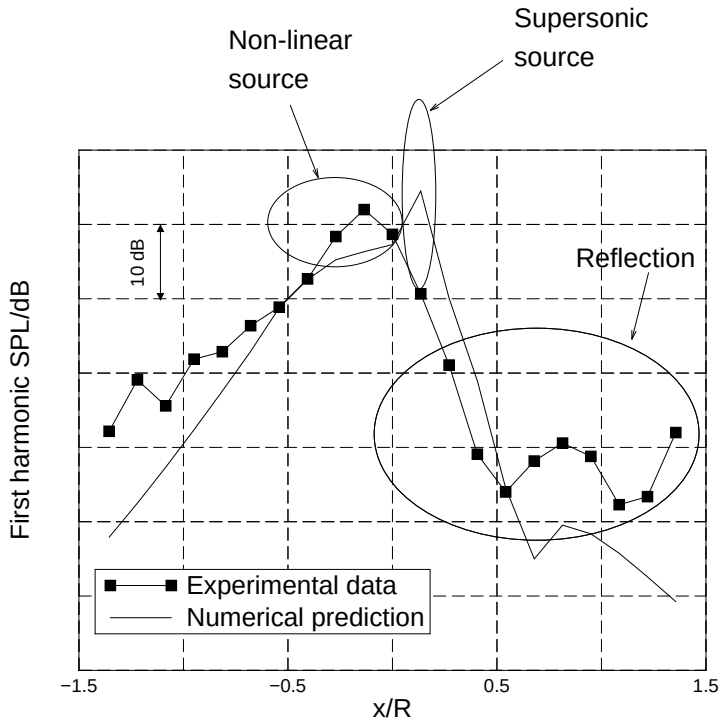

Figure 5.31: Possible sources of error in numerical predictions

the number of pressure tappings which can be built into a blade, and there is also a limit on where those tappings can be placed. In particular, tappings cannot be placed very close to a tapered blade tip or a fine trailing edge. And since it is known that the blade tip is the dominant region for the sound transmitted to the far field (Parry and Crighton [49]) when the propeller is acoustically subsonic and that the acoustic field is dominated by the gradient of the source strength near the tip, the effect of inaccuracy in the tip pressure distribution is obviously quite important. In this case, the blade pressure was held constant outboard of the last set of pressure tappings, so that loading noise should be underestimated rather than overestimated. This does not necessarily mean that the total acoustic signal should be underpredicted as the net sound pressure depends on the phase relationship between the loading and thickness terms.

Finally, as can be seen in the angle of attack effect plots, figures 5.11 to 5.13, there is a problem in the estimation of the blade unsteady loading. It is known that a fluctuating pressure on the blade surface is a very efficient radiator of sound so that the underestimation of the radiated noise could have any of a number of causes.

The most obvious possibility is that the unsteady loading has been underestimated. Without more extensive dynamic data on the blade surface this is hard to examine. Another possible cause of the error is that the phase of the

sound radiated by the unsteady loading in the model is such as to cause excessive cancellation with the steady loading noise. Finally, it is almost certain that the assumption of the unsteady loading being similar at all blade sections is unsound. Again, without greater coverage of a blade it is difficult to say which of these causes is more important. It is perfectly possible that all are involved to some degree.

5.6.2 Non-linear sources

The theory used in developing the prediction is purely linear; no non-linear sources such as shocks are modelled and it should be expected that at high tip Mach numbers the predictions will break down. According to Magliozzi et. al. [16], the non-linear terms become important for section relative Mach numbers from about 0.9 to 1.1, contributing up to 6 dB to the radiated noise. This would mean that an increased error can be expected around the propeller plane at high tip Mach numbers. This effect can be seen in the high speed propeller plots where the numerical predictions are quite good in regions away from the propeller plane, giving us confidence that the prediction technique is valid, but not so good in and around the propeller plane where the method can be expected to break down. Overall, however, neglecting the non-linear terms does not seem to introduce a large error for reasons explained in §5.6.5.

5.6.3 Wind-tunnel reflections

While the theory developed in this thesis is intended to model the noise generation of a body in free space, the tests were carried out in a wind-tunnel where the measured noise was affected by reflection from the tunnel boundaries. This is visible in regions outside the propeller plane and shows up as a hump in the axial directivity, caused by reinforcement of the noise by sound reflected from the wind-tunnel wall. It is especially clear in the plot used for figure 5.31 but can be seen in a number of other sets of data, for example figure 5.18, where it is visible up- and downstream of the propeller plane, and figures 5.19 to 5.21 where it is visible in the upstream direction in each case. In many of the other plots, even though there is no obvious hump, there is some evidence of tunnel reflection affecting the results as the experimental results do not die off as quickly as one might expect. This is especially evident in the low speed propeller cases where, due to the lower frequency of the sound generated, any reflection effects would be especially serious.

This effect of a wind-tunnel on measured propeller acoustics can be modelled (see, for example, the work of Eversman [51] or Eversman and Baumeister [52]) but would have been beyond the scope of this project.

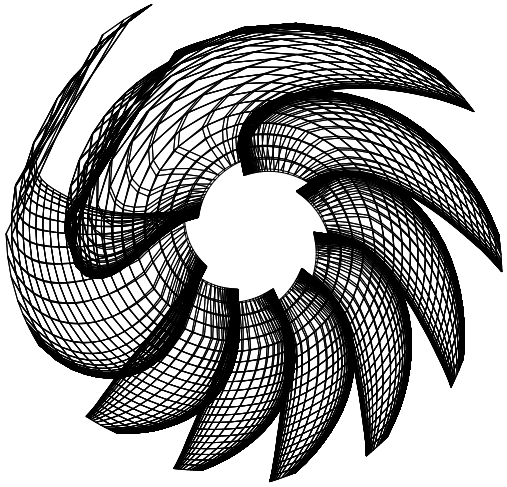

Figure 5.32: Retarded surface for eight observer time points

5.6.4 Supersonic sources

The theory developed in this thesis is strictly only valid for sources which are acoustically subsonic. This amounts to one of two things; either there is only one retarded time per observer time point or $(1 - M_r)$ is always large enough to avoid numerical errors in the Doppler factor $1/(1 - M_r)$ and its derivative. It appears that for the highest tip Mach number case considered, the source does become acoustically supersonic in one test, around the propeller plane, in figure 5.21. A predicted time record for this case is shown in figure 5.33. The set of sharp, tall spikes corresponds to points in the time record at which the Doppler amplification becomes very large indeed indicating that the source has become acoustically supersonic. It *is* possible and valid to use a 'subsonic' code to carry out predictions on aerodynamically supersonic propellers under certain circumstances if care is taken to ensure that the source-observer Mach number is never too high, see §5.6.5. Since the effect of non-linear terms is also greatest when the source-observer Mach number is unity (see §5.6.5) this is a double advantage of using the subsonic source technique.

The effect of the supersonic tip speed can be studied using the retarded surface (also known as the acoustic planform), figures 5.32 and 5.34. This is a plot of the position of each point on the blade mesh at the corresponding retarded time for some fixed observer time. In other words, for a given time point in the acoustic signal, it shows the position of the blade mesh points at

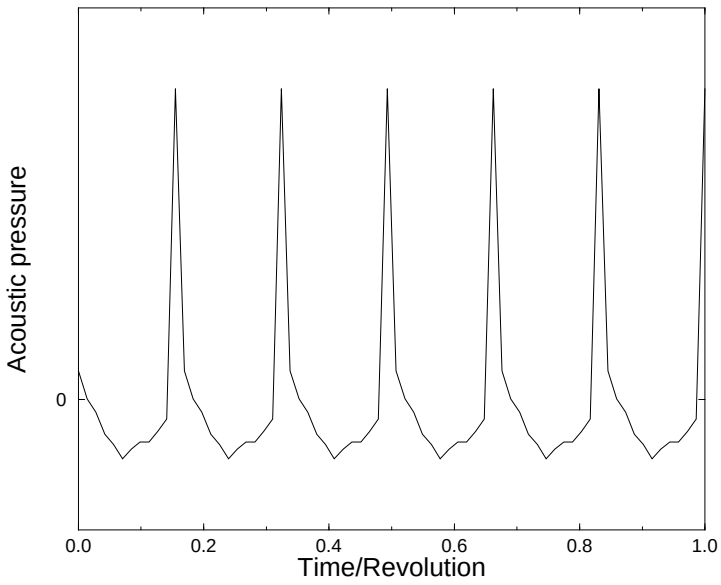

Figure 5.33: Numerically predicted time record for supersonic blade tip case

their retarded time.

Figure 5.32 shows the retarded surface of a single blade for eight equally spaced observer time points for the case of figure 5.21 already mentioned. A large variation in acoustic planform is evident, with the blade positions in the lower right-hand region being comparatively undistorted while those at the upper left are much more affected. It is important to remember that, since the blade shapes are drawn at equal intervals of observer time, the angular distance between a point on one blade image and its position on the next image depends on its Mach number in the observer direction. This means that the most highly distorted images are those in the region where the source is moving most rapidly relative to the observer.

Viewed in this light, the extreme distortion of the blade shape in figure 5.32 is only to be expected. Figure 5.34 shows the most distorted of the blade images in more detail. The effect of retarded time variations shows up most clearly in the tip region. The images of the blade at the other positions, while distorted, remain smooth and well-defined. For this image, however, the tip region is very distorted and jagged, an effect caused by supersonic motion towards the observer. The singularities caused by supersonic motion can be related to the discontinuities in this retarded surface using, for example, Farassat's formulation 3 [41] or Wells and Han's moving medium form of Farassat's formulation, [39]. Because these techniques use an integration over the retarded surface (rather than the real blade surface used here), discontinuities

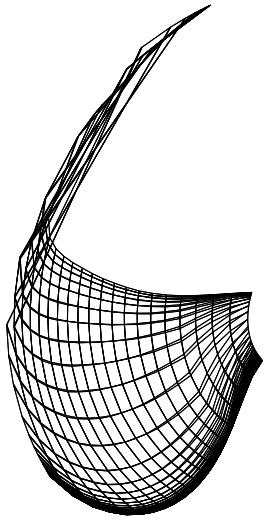

Figure 5.34: Retarded surface for single observer time point

in the surface can be linked directly to discontinuities in the time record.

5.6.5 A note on the use of subsonic formulae for supersonic propellers

As indicated above, the formulation developed in this thesis for subsonic source acoustics also works quite well for a supersonic propeller. There are two conditions which must hold for this to be true, both related to the observer position. The first is that the source must be *acoustically* subsonic, as explained in §2.1. For observer positions near the propeller axis this is not a difficulty; the blade tip has quite a small velocity in the direction of the observer. For the highest speed case considered in this thesis ($M_\infty = 0.78$, $M_t = 1.08$), figure 5.35 shows the Doppler amplification $(1 - \mathbf{M}_s.\mathbf{D})$ plotted for the blade tip over one revolution for a number of observer points near the propeller plane.

Figure 5.36 shows an enlarged view of the region in figure 5.35 where the Doppler amplification becomes zero. It can be seen that only for the observer positions nearest the propeller plane does the source approach at sonic velocity. In other words, the subsonic source method is quite valid for all other observer positions on the sideline and for the lower speed cases no difficulty should arise.

The other possible difficulty in using the method of this thesis for supersonic propellers is the presence of non-linear (quadrupole) sources. Hanson and Fink [53] examined this problem and found that the quadrupole is "negligible" for thin propeller blades "outside the transonic speed range". Since the high speed propeller blade was thin it is perhaps no surprise that the linear

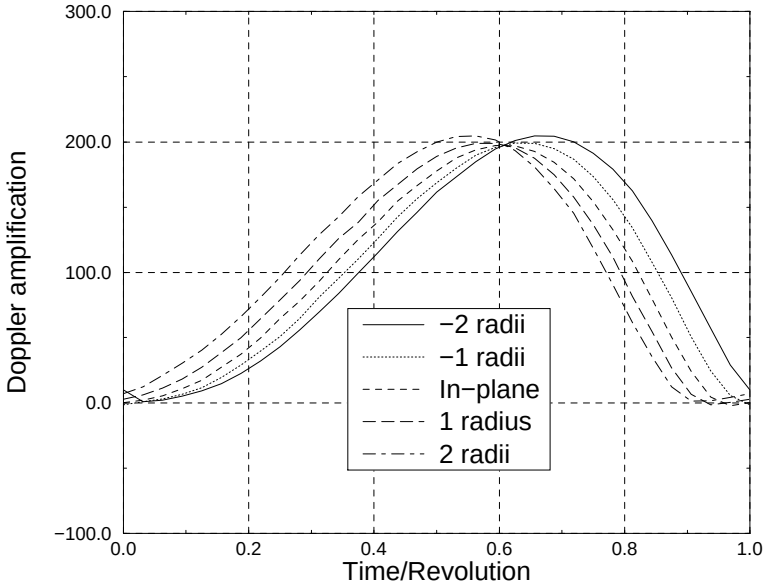

Figure 5.35: Doppler amplification for one revolution of blade tip. $M_\infty = 0.78$, $M_t = 1.08$.

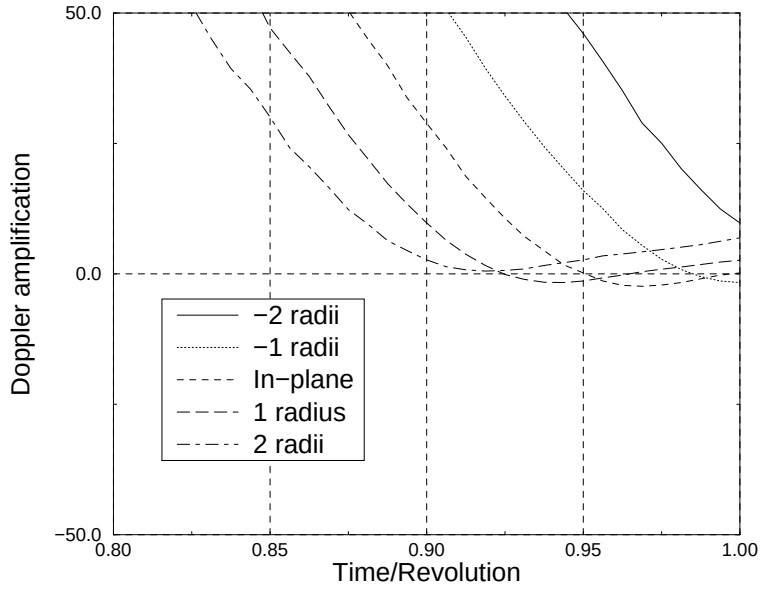

Figure 5.36: Enlargement of figure 5.35

theory given here worked well over most test conditions for the high speed propeller, including the very high speed cases. Envia [54] gives numerically computed results and asymptotic formulae for quadrupole noise which show the quadrupole contribution from a supersonic tip propeller having a maximum in the propeller plane and falling by 20dB over a distance of 1 blade radius, figure 5.37. Reference to the supersonic tip speed tests shows an underprediction in this region which may be due to neglecting the quadrupole terms.

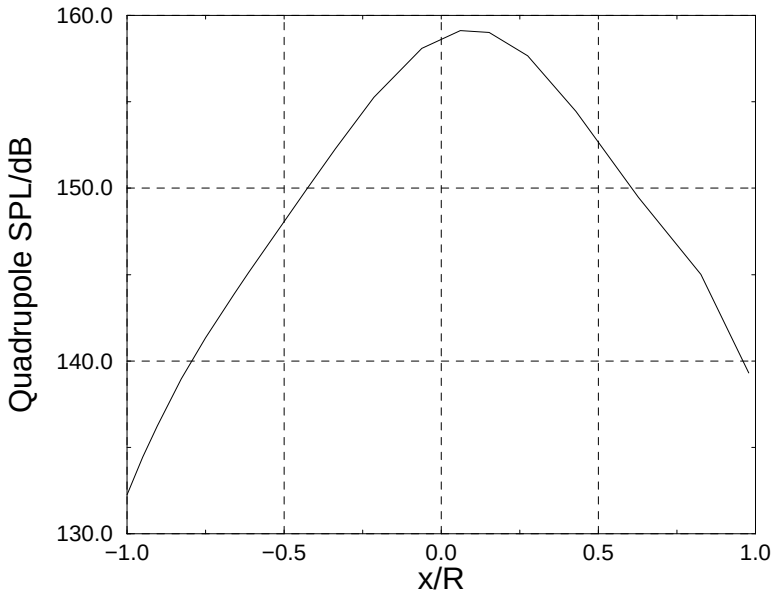

Figure 5.37: Sideline directivity of quadrupole source, $M_t = 1.15$, $M_\infty = 0.8$. Data from Envia [54].

Finally, Peake and Crighton [55], in developing an asymptotic analysis, show that the quadrupole noise is dominated by the contribution from the Mach radius (the radius where the source approaches the observer at sonic velocity). In the case of the high speed tests considered here there is usually no Mach radius (no part of the blade approaches the observer at sonic velocity) so that the quadrupole contribution can be neglected. Also, it should be noted that the condition for quadrupole noise being important is the same as the condition that the Doppler factor not be zero. Ensuring that there is no Doppler singularity also ensures that non-linear sources are not important.

Based on the results presented in this chapter, it is concluded that the subsonic source method can legitimately be used for certain supersonic blade cases.

Chapter 6

Conclusions

> *The high speed propellers will be noisy in operation (for reasons quite different from those that make marine propellers noisy). The noise, however, will be chiefly "near field" noise which can be made tolerable by improving the sound insulation of the fuselage. The "far field" noise may actually be less than that of existing turbofan engines. ...*
>
> *After more than a century of application in hydronautics and aeronautics the screw propeller is very much alive and turning; I expect it will survive for as long as man uses water and air for transport.*
>
> *The Screw Propeller*, E. Eugene Larrabee [56]

6.1 The thesis

A linear acoustic time domain technique for the prediction of noise from a subsonic propeller operating at incidence in a flow has been developed using a moving medium approach. This approach, equivalent to previously published frequency domain methods (those of Hanson [40], Hanson and Parzych [45] and Mani [11] for example) fits in with the previously published time domain techniques. It can be considered a moving medium equivalent of Farassat's formulation 1A [22] or as a subsonic rotor equivalent of Wells and Han's method [39].

A numerical code based on this formulation [57] has been developed and used to predict the noise generated in a number of wind-tunnel tests. Comparisons with these experimental results have, in the main, been quite good, in particular those for a high tip speed (supersonic) advanced design. The theory breaks down, as it should, for acoustically supersonic blades and for conditions where non-linear sources are important. However, as shown in the discussion of §5.6.5, it is possible to use a subsonic method of the type given here for the prediction of noise from supersonic propellers if care is taken to ensure that no part of the blade approaches the observer at sonic velocity.

6.1.1 Future work

Future development of the work in this thesis is planned to include the use of the moving-medium approach for integrated aeroacoustic/aerodynamic calculations as in the work of Long [18] and Farassat [19]. Such an approach offers a middle way for aerodynamic calculations on installed propellers somewhere between Navier-Stokes and incompressible potential methods. Steering between Scylla's complexity and Charybdis' limitations, it gives an inviscid, compressible formulation which can include a full propeller model and a fuselage without needing to use complex meshing techniques simply to map the computational domain. It should also make the calculation of the sound scattered by a fuselage somewhat easier—a byproduct of the aerodynamic calculation is a complete acoustic pressure distribution over the fuselage.

References

[1] T. S. Kuhn. Mathematical versus experimental traditions in the development of physical science. In *The essential tension: Selected studies in scientific tradition and change*, pages 31–65. University of Chicago Press, London, 1977.

[2] F. V. Hunt. *Origins in acoustics.* Acoustical Society of America, New York, 1992.

[3] A. Koestler. *The sleepwalkers: A history of man's changing vision of the universe.* Penguin, 1986.

[4] J. W. S. Rayleigh. *The theory of sound.* Dover, New York, 2nd edition, 1945.

[5] N. Marsh. An introductory Essay to the Doctrine of Sounds containing some proposals for the improvement of Acoustics, as it was presented to the Society of Dublin, Nov 12. 1683. *Phil. Trans. Roy. Soc. Lond.*, 156:472–486, February 1683/4.

[6] M. J. Lighthill. The fourth annual Fairey lecture: The propagation of sound through moving fluids. *Journal of Sound and Vibration*, 24(4):471–492, 1972.

[7] D. G. Crighton. Computational aeroacoustics for low Mach number flows. In Jay C. Hardin and M. Y. Hussaini, editors, *Computational aeroacoustics*, ICASE/NASA LaRC, pages 50–68. Springer-Verlag, New York, 1993.

[8] M. J. Lighthill. On sound generated aerodynamically: I General theory. *Proc. Roy. Soc. Lond. A.*, 231:505–514, 1952.

[9] J. E. Ffowcs Williams and D. L. Hawkings. Sound generation by turbulence and surfaces in arbitrary motion. *Phil. Trans. Roy. Soc. Lond. A.*, 264:321–342, 1969.

[10] M. S. Howe. Contributions to the theory of aerodynamic noise, with application to excess jet noise and the theory of the flute. *J. Fluid Mech.*, 71(4):625–673, 1975.

[11] R. Mani. The radiation of sound from a propeller at angle of attack. *Proc. R. Soc. Lond. A*, 431:203–218, November 1990.

[12] T. D. Crouch. *The Bishop's boys: A life of Wilbur and Orville Wright.* Norton, New York, London, 1989.

[13] F. B. Metzger and J. S. Preisser. A history of propeller tone noise prediction methodology 1919 to 1994. In *First Joint CEAS/AIAA Aeroacoustics Conference*, volume 1, pages 17–43, Godesberger Allee 70, D-53175 Bonn, Germany, June 1995. AIAA/CEAS, DGLR.

[14] D. L. Hawkings and M. V. Lowson. Theory of open supersonic rotor noise. *Journal of Sound and Vibration*, 36(1):1–20, 1974.

[15] L. Gutin. On the sound field of a rotating propeller. Technical Memorandum 1195, NACA, Langley Aeronautical Laboratory, Langley Field, VA, USA, 1948.

[16] B. Magliozzi, D. B. Hanson, and R. K. Amiet. Propeller and propfan noise. In H. H. Hubbard, editor, *Aeroacoustics of Flight Vehicles*, volume 1, pages 1–64. Acoustical Society of America, New York, 1995.

[17] A. Powell. Some aspects of aeroacoustics: From Rayleigh until today. *ASME Journal of Vibration and Acoustics*, 112:145–159, 1990.

[18] L. N. Long. An aerodynamic theory based on time domain aeroacoustics. *AIAA Journal*, 23(6):875–882, June 1985.

[19] F. Farassat. A new aerodynamic integral equation based on an acoustic formula in the time domain. *AIAA Journal*, 22(9):1337–1340, September 1984.

[20] M. V. Lowson. The sound field for singularities in motion. *Proc. Roy. Soc. A*, 286:559–572, 1965.

[21] A. P. Dowling and J. E. Ffowcs-Williams. *Sound and Sources of Sound.* Butterworth, 1983.

[22] F. Farassat. Linear acoustic formulas for calculation of rotating blade noise. *AIAA Journal*, 19(9):1122–1130, September 1981.

[23] D. B. Hanson. Compressible helicoidal surface theory for propeller aerodynamics and noise. *AIAA Journal*, 21(6):881–888, 1983.

[24] B. W. McCormick. *Aerodynamics, aeronautics, and flight mechanics.* John Wiley and Sons, Inc., New York, second edition, 1995.

[25] T. J. Kirker. Procurement and testing of a 1/5 scale advanced counter rotating propfan model. In *AIAA 13th Aeroacoustics Conference*, October 1990.

[26] R. P. Woodward and I. K. Loeffler. In-flight source noise of an advanced large-scale single-rotation propeller. *Journal of Aircraft*, 30(6):918–926, 1993.

[27] S. L. Sarin and R. P. Donnelly. Angle of incidence effects on the farfield noise of an isolated propeller. In *DGLR-AIAA 14th Aeroacoustics Conference*, 1992.

[28] W. J. G. Trebble. Investigations of the aerodynamic performance and noise characteristics of a Dowty Rotol R212 propeller at full-scale in the 24 ft wind tunnel. *Aeronautical Journal*, pages 275–284, 1987.

[29] W. J. G. Trebble. Investigation of the aerodynamic performance and noise characteristics of a 1/5th scale model of the Dowty Rotol R212 propeller. *Aeronautical Journal*, pages 225–236, 1987.

[30] S. Meijer, I. A. Lindblad, S. Wallin, and R. P. Donnelly. Acoustic predictions and measurements on a transonic propeller. In *15th AIAA Aeroacoustics Conference*. AIAA, AIAA, October 1993.

[31] J. H. Dittmar and D. B. Stang. Cruise noise of the 2/9 scale model SR-7A propeller. *Journal of Aircraft*, 25(8):740–746, 1988.

[32] H. Shin, C. E. Whitfield, and D. C. Wisler. Rotor-rotor interaction for counter-rotating fans, part 1: Three-dimensional flowfield measurements. *AIAA Journal*, 11:2224–2233, November 1994.

[33] D. P. Garber and W. L. Willshire, Jr. En route noise levels from the Propfan Test Assessment airplane. NASA Technical Paper TP 3451, NASA, National Aeronautics and Space Administration, Langley Research Center, Hampton, Virginia 23681-0001, USA, September 1994.

[34] D. G. Crighton and A. B. Parry. Asymptotic theory of propeller noise part II: Supersonic single rotation propeller. *AIAA Journal*, 29(12):2031–2037, 1991.

[35] D. G. Crighton and A. B. Parry. Higher approximations in the asymptotic theory of propeller noise. *AIAA Journal*, 30(1):23–28, 1992.

[36] N. Peake and D. G. Crighton. An asymptotic theory of nearfield propeller acoustics. *J. Fluid. Mech.*, 232:285–231, 1991.

[37] C. A. Powell and J. M. Fields. Human response to aircraft noise. In H. H. Hubbard, editor, *Aeroacoustics of Flight Vehicles*, volume 2, pages 1–52. Acoustical Society of America, New York, 1995.

[38] T. F. W. Embleton and G. A. Daigle. Atmospheric propagation. In H. H. Hubbard, editor, *Aeroacoustics of Flight Vehicles*, volume 2, pages 53–99. Acoustical Society of America, New York, 1995.

[39] V. L. Wells and A. Y. Han. Acoustics of a moving source in a moving medium with application to propeller noise. *Journal of Sound and Vibration*, 184(4):651–663, 1995.

[40] D. B. Hanson. Sound from a propeller at angle of attack: A new theoretical viewpoint. *Proc. R. Soc. Lond. A.*, 449:315–328, 1995.

[41] F. Farassat. Theoretical analysis of linearized acoustics and aerodynamics of advanced supersonic propellers. In *CP-366, Aerodynamics and acoustics of propellers*, volume 10. AGARD, October 1985.

[42] P. Spiegel. *Prévision et analyse du bruit émis par un rotor principal d'hélicoptère en présence d'interactions pale-tourbillon.* PhD thesis, Université du Maine, July 1995.

[43] K. S. Brentner. Numerical algorithms for acoustic integrals—the devil is in the details. In *2nd AIAA/CEAS Aeroacoustics Conference*. AIAA, 1996.

[44] R. Stuff. Noise field of a propeller with angular inflow. *AIAA Journal*, 26(7):777–782, July 1988.

[45] D. B. Hanson and D. J. Paryzch. Theory for Noise of Propellers in Angular Inflow With Parametric Studies and Experimental Verification. NASA Contractor's Report 4499, Hamilton Standard Division, United Technologies Corporation, P.O. Box 100, Windsor Locks, Connecticut, 06096, U.S.A., March 1993.

[46] A. Lakhtakia, V. K. Varadan, and V. V. Varadan. Green's functions for propagation of sound in a simply moving fluid. *J. Acoust. Soc. Am.*, 85(5):1852–1856, 1989.

[47] F. Farassat. Introduction to generalized functions with applications in aerodynamics and aeroacoustics. NASA Technical Paper TP 3428, NASA, National Aeronautics and Space Administration, Langley Research Center, Hampton, Virginia 23681-0001, May 1994 (corrected April, 1996).

[48] R. L. Panton. *Incompressible Flow.* John Wiley & Sons, Inc., 1984.

[49] A. B. Parry and D. G. Crighton. Asymptotic theory of propeller noise part I: Subsonic single rotation propeller. *AIAA Journal*, 27(9):1184–2037, 1989.

[50] William H. Press, Saul A. Teukolsky, William T. Vetterling, and Brian P. Flannery. *Numerical Recipes in C.* Cambridge University Press, second edition, 1992.

[51] W. Eversman. Analytical study of wind-tunnel acoustic testing of propellers. *Journal of Aircraft*, 27(10):851–858, 1990.

[52] W. Eversman and K. J. Baumeister. Modeling wind tunnel effects on the radiation characteristics of acoustic sources. *Journal of Aircraft*, 23(6):455–463, 1986.

[53] D. B. Hanson and M. R. Fink. The importance of quadrupole sources in prediction of transonic tip speed propeller noise. *Journal of Sound and Vibration*, 62(1):19–38, 1979.

[54] E. Envia. Asymptotic theory of supersonic propeller noise. *AIAA Journal*, 32(2):239–246, February 1994.

[55] N. Peake and D. G. Crighton. Lighthill quadrupole radiation in supersonic propeller acoustics. *Journal of Fluid Mechanics*, 223:363–382, 1991.

[56] E. E. Larrabee. The screw propeller. *Scientific American*, pages 114–124, July 1980.

[57] M. Carley. SCRUMPI (Sound Calculation for Rotation of Unsteady-source Multibladed Propellers with Incidence) user manual. Technical report, Department of Mechanical Engineering, Trinity College, Dublin 2, Ireland, 1996.

[58] S. E. Wright. Sound radiation from a lifting rotor generated by asymmetric disk loading. *Journal of Sound and Vibration*, 9(2):223–240, 1969.

[59] H. Jeffreys and B. Swirles (Lady Jeffreys). *Methods of Mathematical Physics*. Cambridge University Press, third edition, 1956.

Appendix A

Frequency domain equivalent of time domain point source calculation

To calculate an equivalent to the time domain point source model, equation 3.7, the idea of Wright [58] can be used with the source modelled as a sum of azimuthal modes. For the case of a point source at a radius a_0, the source strength can be written

$$s(a,\psi,t) = \frac{1}{\pi}\sum_{m=1}^{m=N}\delta(a-a_0)\Re(e^{j(m\Omega t - m\psi)}) \tag{A.1}$$

if N harmonics of the sound are considered. In effect this is a repetition of equation 3.4 except that now the integration over space is performed first and the integration over retarded time is catered for by replacing the point source by a Fourier series in azimuth. The convenience of this is that the retarded time calculations are trivial since the source does not move; the Fourier series does the work. As noted in chapter 2, a frequency domain formulation of this type reduces by one the number of degrees of freedom that must be allowed to the source motion.

The strength of the mth harmonic of the sound from the distribution is then an integral over the disc,

$$h_m = \frac{1}{\pi}\int_{a_{hub}}^{a_{tip}}\int_0^{2\pi}\delta(a-a_0)G(r,\theta,z;a_0,\psi,0;\Omega)\exp(j\,(m\Omega t - m\psi))a\,da\,d\psi \tag{A.2}$$

which becomes, after inserting the Green's function, equation 3.2,

$$h_m = \frac{1}{\pi}\int_{a_{hub}}^{a_{tip}}\int_0^{2\pi}\delta(a-a_0)\exp(-jm\psi)a \times\gamma\frac{\exp(-j\Omega(\gamma R'/c - \gamma^2\mathbf{M}_\infty.(\mathbf{x}-\mathbf{y})/c))}{4\pi R'}\,d\psi\,da \tag{A.3}$$

This can be approximated for the far field if required by using a first order expansion for σ in the phase term. Then, holding R' constant in the amplitude the integral over ψ becomes a Bessel function in a representing the radiation efficiency as a function of disc radius (see Wright [58] and Mani [11] for example). Alternatively, it can be left in this exact form as in the work of Hanson [40].

Appendix B

Multidimensional delta function as a surface integral

The identity

$$\int_{\mathbf{x}} \phi(\mathbf{x})\delta(f)\, d\mathbf{x} = \int_{f=0} \phi(\mathbf{x})\, dS \tag{B.1}$$

is used in chapter 4 to develop the surface integral form of the acoustic equations. It can be proven by setting up a curvilinear coordinate system (ξ_1, ξ_2, ξ_3) with ξ_1 and ξ_2 lying in the surface $f = 0$ and ξ_3 perpendicular to it. Since the convention that $|\nabla f| = 1 = \partial f/\partial \xi_3$ has been adopted, ξ_3 is the distance from the surface f. Then

$$\int_{\mathbf{x}} \phi(\mathbf{x})\delta(f)\, d\mathbf{x} = \int_{\mathbf{x}} \phi(\xi)\delta(f(\xi))\frac{\partial(x_1, x_2, x_3)}{\partial(\xi_1, \xi_2, \xi_3)}\, d\xi_1\, \xi_2\, \xi_3,$$

with $\partial(x_1, x_2, x_3)/\partial(\xi_1, \xi_2, \xi_3)$ the Jacobian of the transformation of $\mathbf{x}$ to ξ (Jeffreys and Jeffreys [59]). Then

$$\begin{aligned}
\int_{\mathbf{x}} \phi(\mathbf{x})\delta(f)\, d\mathbf{x} &= \int_{\mathbf{x}} \phi(\xi)\delta(\xi_3)\frac{\partial(x_1, x_2, x_3)}{\partial(\xi_1, \xi_2, \xi_3)}\, d\xi_1\xi_2\xi_3, \\
&= \int_{\xi_3=0} \phi(\xi_1, \xi_2)\frac{\partial(x_1, x_2, x_3)}{\partial(\xi_1, \xi_2, \xi_3)}\, d\xi_1\, d\xi_2 \\
&= \int_{f=0} \phi(\mathbf{x})\, dS.
\end{aligned} \tag{B.2}$$

As a concrete example, consider the function $f = (x_1^2 + x_2^2 + x_3^2)^{1/2} - 1$ which represents the surface of a sphere of unit radius. The coordinates ξ_i can be chosen as the coordinates of a spherical polar system so that

$$\begin{aligned}
x_1 &= (1 + f)\sin\xi_1 \cos\xi_2, \\
x_2 &= (1 + f)\sin\xi_1 \sin\xi_2, \\
x_3 &= (1 + f)\cos\xi_1,
\end{aligned}$$

noting that $\xi_3 = f$. The Jacobian of this transformation is $(1+f)^2 \sin\xi_1$ (Jeffreys and Jeffreys [59]) so that the integral becomes

$$\begin{aligned}\int_{\mathbf{x}} \phi(\mathbf{x})\delta(f)\, d\mathbf{x} &= \int_{\mathbf{x}} \phi(\xi)\delta(\xi_3)(1+f)^2 \sin\xi_1\, d\xi_1\, d\xi_2, \\ &= \int_{f=0} \phi(\mathbf{x}) \sin\xi_1\, d\xi_1\, d\xi_2,\end{aligned}$$

which is the familiar integral of $\phi(\mathbf{x})$ over the surface of a sphere of unit radius.

Appendix C

Numerical implementation

Two aspects of the numerical component of the work presented in this thesis are important—the actual numerical calculation of the sound generated by the propeller and the interpolation of the measured blade loading to generate the aerodynamic input for the acoustic calculation.

C.1 Sound prediction

The numerical code (called SCRUMPI) used to predict the generated noise is described in detail in its manual [57]. It was intended that it be capable of modelling the loading and thickness sources in as much detail as possible, including in particular the unsteady effects due to incidence. Two aspects of the evaluation of the acoustic integrals are of interest. The first is the estimation of the retarded time and the associated kinematic quantities for a given observer time-point while the second is the actual evaluation of the integral over a blade surface element for the calculation of the radiated sound.

C.1.1 Retarded time calculation

The calculation of retarded time for some point on the blade and for some observer time is a question of solving equation 3.5 for $g = 0$. This can be done quite easily using the Newton-Raphson method, [50], which requires as input g and $dg/d\tau$,

$$g = \tau - t + \gamma R'/c - \gamma^2 \mathbf{M}_\infty.(\mathbf{x} - \mathbf{y})/c$$
$$dg/d\tau = 1 + \gamma \partial R'/\partial\tau/c + \gamma^2 \mathbf{M}_\infty.\dot{\mathbf{y}}/c$$

with $dg/d\tau$ given in equation 3.6. For efficiency, it is important to note that almost all of the important kinematic variables are calculated in solving for τ so that they do not need to be recalculated once τ has been found.

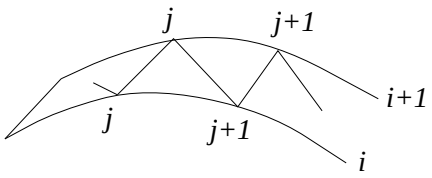

Figure C.1: Blade surface element generation

C.1.2 Blade surface integration

Integration over the blade surface is performed by dividing it into triangular patches. The geometry is supplied in the form of a section description at a number of radial stations. Triangular elements are formed by connecting two adjacent points of one section with a corresponding point of the next section. Figure C.1 shows the assignment of nodes to the element shown. For the area bounded by the ith and $i+1$th blade sections, and the jth and $j+1$th points of each of those sections, the two triangular elements formed are $<(i,j)\,(i+1,j+1)\,(i+1,j)>$ and $<(i,j)\,(i,j+1)\,(i+1,j+1)$. Note that the ordering of nodes in an element is anticlockwise for both elements. Then a plane through the three points of an element can be defined. The integral of a function defined over a triangular patch, varying linearly between the nodes, is easily found to be the area of the patch multiplied by the mean value of the function at the nodes,

$$I = A(f_1 + f_2 + f_3)/3$$
$$A = \text{area of triangular patch}$$
$$f_i = \text{value of function at each of triangle nodes}$$

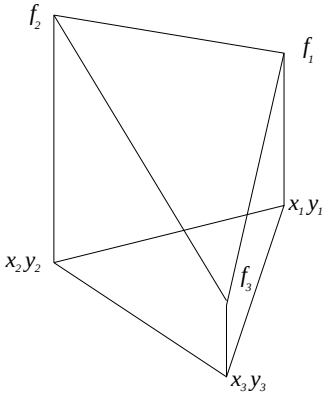

Figure C.2: Integration over triangular patch

C.2 Pressure interpolation

The interpolation technique used to generate the blade surface loading from the measured pressures proceeded in two stages—the estimation of a loading distribution around each section where pressure measurements were available followed by the interpolation of the section data to generate a full blade distribution.

C.2.1 Steady pressure estimation

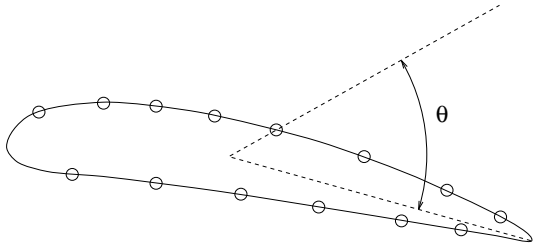

Figure C.3: Section interpolation

The first part of calculating the steady pressure distribution was the calculation of a pressure distribution for one section where tappings were available. At each radial station, a description of the section and an ordered list of the tapping positions were generated. Each tapping position i was then assigned an angular position variable θ_i which is the angle formed by the tapping, the centroid of the section and the section trailing edge, figure C.3. For each point on the section curve, a similar variable was generated and a linear interpolation routine was used to estimate the pressure at each position on the tapping. To ensure that a full set of data were available to cover the range $0 \leq \theta \leq 2\pi$ the list of data points (θ_i, p_i) was expanded by prepending the list $(\theta_i - 2\pi, p_i)$ and appending the points $(\theta_i + 2\pi, p_i)$. The use of this 'polar' interpolation scheme guaranteed that the leading and trailing edges could be handled correctly and avoided the numerical difficulties of interpolating using a Cartesian coordinate as a variable.

When the section interpolation was generated at each tapping radial station, linear interpolation using section radius as the interpolation variable was performed.

C.2.2 Unsteady pressure

As can be seen in figures E.2 and E.3 the unsteady pressure transducers were mostly concentrated at one section. Certainly, at those sections with only one measurement point, no meaningful interpolation was possible so for the estimation of the blade unsteady loading distribution a different approach was

used. For each propeller, one section was well covered by unsteady pressure transducers and this section was used as a reference. The unsteady pressure at each section was estimated as a scaled version of this reference set of measurements on the assumption that the ratio of unsteady to steady pressure did not vary with radius.

C.3 Output

The results from SCRUMPI are output as a file containing the value of each of the four integrals of equations 4.12 and 4.15 as well as an index. The single-blade records are written first, followed by the superposed whole-propeller signal. For example, part of the output file for a 72 point time record reads as follows.

```
0 -5.139522e-02 -9.434133e+00 -4.777253e+00 2.788415e+01
1 2.031973e-02 -9.451475e+00 -4.818794e+00 2.800561e+01
⋮

70 -1.831733e-01 -9.175837e+00 -4.457486e+00 2.753205e+01
71 -1.189177e-01 -9.340992e+00 -4.658111e+00 2.772676e+01

0 -2.463184e+01 3.079602e+01 -1.116277e+02 -7.850605e+00
1 -2.095172e+01 -4.421509e+01 -2.346421e+02 -2.189417e+01

⋮

70 -2.218767e+01 1.336083e+02 1.092495e+02 -1.211110e+01
71 -2.871216e+01 9.578926e+01 7.262131e+00 -3.226573e+00
```

The columns of the file contain

(1) time point index,

(2) $$\frac{\gamma}{4\pi c}\int_S\left[\frac{1}{1-\mathbf{M}_s.\mathbf{D}}\frac{d}{d\tau}\left(\frac{\mathbf{l}.\mathbf{D}}{R'(1-\mathbf{M}_s.\mathbf{D})}\right)\right]dS,$$

(3) $$\frac{\gamma}{4\pi}\int_S\left[\frac{\mathbf{l}}{R'(1-\mathbf{M}_s.\mathbf{D})}.\left(\frac{\mathbf{R}}{R'}-\frac{\gamma}{c}\frac{\dot{\mathbf{R}}}{1-\mathbf{M}_s.\mathbf{D}}\right)\right]dS,$$

(4) $$\frac{\gamma}{4\pi}\int_S\left[\frac{1}{1-\mathbf{M}_s.\mathbf{D}}\frac{d}{d\tau}\left(\frac{\rho_0 v_n(1-\mathbf{M}_\infty.\mathbf{D})}{R'(1-\mathbf{M}_s.\mathbf{D})}\right)\right]dS,$$

(5) $$-\frac{\gamma}{4\pi c}\int_S\left[\frac{\rho_0 v_n\mathbf{M}_\infty}{R'(1-\mathbf{M}_s.\mathbf{D})}\cdot\left(\frac{\mathbf{R}}{R'}-\frac{\gamma}{c}\frac{\dot{\mathbf{R}}}{1-\mathbf{M}_s.\mathbf{D}}\right)\right]dS.$$

The first 72 lines contain the single-blade time records while the rest of the file holds the superposed signals for the whole propeller.

Appendix D

Acoustic tests and measurement

The experimental data in chapter 5 are supplied courtesy of the partners in SNAAP (Study of Noise and Aerodynamics of Advanced Propellers), a European Union sponsored project which involved a number of European aerospace companies (Aérospatiale, Alenia, Dornier, Fokker, Dowty Aerospace Propellers and Ratier Figeac) and research institutes and universities (CIRA, NLR, ONERA, University College, Galway, IST, Lisbon and Trinity College, Dublin). Two sets of tests were conducted to generate the data used in this thesis. The first set was carried out at ARA, Bedford, England while the second was at DNW, Emmeloord, The Netherlands. In each case, acoustic and on-blade unsteady pressure data were acquired using an LMS data acquisition system running on a Hewlett-Packard 382 controller. Details of the blade-mounted instrumentation are given in appendix E. Quarter-inch Bruel & Kjäer microphones fitted with nose-cones were used.

D.1 ARA tests

The tests at ARA were conducted in the transonic wind-tunnel with the addition of an acoustic liner. For the axial directivity data presented in this thesis the microphone traverse rig swept the measuring microphone along a sideline 1.22 blade radii from the propeller centre, figure D.1. The microphone was moved over a traverse of 1 blade radius up and downstream of the low speed propeller and 1.36 blade radii up and downstream of the high speed propeller.

Tables D.1 and D.2 show the conditions for the tests which were carried out at ARA on the LSP and HSP respectively. Those test cases for which predictions are presented in chapter 5 are shown boxed. For the LSP tests and a number of the HSP tests, the driving parameter was the advance ratio $J = M_\infty/\pi M_r$, the ratio of the flight Mach number to the tip rotational Mach number. The test cases chosen correspond to flight conditions of interest, i.e. high speed cruise at zero or low incidence and lower speed flight at higher angles of attack related to climb and descent conditions. The DNW tests, conducted at lower speed concentrated more on the high incidence angles

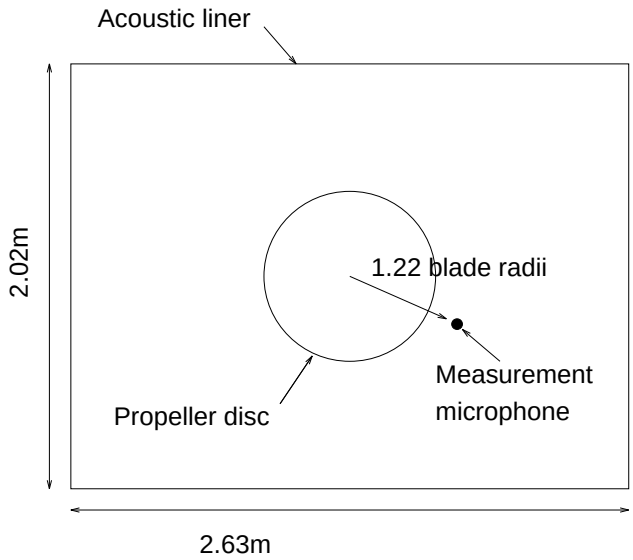

Figure D.1: ARA traverse geometry

related to takeoff and approach.

	M_∞					
J	0.6		0.65		0.7	
3.238	0.84	**0°**	0.91	**0°**	0.98	**0°**
3.597	0.80	**0°**	0.86	**0°**	0.93	**0°**
4.047	0.76	0°	0.82	0°, 1.5°, 3°	0.89	**0°**, 1.5°, **3°**
4.625	0.73	**0°**	0.79	**0°**	0.85	**0°**, 3°
	M_t	α	M_t	α	M_t	α

Table D.1: LSP tests conducted at ARA. Chapter 5 contains data for the boxed entries, see table 5.1

D.2 DNW tests

For the DNW tests, noise was measured in the propeller's far field as shown in figure D.2. The measurement microphone was traversed from 6.74 blade radii upstream of the propeller to 6.9 blade radii downstream.

	M_∞									
N/rpm	0.5		0.6		0.74		0.76		0.78	
4200					0.96	0°	0.97	0°	0.99	0°
4500	0.81	0°								
4750	0.83	0°, 1.5°, 3°								
5123			0.95	0°	1.05	0°	1.06	0°	1.08	0°, 1.5°
	M_t	α	M_t	α	M_t	α	M_t	α	M_t	α

Table D.2: HSP tests conducted at ARA. Chapter 5 contains data for the boxed entries.

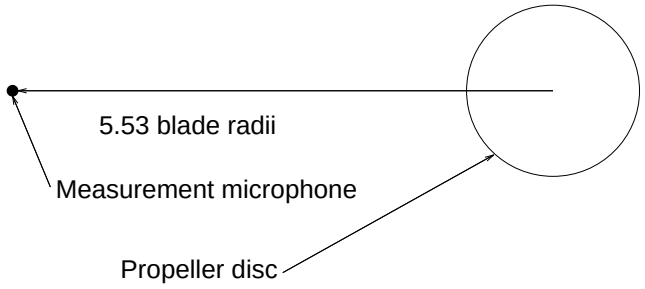

Figure D.2: DNW traverse geometry

	M_∞					
J	0.1		0.15		0.2	
0.945					0.69	0°, 5°, 10°, 15°
0.998			0.50	0°	0.66	0°, 7.5°, 15°
1.065					0.62	0°
1.140			0.44	0°	0.59	0°, 7.5°, 15°
1.267					0.53	0°
1.422	0.24	0°	0.36	0°	0.48	0°, 7.5°, 15°
	M_t	α	M_t	α	M_t	α

Table D.3: LSP tests conducted at DNW. Chapter 5 contains data for the boxed entries.

Appendix E

Blade instrumentation

The two propellers examined in this thesis were instrumented with both static pressure tappings and unsteady pressure transducers. The static tappings were distributed over three blades as were the dynamic transducers. Figures E.2 and E.3 show the distribution of the measurement points in a composite form, i.e. showing the transducer positions referred to a single blade for the LSP and HSP respectively. Each figure shows the positions of the pressure measurements for the suction (low pressure) side and pressure (high pressure) side respectively. The propellers themselves are shown in figure E.1.

Signals were read from the transducers using a slip-ring on the propeller shaft. All of the unsteady pressures were read during each test, while one third of the pressure tapping readings were logged. This was a compromise between the need to have a large number of tappings to give a complete pressure distribution and the limitations imposed by the number of available slip-rings and the number of tappings that could be read by the hub-mounted "Scanivalve" system. The tappings not in use in a test were taped over.

Data were acquired using Hewlett-Packard 382 workstation controlled Hewlett-Packard and DIFA Scadas acquisition systems and LMS processing software. Eight microphones were sampled at 16384 Hz on one system and the twenty-five channels of unsteady pressure data were taken on the other at a sample rate of 8192 Hz. Both systems also acquired the once-per-revolution ('1P') pulse from the propeller shaft for synchronisation purposes. The 1P signal was used in the generation of the time averaged waveforms used for the unsteady loading calculations (appendix C) and for the comparisons with numerical predictions shown in chapter 5.

Low speed propeller

High speed propeller

Figure E.1: Propellers used in the acoustic tests

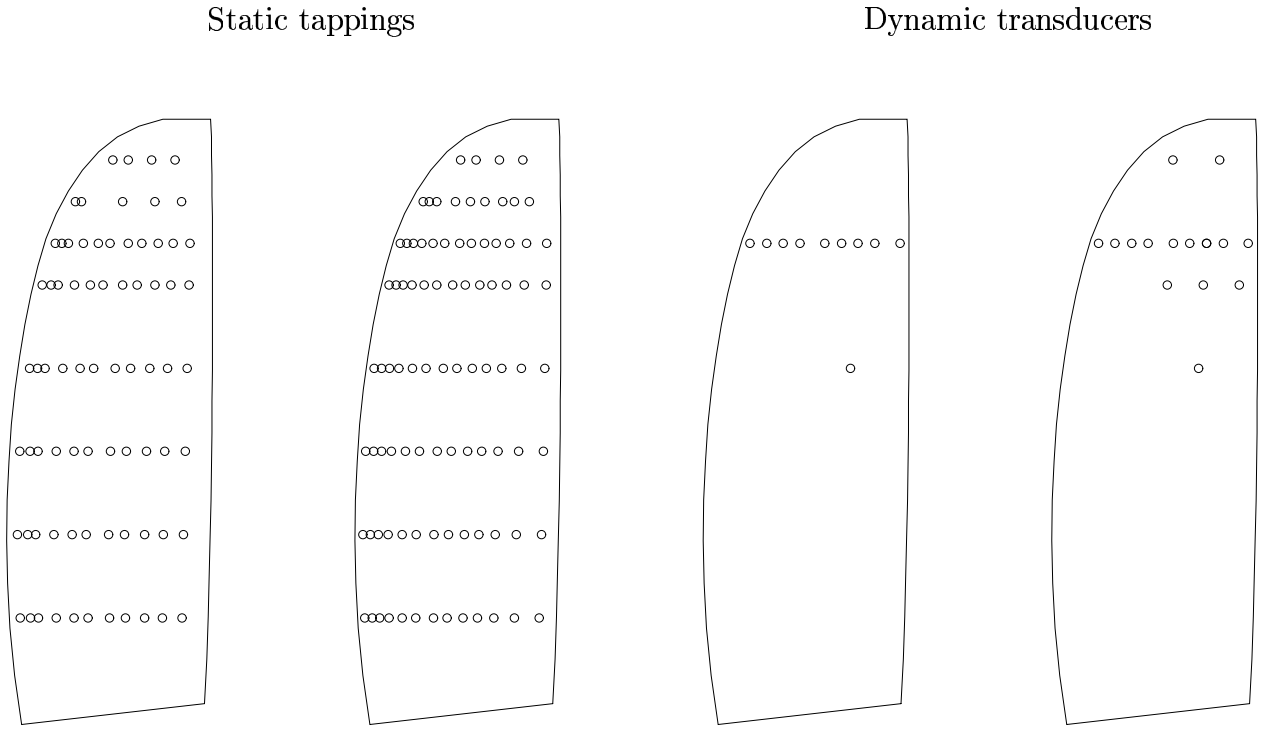

Figure E.2: LSP instrumentation

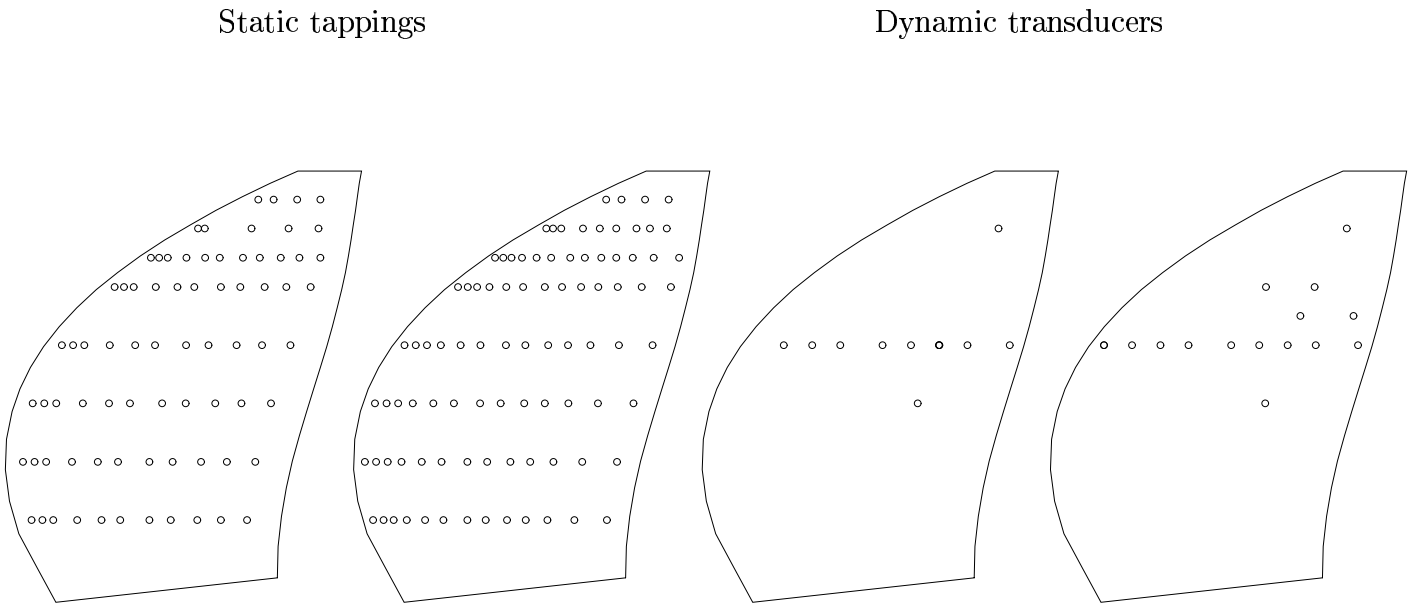

Figure E.3: HSP instrumentation

He has never again encountered the most esteemed Arkady Apollonovich Sempleyarov in connection with acoustical problems. The latter was quickly transferred to Bryansk and appointed director of a mushroom-growing center. Nowadays, Moscow residents eat pickled saffron milk caps and marinated white mushrooms with endless relish and praise, and never stop rejoicing in the lucky transfer. Since it is all a matter of the past now, we feel free to say that Arkady Apollonovich never did make any headway with acoustics, and, for all his efforts to improve the sound, it remained as bad as it was.

The Master and Margarita, Mikhail Bulgakov